Theoretical characterization of new dynamic bonds for responsive materials and their optical properties

eman ta zabal zazu

UPV EHU

NAZIOARTEKO
BIKAINTASUN
CAMPUSA

CAMPUS DE
EXCELENCIA
INTERNACIONAL

Author: Maialen Galdeano Fraile
Directors: Jon Mattin Matxain and Fernando Ruipérez

Donostia
2023

Theoretical characterization of new dynamic bonds for responsive materials and their optical properties

POLYMAT

Basque Center for
Macromolecular Design and Engineering
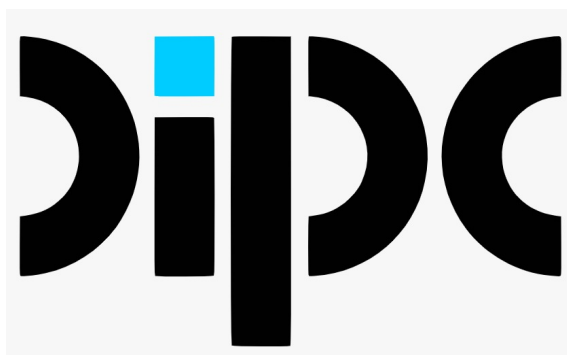
Author: Maialen Galdeano Fraile
Directors: Jon Mattin Matxain and Fernando Ruipérez

Eskerrik beroenak

Lau urte eta erdi igaro dira tesia hasi nuenetik eta, azkenean, hemen nago eskerrak idazten. Lehenik eta behin, bidaia honetan oso garrantzitsuak izan diren bi pertsonei eskerrak eman nahiko nizkieke. Txoni, badira 7 urte ezagutu ginela, erraz esaten da. Orduantxe erakutsi zenidan nire lehenengo kalkulua bidaltzen, gogoan dut amoniako molekula zela! Ez dakizu zenbat eskertzen dudan momentu horretan nigatik apustu egin izana, zure konfidantzak asko lagundu dit. Mila esker ere nigatik egin duzun guztiagatik, irekitako eta botatako ate bakoitzagatik, konfiantza kiloka emateagatik eta eskainitako animo guztiengatik (batez ere, tesiaren amaieran jaja), zu gabe hau ez litzateke posible izango. Fernando, nire beste euskarria, duela 6 urte ezagutu zintudan gradu amaierako lanean. Hasieran, niretzat izen bat zinen, orain nire sostengua. Mila esker nigan itsu-itsuan sinesteagatik, batez ere, ezagutzen ez ginenean eta nire zuzendaria izatea onartu zenuenean. Bioi, eskerrik asko azkar erantzundako email bakoitzagatik, egunero laguntzeko prest egoteagatik, nire zalantzak (existentzialak eta akademikoak) argitzen laguntzeagatik eta erakutsi didazuen guztiagatik. Bidaia honetan nire aingeru guardakoak izan zarete!!!

Ekipo, azkeneaaaannnn!!! Eskerrik asko hainbeste urtetan nere negarrak eta pozak entzuteagatik, benetan! Ez dakizue ze garrantzitsuak bihurtu zareten niretzat Txantxot, Telle, Julen, David, Iker, Lanuza, Jon, Oksana, Andoni, Erramun, eta nola ez, Maria. Eskerrik asko hainbeste kafe partekatzeagatik. Eta, Maria, gure Mariapedia maitea, bihotz-bihotzez eskerrak hor egoteagatik, masterretik tesira, nire despisteak saihesten eta konpontzen. Maite zaituztet ekipo!!! Bulegokoei ere eskerrak eman nahi dizkiet, Eli, Txema eta Xabi, emandako aholku bakoitzagatik (ez direla gutxi izan) eta nire arrakastak ospatzeagatik.

Lagunak, eskerrak alboan izan zaituztedan! Mila esker Maider eta Esti urteotan zehar nire ondoan egoteagatik eta beti laguntza eskaintzeagatik. Eskerrik asko Maddi eta Miriam, txakurrekin emandako paseo terapeutikoengatik; kuadrila, beti hor egoteagatik; Lastreak, hainbeste (beharrezko) parrandengatik; Domin y Ander, por aguantar mis lloros y convertirlos en risas; Gym Bros, por insistir taaaanto en que ir al gimnasio y estar con vosotros me hará bien, no os falta razón; Eli y Javi, por hacerme sentir como en casa durante tantos años, de ser jefes habéis pasado a ser muy buen amigos. Hoberenak zarete, maite zaituztet!

Aita, Ama, Jon: POR FIN! Orain lasai egingo dugu lo. Eskerrik asko 29 urtetan ni ondo zaintzeagatik eta eman didazuen guztiagatik. Nola ez, mila esker ere Galdeano-Fraile familiei, beti nire ondoan goxo-goxo egoteagatik. Gracias a mi familia adoptiva, Stella, Jesus, Maitane, Rocio y Dani, gracias por apoyarme incondicionalmente desde

los 15 años hasta hoy, gracias por hacerme sentir otra hija-hermana más, sin vosotros nada sería igual. Y, muchas gracias Dani, por crear el lema de ¡*QUIEN LA SIGUE, LA CONSIGUE!*

Mila mila mila esker Eneko, nire bide lagun gustokoena. Eskerrik asko nire alboan egoteagatik, azken hilabeteotan etxekogizon izateagatik, nahi nuen familia sortzen laguntzeagatik, nire malkoak lehortzeagatik eta pazientzia kiloka emateagatik. Badakizu dena. Eta orain notizi ona, BUKATU DA!

Azkenik, eskerrak eman nahi dizkiot nire buruari ere, amore ez emateagatik. Mila esker denoi, zuek gabe ez litzateke posible izango. Onenak zarete!!!

Contents

Chapter 1

Introduction

The Natural Sciences encompass a range of disciplines aimed at understanding the universe we inhabit. These fields can be broadly divided into two categories: Physical Sciences, which focus on non-living systems such as matter, energy, and the universe, and Life Sciences, which study living organisms and their interactions with the environment. Chemistry is a branch of Physical Sciences that is concerned with the composition, structure, properties, and reactions of matter. While it primarily falls under the Physical Sciences category, it is also closely linked to the Life Sciences through the study of the chemical processes within living organisms.

Chemistry can be defined in various ways. According to Oxford Dictionary, "Chemistry is the branch of science concerned with the substances of which matter is composed, the investigation of their properties and reactions, and the use of such reactions to form new substances." Cambridge Dictionary defines it in a similar manner, while British Encyclopedia also includes the concept of energy released or absorbed during chemical processes. This fact opens the possibility of including in Chemistry also the interaction of matter with light, being light a source of energy that can take part in photochemical or photophysical processes.

There are different classifications within chemistry. Based on the type of the molecules under study, areas such as Organic, Inorganic Chemistry, Biochemistry can be distinguished. On the other hand, if we focus on the manner molecules and their processes are studied, other areas such as Analytical Chemistry or Physical Chemistry arise. The latter enables the study of chemical reactivity based on two main criteria. On one hand, the reversibility or irreversibility of a given reaction, and on the other hand, the velocity at which the reaction takes place. In this context, reversible reactions that occur at room temperature (or near it) and are kinetically allowed have opened a new branch of chemistry, named Dynamic Chemistry, with high impact in the development of new materials.

1.1   Dynamic chemistry

Traditionally, the synthesis of organic compounds has been controlled kinetically resulting in irreversible covalent bond formation. This strong covalent bond formation is a consequence of very carefully chosen reagents and conditions, looking for the most efficient pathway of the chemical reaction. Indeed, a more energetically favourable pathway to the formation of a particular product is sought to obtain an irreversible covalent bonding reaction. Hence, a detailed comprehension of the different transition states and pathways is needed to obtain a controlled product distribution. This irreversible nature of the reaction ensures that, once the product is formed, there is no way for it to become again the starting reagents or to transform into another product under the conditions of the reaction. In this context, chemists have provided with efficient syntheses of natural and unnatural products. [1,2]

Nevertheless, in recent years, reversible chemistry has been widely recognised since it is expected to yield great advances in materials science. This reversible chemistry is based on the ability of a covalent or non-covalent bond to be formed, broken and reformed reversibly at equilibrium. [3] If this equilibrium is achieved fast enough, the process is called dynamic chemistry and leads to efficient formation of products under thermodynamic control.

Dynamic chemistry is gaining significance in polymer science and engineering, since a large variety of materials have been developed with unique properties attributed to the nature of the dynamic bond, such as reprocessing, recycling or self-healing capacity. [4] These dynamic bonds must experience a fast reversible cleavage, so that an effective and well-planned structural design is decisive to adjust the dissociation and activation energies. This tailoring includes the use of both steric [5–7] and electronic effects. [8,9] The reversible response may be triggered by different stimuli, such as chemical, biological or physical, producing a change of one or more properties in the material. The development of this field of research may outcome in dynamically controlled systems for diverse applications such as drug delivery, robotics, (bio)sensors and self-healing materials. [10] In this context, synthetic polymers are good candidates to include dynamic features, since they can be chemically altered easily resulting in a responsive mechanism that can be readily manipulated.

In conclusion, dynamic chemistry is a field with numerous practical applications, see Figure 1.1. Some examples of these applications include drug delivery systems that release medication in a controlled manner, molecular machines that can execute mechanical tasks at the molecular level, responsive materials that can sense and adapt to changes in their environment, shape-memory materials that can modify their configuration in response to external stimuli, chemical amplification that can amplify small signals or changes for more precise detection, catalysis that allows for efficient formation and disconnection of covalent bonds in response to external stimuli, self-assembly where molecules or components organize themselves into arranged structures without external intervention, and self-healing materials that can autonomously repair themselves
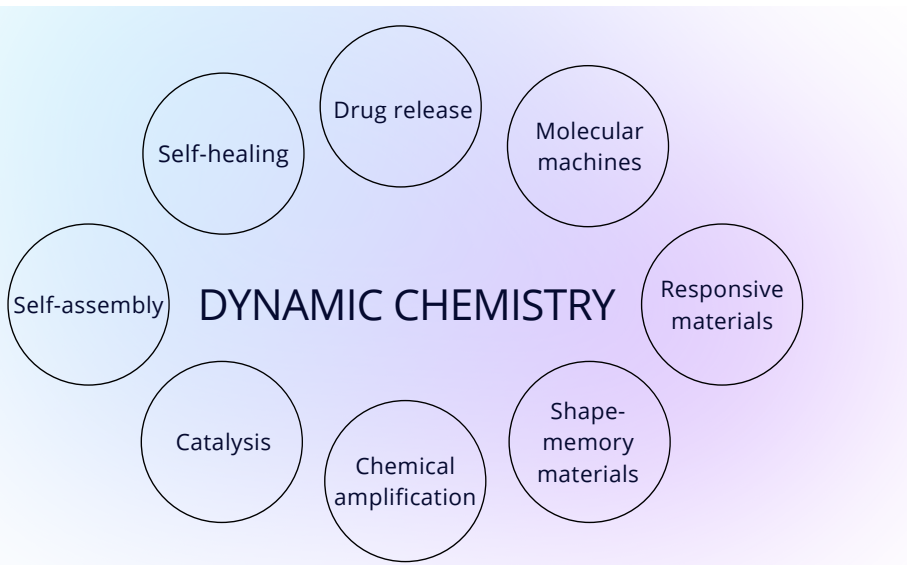
Figure 1.1: Selected applications of dynamic chemistry in different fields.

after being harmed or distorted (see the following section for more details). Therefore, advances in dynamic chemistry could potentially transform fields such as medicine, materials science, and nanotechnology.

1.2 Self-healing materials

The inspiration for the development of self-healing materials may be found in Nature, where many living organisms show the ability to self-heal employing different strategies. Some of them are depicted in Figure 1.2. Salamanders can regenerate lost body parts by forming a mass of cells called the blastema after a limb is amputated. Reptiles shed their skin to facilitate their growth as they are constrained by it; the new skin develops underneath the old skin and the outermost layer dies and falls away. Mussel byssal threads repair themselves through histidine-metal interactions after exposure to mechanical stress in the ocean, allowing them to remain attached to their substrates. Cells have the ability to detect and repair any damage that occurs to the DNA molecules that make up its genome. In leaves, the exposure of the wound site to air triggers a process in which cells enlarge and reproduce, resulting in the closure of the wound. Cell signaling is crucial for coordinating the activities of platelet clotting, immune response, tissue repair and infection prevention during wound healing. Overall, it is evident that in nature one can find the self-healing process occurring not only at the molecular level, but also at macroscopic level.

Inspired in these natural examples, scientists have been able to design different approaches to synthesize non-living materials with self-healing capacity. In the last years, functional materials that are able to endure environmental stress by repairing themselves

Self-healing in nature
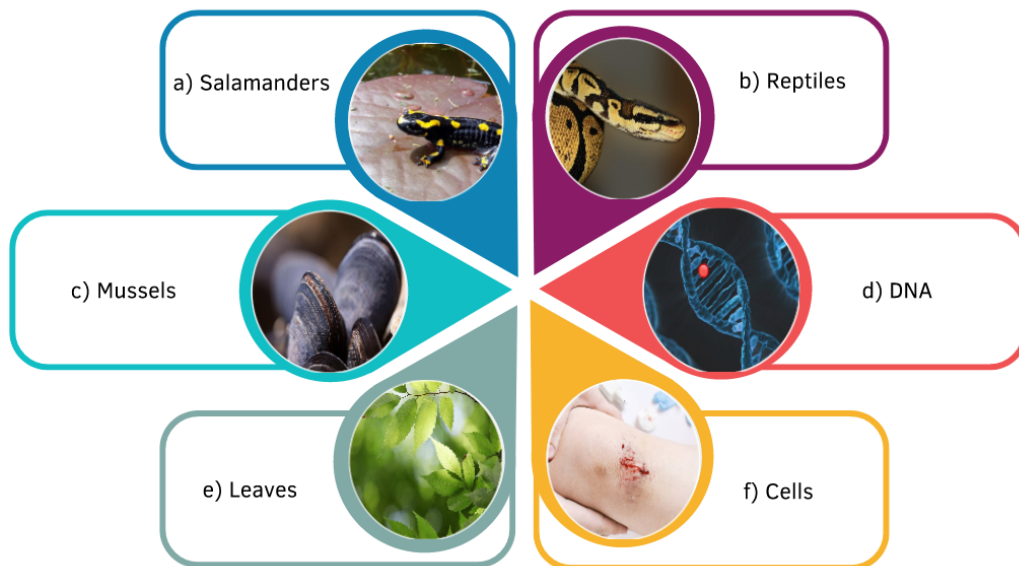
Figure 1.2: Examples of different self-healing processes found in nature, such as those observed in a) salamanders, b) reptiles, c) mussels, d) DNA, e) leaves, and f) cells.

either automatically[11] or in response to an external stimulus, like heat[12] or pressure,[13] are of great technological interest and is a rapidly expanding area of research.[14–17] Thus, self-healing polymers have been intensively explored because of their broad applications and the range of healing mechanisms available.[18–21] These smart materials are created particularly to prolong the life of products that guarantee their chemical integrity or function and are based on reversible chemistry, in such a way that the reorganization of the chemical bonds leads to a reconnection of the damaged parts, resulting in a partial or complete recovery of the material.

Many different chemistries have been explored to introduce healing functionality in polymeric materials, and two main approaches, depending on the nature of the reversible bond, can be devised: i) materials based on dynamic covalent bonds,[4,22–29] making use of the retro-Diels-Alder reaction,[12,30,31] dichalcogenide bonds,[32–36] siloxane chemistry,[37] transesterification,[38] transcarbamoylation,[39] transamidation[40] or alkoxyamine chemistry,[41] for instance, and ii) based on non-covalent interactions, such as π-π stacking,[42–44] hydrogen bonds,[13,45–48] metal-ion interactions[49–54] or ionomers.[21,55]

The presence of non-covalent interactions, such as hydrogen bonds, in self-healing polymers is important, since the chain dynamics influences the ability to flow and reshuffle, which remarkably determine the healing capacity of the material. However, the use of dynamic covalent bonds results in materials with higher mechanical stability and strength. In this vein, the use of weaker covalent bonds can be beneficial to achieve

an autonomously healing material while keeping a reasonable level of bond strength.[56] Aromatic dichalcogenides are found to be especially promising,[33,34,57,58] and exchange reactions have been reported at room temperature both in solution[59] and in the solid state.[60] Recently, the mechanism responsible for the exchange of disulfide-based compounds has been proposed theoretically by using quantum chemical calculations[35] and confirmed experimentally, in the absence of catalyst.[61] Furthermore, non-covalent interactions are, in general, more susceptible to external stimuli compared to covalent bonds, and self-healing materials based on these interactions display remarkable healing features.[62]

Another example of responsive materials based on dynamic covalent chemistry are the so-called vitrimers,[63] cross-linked materials firstly proposed by Leibler and coworkers[38] designed to enhance the robustness of thermosets with the processability of thermoplastics. The crosslinks undergo dynamic exchange by an associative exchange process[64] that leads to a constant crosslinking density which does not change with time and temperature. In this way, the material can be processed like traditional glass, in a liquid state, without losing network integrity. Different materials and associative exchange reactions have been used to synthesize vitrimers, for example, the exchange between the urea group and free aromatic amine groups in poly(urea-urethane) polymers.[65]

In summary, in order to achieve a reversible self-healing material which is autonomous or needs weak stimulation, an appropriate choice of the dynamic bond is mandatory. In this Thesis we focus on the chemistry of Frustrated Lewis Pairs (see section 1.3) and Metal-Pincer ligands (see section 1.4).

1.3 Dynamic bonds based on frustrated Lewis pairs

Despite the large number of reversible chemistries available, it is still challenging to develop self-healing materials based on dynamic bonds without changing the overall performance of the material.[66] For instance, certain dynamic bonds can only be applied to a particular polymer and, therefore, it would be desirable to identify new bonds that may expand the application field and be easily integrated into a larger number of polymeric systems. Following this approach, Shaver and coworkers explored a new type of self-healing material based on the reversible interaction between a frustrated Lewis pair (FLP) and a specific small molecule (diethyl azodicarboxylate, DEAD).[67] For the first time, an experimental research team took the FLP concept into a new area by producing dynamic cross-linked networks that provide polymer gels with self-healing properties.

The concept of FLP was introduced by Stephan and coworkers back in 2006.[68] This is a recent paradigm for chemical reactivity based on impeded dative bonding between a Lewis acid and a Lewis base. In the last decade, it has been shown that the introduction of steric hindrance or a dissociative equilibrium results in free electron donors and acceptors that no longer have the capacity to form a dative bond, creating

a FLP[69–71] and promoting activation of small molecules such as H_2, CO_2, NO or CO. The description of the FLP concept is depicted in Figure 1.3 top.
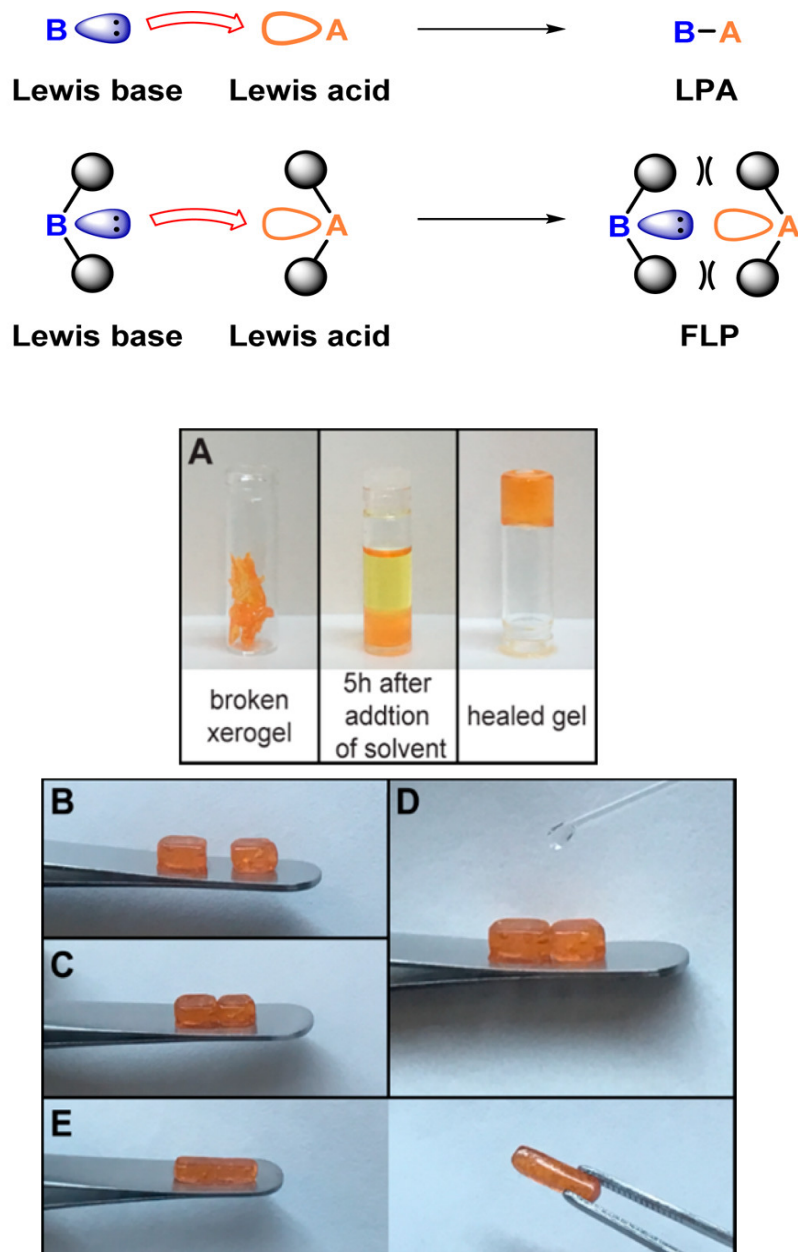
Figure 1.3: Top: Description of a frustrated Lewis pair. Bottom: Self-healing process of a broken xerogel (A) and a cut brickshaped swollen gel (B-E). Image reproduced from Ref. 67.

Shaver and coworkers designed a polymer containing FLP-based cross-links, that is, including electron donor and acceptor molecules that may interact reversibly with a small molecule to generate a responsive network. In particular, the monomers 4-styryl-

diphenylborane and 4-styryl-dimesitylphosphine were incorporated in a polystyrene main chain. In this way, the diethyl azodicarboxylate (DEAD) molecule reacts with boron and phosphorus atoms forming a gel (see Figure 1.3 bottom). Since the FLP-DEAD interactions are dynamic, high temperatures (100°C) may cleave the dative bonds.[67,72] Apart from this pioneering work, the introduction of FLPs into molecular materials has been, to our knowledge, scarcely considered.[73,74]

Weak interaction energies have been calculated in the activation of small molecules by FLPs. For example, the binding energy of CO_2 with the phosphine-borane pair is only of around 18 kcal/mol,[75] which is in the range of a medium-strength hydrogen bond,[76] and can be comparable to those present in a supramolecular responsive material. Thus, based on these results, we believe that the theoretical characterization of the interactions present in the material proposed by Shaver will provide information relevant for the development of new responsive materials activated by small molecules, exploiting the dynamic nature of the FLP bonding.

1.4 Dynamic bonds based on pincer ligands

Among non-covalent interactions, metal-ligand interactions provide great versatility regarding bond strength and binding dynamics, producing metallopolymers with controlled mechanical properties.[77] This type of interaction is also found in natural systems. For example, in mussels, byssus threads anchor the mussel on a substrate, where reversible Fe(III)-aminoacid interactions in the mussel foot proteins play an important role in adapting to the mechanical stress of turbulent water.[78,79] Inspired by this phenomenon, the first self-healing metallopolymer was described by Rowan and Weder.[53] Since this pioneering work, many efforts have been devoted to understand the underlying mechanism and devise new materials with improved features.[80–84]

The metal-ligand bond can be tuned in a broad range by a careful selection of both the metal and the ligand[85–87] to obtain optimal bond strengths for self-healing. Besides, the incorporation of metal-ligand bonds in supramolecular structures leads to the development of materials with advanced functionalities, such as thermoresponsive[88] or luminiscent materials.[89] So far, different ligands have been used to develop self-healing materials, i.e., histidine,[90,91] imidazole,[92,93] carboxylate,[94–96] pyridyl[53,97,98] or sulfur-containing ligands,[99] to mention some. Pyridine-containing ligands have been used to synthesize a large number of self-healing polymers, based on the Lewis basic character of the nitrogen lone pair.

The use of multidentate ligands increases the binding affinity towards a wider range of metals due to the chelating effect[100] and the $d\pi$-$p\pi$ back bonding of the metal to the ligands.[101] Thus, the so-called pincer ligands are chelating agents that bind tightly to three adjacent coplanar sites in a meridional configuration, see Figure 1.4. The terdentate coordination provides strong binding and results in high thermal stability.

Early examples of pincer ligands referred to ligands with a carbanion as the central donor site and flanking binding units that enforced meridional coordination, referred as η^3-ECE coordination, where E represents a neutral two-electron donor, usually coordinating by N and P atoms (NCN and PCP-type pincer ligands). In recent times, the *ECE* coordination has been extended to NNN, PNP, or SNS systems, to mention some.[102]
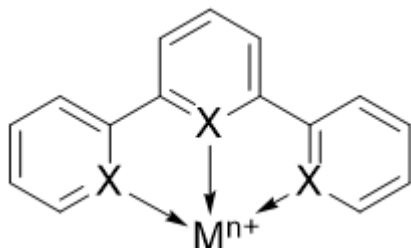
Figure 1.4: Schematic representation of a metal-pincer ligand complex, where the pincer is usually a terpyridine ligand (X = N) and M refers to a transition metal with its corresponding oxidation number. The arrows represent the interaction between the pincer and the metal.

Thus, a variety of terpyridine-containing (NNN coordination) polymers have been developed using metals such as Fe(II),[103] Cd(II),[103,104] Zn(II)[105,106] or Co(II).[107] The self-healing metallopolymer developed by Rowan and Weder, mentioned above, is based on the interaction between Zn(II) and La(III) with a pyridyl-based terdentate ligand.[53] In all these works, the relevance of the nature of the metal-ligand bond is highlighted. Thus, in terms of reversible interactions, Fe(II) seems to be the best candidate for self-healing features; other metals such as Ru(II) yield a too strong interaction,[101] while Cd(II) leads to a too weak interaction.[105] It is clear that the behaviour of the metal-ligand interaction is influenced by both the nature of the chelating ligands and the coordinated metal, which is a manifestation of the electronic structure.

Unlike terpyridine (TPY), metal-ligand complexes using the phosphorus analogue, terphosphinine (TPPh), have not been reported yet, although similar ligands have been used for the coordination of Rh and Ir, where the strong π-acceptor character of phosphinine is revealed.[108] The inclusion of a phosphorus atom in the aromatic moiety influences on the electronic, steric and coordination properties. Thus, although phosphinines are planar aromatic systems with delocalized π electrons, due to the overlap of phosphorus *3p* and carbon *2p* orbitals, the electronic properties of phosphinines differ from those of pyridines. The phosphorus lone pair occupies a more diffuse, partly delocalized and less directional orbital than that of pyridine and a low-lying LUMO orbital enables phosphinine to act as a good π-acceptor ligand.

While most of the research has been directed to the synthesis and characterization of new self-healing metallopolymers, few studies deal with the relationship between nature and dynamics of the metal-ligand bond with self-healing properties. In recent years, there have been a number of approaches focusing on the interaction between terpyridines with transition metals, concretely, Fe(II), Rh(II) and Cd(II)[101,105,109,110] metals. The only computational work in the literature, to our knowledge, is the one of Kupfer et

al.,[103] where thermally induced self-healing mechanisms in metallopolymers based on bisterpyridine complexes of Fe(II) sulfate and Cd(II) bromide were studied.

Therefore, it is clear that a computational insight into the metal-ligand interaction will provide valuable information for the development of new materials with self-healing capability.

1.5 Light-induced properties in self-healing materials

According to the broad definition of Chemistry given at the beginning of the Introduction, the matter-light interaction may also be studied within Chemistry. The absorption or emission of light represents a form of energy absorption or release. Absorption of UV/Vis light can trigger transitions between electronic states, changing the system from a ground to an excited electronic state. Therefore, the behavior of the excited state will be relevant to understand the characteristics of the system. Regarding polymeric materials, there are two noteworthy outcomes. First, light absorption can trigger self-healing processes (see Figure 1.5). Second, in materials already possessing self-healing ability, light absorption can provide the system with photoluminescent properties like fluorescence or phosphorescence. Thus, photoresponsive polymers undergo a change in their properties in response to light. The light-induced molecular change is reflected in a macroscopic change of the material properties.[111] The use of light may be advantageous, since it can be used locally and the wavelength may be tuned to selectively address the damaged part.[112]
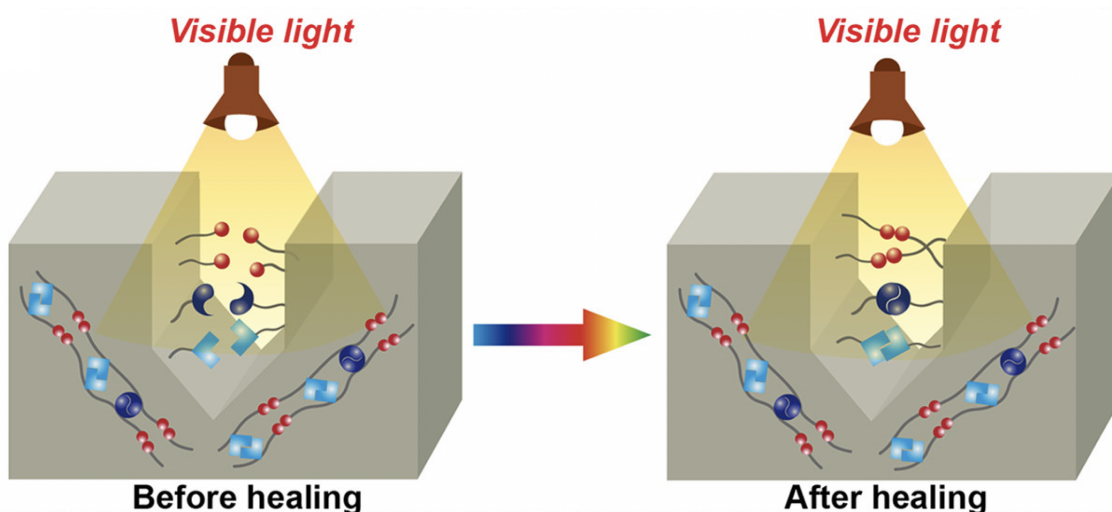
Figure 1.5: Light-induce self-healing process in a polymeric material. Figured adapted from Ref. 113.

One example of polymeric materials that exhibit light-induced self-healing properties

can be found in dichalcogenide-based materials. These materials derive their self-healing properties from the generation of sulfur or selenium radicals after the cleavage of the S-S or Se-Se bond, which can be activated by exposure to UV or visible light. Accordingly, when the material is irradiated, an electron transfer from the bonding (σ) to the antibonding (σ^*) sigma orbital takes place, resulting in a decrease in the bond order and weakening the S-S or Se-Se bond, promoting the radical formation.[36]

Another example of light induced self-healing process can be found in the pioneering work of Rowan and Weder,[53] where the healing process takes place after irradiating with UV light. The authors propose that the healing is a consequence of photothermal conversion. So, the complexes exhibit low fluorescence quantum yield, suggesting that part of the absorbed light is transformed into heat and used for the dissociation of the metal-ligand bond. Moreover, after irradiating with light of wavelengths different than that in which the complex absorbs, the material showed no healing, supporting that the process is indeed produced by light absorption.

The nature of the metal is relevant in both the self-healing and photophysical properties of the metallopolymers.[54,114,115] A well-known transition metal that creates complexes with cyclometallic compounds is, for instance, Ir(III).[116,117] The spectroscopic and electrochemical features of these complexes have been used for various applications including organic light-emitting diodes (OLEDs),[118] light-emitting electrochemical cells (LEC),[119] oxygen sensing,[120,121] sensitizers for solar cells,[122] hydrogen production[123] and photoredox catalysts.[124] For example, the use of cyclometallated Ir(III) complexes as phosphorescent dopants in OLEDs shows advantages compared to other compounds due to their strong phosphorescent emission. Therefore, the singlet excited states are converted into triplet states by a fast intersystem crossing due to the large spin-orbit coupling exerted by the Ir(III) atom. This spin-orbit coupling also facilitates the phosphorescent emission.[125] Besides, the colour changes within electrophosphorescent devices can be fine-tuned by using a variety of ligands that may alter the emission energy and electrochemical behavior. For example, the green emission of [Ir(ppy)$_3$] complex can be easily converted to yellow and red by replacing the cyclometalated ligands and/or by lowering the LUMO orbital choosing suitable auxiliary ligands.[126–128]

In recent years, an increasing number of studies have focused on light-induced self-healing materials. Accordingly, the investigation of the electronic structures of both the ground and excited states, particularly in self-healing materials based on pincer-metal complexes, will play a fundamental role in the understanding of the processes involved and in the development of new materials. Thus, modifications of the electronic structures by computationally guided molecular design may give rise to new materials with unprecedented properties.

1.6 Motivation and goals of the thesis

Although the correlation between bond dynamics and macroscopic properties is not straightforward, a detailed characterization and rational design of these bonds may provide very valuable information for the design of new, improved self-healing materials.

It is clear that the design of a novel dynamic bond or interaction combined with reasonable mechanical properties is crucial in the development of self-healing materials, in which computational chemistry becomes a powerful tool, since it may assist in understanding the experimental results and suggesting promising candidates. Consequently, this thesis is devoted to the theoretical characterization of dynamic bonds based on new frustrated Lewis pairs and pincer ligands that may be easily incorporated in polymeric materials to provide with new improved features. The detailed knowledge of the electronic structure and interactions will allow the development of new dynamic bonds that will help in the advancement of such materials.

To achieve this, the following general and specific goals are presented:

1. Detailed characterization of the dynamic interactions of cross-linkers in polymeric chains that may be represented as complexes with a general structure as depicted in Figure 1.6, to find out general trends that may assist the development of new self-healing materials. In order to accomplish this goal, the following investigations have been performed:

    (a) Computational study of the interaction between different frustrated Lewis pairs and the diethyl azodicarboxylate (DEAD) molecule. The results are presented in Chapter 3.

    (b) Computational study of the interaction between different pincer ligands and transition metal atoms. The results are presented in Chapter 4.

2. Investigation of the photophysical features of metallopolymer-based self-healing materials to understand the luminescent properties of these systems and their influence in the healing process. In order to accomplish this goal, the following investigations have been performed:

    (a) Computational study of the light absorption properties in selected metal-pincer ligand complexes. The results are presented in Chapter 5.

    (b) Computational study of the light emission properties in selected metal-pincer ligand complexes. The results are presented in Chapter 5.
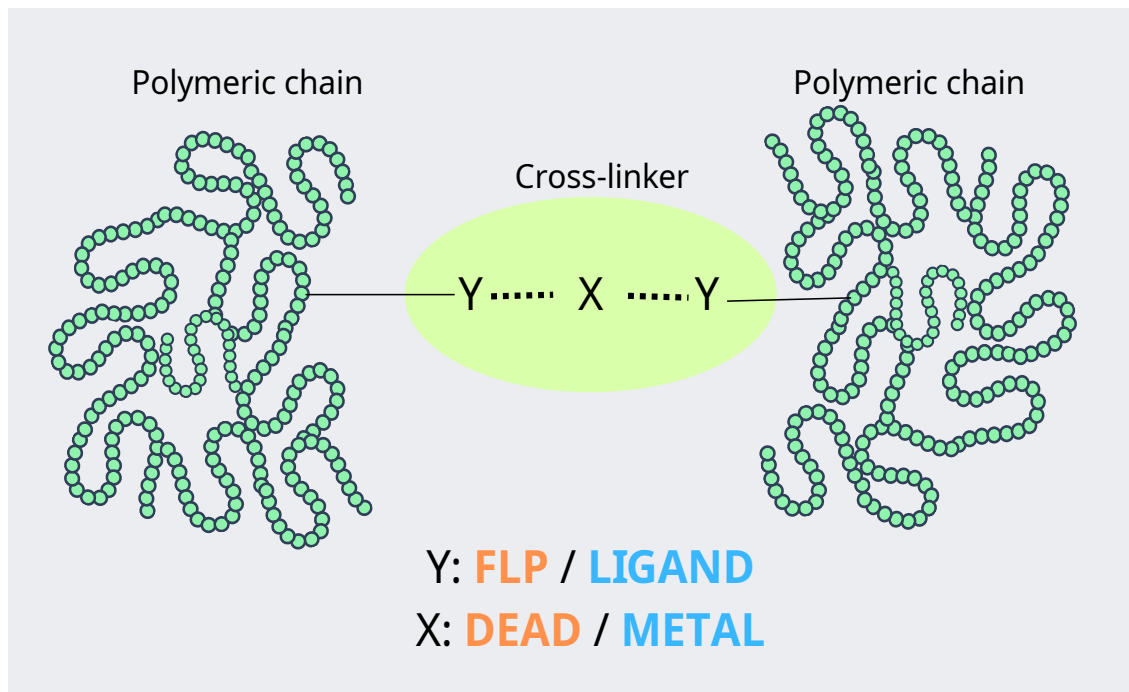
Figure 1.6: Schematic description of the systems studied in this thesis work. The cross-linker is represented as a Y-X-Y cluster, in which Y letter corresponds to either FLP or ligand compounds, whereas X letter corresponds to either DEAD molecule or a transition metal.

The work has been organized in the following manner: in Chapter 1 an introduction of the thesis is provided, in Chapter 2 the methods of Quantum Chemistry used are described. Then, in Chapters 3, 4 and 5, the results of this thesis are presented and discussed. Finally, the main conclusions are summarized in Chapter 6.

Chapter 2

Computational Methods

In this chapter, the background of the methodology used is explained to put the reader in context. In order to provide a good comprehension of the methodology and its background, the section is divided in different parts with the corresponding subsections.

2.1 Introduction to Quantum Chemistry

Along the 20th century, the development of quantum theory changed the view of scientists about the microscopic world.[129–132] Before its development, the proposed theories to explain the structure and stability of an atom failed utterly until Bohr's theory emerged in an attempt to explain the structure of the simplest atom known, hydrogen. In their model, Bohr and Sommerfeld proposed that electrons were fixed around the nucleus in stationary orbits and defined energy. According to the Planck's theory of radiation, it is known that electrons can gain or loose energy hopping between allowed orbitals, absorbing or emitting radiation. This theory was extended to chemistry and the concept of quantum chemistry was conceived. Nowadays, quantum chemistry is an important tool in order to predict and calculate molecular properties and reactivity.[133–137]

In the background of quantum chemistry lies the Schrödinger equation, which is a differential equation in space and time, depending only on the mass and velocity of particles, and is defined as:

$$i\hbar\frac{\delta}{\delta t}\Psi(r, R, t) = \hat{H}\Psi(r, R, t) \qquad (2.1)$$

For a stationary system, the time-independent Schrödinger equation reads:

$$\hat{H}(r, R)\Psi(r, R) = E\Psi(r, R) \qquad (2.2)$$

where the Hamiltonian operator, $\hat{H}$, corresponds to the system's total energy, Ψ is the wavefunction, which depends on the position of nuclei and electrons, and contains all

the measurable information about the system and, finally, *E* is the energy related to the wavefunction.

For systems with *N* electrons and *M* nuclei, the non-relativistic Hamiltonian involves the kinetic energy of nuclei ($\hat{T}_N$) and electrons ($\hat{T}_e$), the electron-nucleus attraction ($\hat{V}_{eN}$), the electron-electron repulsion ($\hat{V}_{ee}$) and nuclei-nuclei repulsion ($\hat{V}_{NN}$):

$$\hat{H}(r,R) = \hat{T}_e(r) + \hat{V}_{eN}(r,R) + \hat{T}_N(R) + \hat{V}_{NN}(R) + \hat{V}_{ee}(r) \tag{2.3}$$

where, in atomic units:

$$\hat{T}_e(r) = \sum_{i=1}^{N} -\frac{\nabla_i^2}{2} \tag{2.4}$$

$$\hat{V}_{eN}(r,R) = \sum_{i=1}^{N}\sum_{A=1}^{M} -\frac{Z_A}{|\vec{r}_i - \vec{R}_A|} \tag{2.5}$$

$$\hat{T}_N(R) = \sum_{A=1}^{M} -\frac{\nabla_A^2}{2m_A} \tag{2.6}$$

$$\hat{V}_{NN}(R) = \sum_{A>B}^{M} \frac{Z_A Z_B}{|\vec{R}_A - \vec{R}_B|} \tag{2.7}$$

$$\hat{V}_{ee}(r) = \sum_{i>j}^{N} \frac{1}{|\vec{r}_i - \vec{r}_j|} \tag{2.8}$$

$$\tag{2.9}$$

and, hence, $\hat{H}$(r,R) is expressed as:

$$\hat{H}(r,R) = \sum_{i=1}^{N}\left[-\frac{\nabla_i^2}{2} + \sum_{A=1}^{M} -\frac{Z_A}{|\vec{r}_i - \vec{R}_A|}\right] + \sum_{i>j}^{N}\frac{1}{|\vec{r}_i - \vec{r}_j|} + \sum_{A=1}^{M} -\frac{\nabla_A^2}{2m_A} + \sum_{A>B}^{M}\frac{Z_A Z_B}{|\vec{R}_A - \vec{R}_B|} \tag{2.10}$$

Equation 2.10 can only be exactly solved for one-electron systems such as the hydrogen atom, due to the presence of the electron-electron interaction term ($|\vec{r}_i - \vec{r}_j|$) and, therefore, approximations must be done to solve it for more complex systems.

The most significant approximation is that proposed by Max Born and Julius Robert Oppenheimer, the so-called adiabatic Born-Oppenheimer approximation (BO hereafter),[138] which consists in assuming that nuclei are heavier than electrons and, therefore, the motion of the electrons is several orders of magnitude faster than the motion of nuclei. In consequence, nuclei can be considered as stationary objects while electrons are assumed

to respond instantaneously to changes in the nuclear configuration, hence, the nuclei can be considered to move in the mean field generated by the electrons.

In this way, the nuclear and electronic parts of the Schrödinger equation can be treated separately and the molecular equation is divided into the electronic and the nuclear Schrödinger equations. In the case of the electronic equation, the nuclear kinetic energy term ($\hat{T}_N$) is ignored, the nuclear repulsion term ($\hat{V}_{NN}$) remains constant and the interaction between electrons and nuclei ($\hat{V}_{eN}$) depends on the coordinates of the fixed nuclei. Thus, the electronic Schrödinger equation is expressed as:

$$\hat{H}_e(r_i; R_\alpha)\Psi_e(r_i; R_\alpha) = (\hat{T}_e + \hat{V}_{ee} + \hat{V}_{eN} + \hat{V}_{NN})\Psi_e = E_e\Psi_e \tag{2.11}$$

The obtained wavefunction, ψ_e, depends parametrically on the nuclear coordinates:

$$\hat{H}_e(r_i; R_\alpha)\Psi_e(r_i; R_\alpha) = E_e(R_\alpha)\Psi_e(r_i; R_\alpha) \tag{2.12}$$

Once the electronic Schrödinger equation is solved, the nuclear equation may then be figured out, where the electronic energy and the internuclear repulsion determine the potential energy surface (PES) that defines nuclear motion. The nuclear equation is expressed as follows:

$$\hat{H}_N(R_\alpha)\Psi_N(R_\alpha) = (\hat{T}_N + E_e + \hat{V}_{NN})\Psi_N(R_\alpha) = E_{TOT}(R_\alpha) \tag{2.13}$$

PES describes equilibrium and transition state (TS) geometries and, then, chemical reactivity and roto-vibrational levels are calculated from the nuclear equation.

The BO approximation reduces the original molecular quantum mechanical problem to a system of electrons interacting under the influence of an external potential induced by the nuclei. Unfortunately, due to the two-particle interaction terms in the electron-electron potential contribution, the electronic Schrödinger equation can only be cast into a closed analytical form for one-electron systems. Therefore, in addition to the BO approximation, more approximations are needed to solve the electronic Schrödinger equation. These approximations gave rise to quantum chemistry and quantum chemical models vary depending on the nature of the approximation. So that, multiple mathematical methods have been developed to find the electronic wave function for any given atomic arrangement. The most emblematic approximation is the so-called Hartree-Fock method (HF),[139,140] for the approximation of the wavefunction of a many-electron system in a stationary state.

In the Hartree-Fock method, the N-body wavefunction of the system is approximated by a single Slater determinant, which is an antisymmetrized determinantal product (in order to fulfill Pauli's principle) of one-electron orbitals depending on the 3N coordinates of the electrons. Taking advantage of the variational principle, a set of N-coupled

equations can be derived and a solution of these equations generates the Hartree-Fock wavefunction and yields the lowest energy of the system.

The Hartree-Fock method provides with rather good equilibrium geometries and conformations, except for systems with transition metals. The main drawback is the incomplete representation of the electron correlation, which is the way in which the motion of one electron influences the motion of the remaining electrons. In order to provide a solution to this incompleteness, different quantum chemical methods were developed. The most significant ones are the configuration interaction (CI),[141] Møller-Plesset perturbation theory (MPn, being n the order of the perturbation)[142] and coupled-cluster approximations (CC),[143] which are extensions of the Hartree-Fock method by mixing ground-state and excited-state wavefunctions, using several Slater determinants.

Another important method to include the electron correlation is the so-called Density Functional Theory (DFT), which is not completely *ab initio* but it is nearly connected with the HF method. This DFT method was chosen to compute all the calculations of this thesis, therefore, in the next section its fundamentals are explained.

2.2 Density Functional Theory

2.2.1 Time-Independent Density Functional Theory

As mentioned before, wavefunction-based methods emerged to give approximated solutions to the electronic Schrödinger equation. However, the complexity of the electronic wavefunction increases with the size of the atomic or molecular system, since it is a 3N-dimensional object. Density Functional Theory arises in order to face this problem and substitutes the concept of the N-electron wavefunction by the electron density $\rho(\vec{r})$, which is a simpler function of the three spatial variables.[144,145]

Hohenberg and Kohn proved that the electronic properties of a system with a non-degenerate ground state are determined by the electron density $\rho(\vec{r})$.[146] In this sense, the ground state energy (E_0) is a functional of $\rho(\vec{r})$, which is defined as the sum of the kinetic energy (T), electron-electron repulsion (E_{ee}) and attraction between electrons and nuclei (E_{eN}):

$$E_0[\rho] = T[\rho] + E_{ee}[\rho] + E_{eN}[\rho] \tag{2.14}$$

As $T[\rho]$ and $E_{ee}[\rho]$ are unknown, they are usually collected in the Hohenberg-Kohn functional (Equation 2.15). In addition, they proposed a variational principle for the energy functional, that is, knowing the exact form of $E[\rho]$ functional, the ground state density can be determined.

$$F_{HK}[\rho] = T[\rho] + E_{ee}[\rho] \tag{2.15}$$

However, the exact form of $E_{ee}[\rho]$ functional is not known. Due to this, Kohn and Sham designed an approximation to define the electronic density in the ground state with a non-interacting system.[147] They demonstrated that the exact electronic energy of a ground state (E_0) for an N-electron system with a ground-state electron density (ρ) is the following:

$$E_0 = -\frac{1}{2}\sum_{i=1}^{N} <\psi_i(1)|\nabla_1^2|\psi_i(1)> + \int v(r)\rho(1)d\vec{r}_1 + \frac{1}{2}\int\int \frac{\rho(1)\rho(2)}{r_{12}}d\vec{r}_1 d\vec{r}_2 + E_{xc}[\rho]$$

(2.16)

where $v(r) = -\Sigma_\alpha \frac{Z_\alpha}{r_{1\alpha}}$ is the external potential of the nuclei, ψ_i are the Kohn-Sham orbitals and $E_{xc}[\rho]$ is the exchange-correlation energy. In the Kohn-Sham procedure, the exact ground state ρ can be calculated from the Kohn-Sham orbitals as stated in Equation 2.17:

$$\rho = \sum_{i=1}^{N} |\psi_i|^2$$

(2.17)

and these orbitals can be calculated solving the one-electron equations:

$$\hat{F}_{KS}(1)\psi_i(1) = \varepsilon_i\psi_i(1)$$

(2.18)

where the Kohn-Sham operator, $\hat{F}_{KS}$, is defined as:

$$\hat{F}_{KS} = -\frac{1}{2}\nabla_1^2 + v(1) + \sum_{j=1}^{n}\hat{J}_j(1) + V_{xc}(1)$$

(2.19)

being $\hat{J}$ the Coulomb operator and V_{xc} the exchange-correlation potential:

$$V_{xc} = \frac{\delta E_{xc}[\rho]}{\delta\rho}$$

(2.20)

Hence, $\hat{F}_{KS}$ works as the Fock operator in Hartree-Fock equations, where the exchange operator has been replaced by V_{xc}. The solutions for these equations are obtained in an iterative way, building $\hat{F}_{KS}$ from a guess density and the equations are solved iteratively until convergence is achieved.

The physical significance of Kohn-Sham orbitals is undefined. In addition, Kohn-Sham orbital energies must not be mistaken with molecular orbital energies. Nevertheless, some authors relate these orbitals with the physical significance of Hartree-Fock canonical orbitals, due to the fact that the exact Kohn-Sham orbital energy for the HOMO is the negative ionization potential, and that the Kohn-Sham equations are analogous to the Hartree-Fock equations. On the other hand, there are some results which show that the results obtained from molecular orbitals using DFT are similar to the ones obtained from standard MO-LCAO methods.[148–150]

Nevertheless, except the case of a uniform electron gas, the exact forms of E_{xc} and V_{xc} are not known. In order to solve this problem, further approaches are needed, the so-called Density Functional Approximations (DFA). The first approximation applied is the

one named as Local Density Approximation (LDA), where each volume element with local density $\rho(\vec{r})$ is considered as a homogeneous electron gas.[151] The main problem of this approach is that the variation of the density in space is not smooth. In order to take into account the non-homogeneous character of the electron density, the Generalized Gradient Approximation (GGA) appears, including the gradient of the density $(\nabla \rho(r))$.[152–154] The exchange-correlation functionals obtained from this approximation are accurate enough for most chemical applications. Still, better solutions may be obtained using the so-called meta-GGA functionals, where the Laplacian of the density $(\nabla^2 \rho(r))$ is involved. Also, a fraction of Hartree-Fock exchange can be included in the functionals, generating hybrid functionals, which are a combination of DFT correlation and Hartree-Fock exchange. These hybrid functionals can be divided into local functionals, where the amount of Hartree-Fock exchange depends on local properties of each particular system, and range-separated functionals, where the Coulomb operator is split into a long-range and a short-range part, and are particularly useful for systems with weak interactions.[155]

2.2.2   Time-Dependent Density Functional Theory

The time-dependent generalization of the density functional theory formalism, TDDFT,[156] offers a rigorous procedure to calculate the dynamic response of the charge density, which combined with linear response theory allows to compute vertical electronic spectra of molecules.[157–161] TDDFT has been applied to very different systems, for example, for metal-containing organic[162–164] or inorganic[165,166] compounds, as well as for extended systems, becoming a very powerful tool to calculate excitation energies.[157–167]

A stationary action principle may be derived, analogous to the minimum energy principle of Hohenberg-Kohn theory, and this can be used, together with appropriate assumptions concerning v-representability, to derive the time-dependent Kohn-Sham equation:

$$[-\frac{1}{2}\nabla^2 + v(r,t) + \int \frac{\rho(r't)}{|r-r'|}dr' + v_{xc}^{\sigma}(r,t)]\psi_{j,\sigma}(r,t) = i\frac{\delta}{\delta t}\psi_{j,\sigma}(r,t) \qquad (2.21)$$

where v_{xc}^{σ}(r,t) is formally the functional derivative of the exchange-correlation action, A_{xc}, in analogy of the Kohn-Sham exchange-correlation term in time-independent DFT, E_{xc}:

$$v_{xc}^{\sigma}(r,t) = \frac{\delta A_{xc}[\rho_{\sigma}]}{\delta \rho_{\sigma}(r,t)} \approx \frac{\delta E_{xc}[\rho_{\sigma}^t]}{\delta \rho_{\sigma}^t(r)} \qquad (2.22)$$

where $\rho_{\sigma}^t(r)$ is the $\rho_{\sigma}(r,t)$ function evaluated at a fixed time. Since the dynamic polarizability, $\alpha(\omega)$, describes the response of the dipole moment to a time-dependent electric field, it may be calculated from the response of the charge density obtained from time-dependent density functional theory, that is, using time-dependent density functional response theory. This allows the determination of the electronic excitation spectrum in the usual dipole approximation because, according to the sum-over-states relation,

$$\bar{\alpha}(\omega) = \sum_l \frac{f_l}{\omega_l^2 - \omega^2} \qquad (2.23)$$

the poles of the dynamic polarizability determine the excitation energies, ω_l, while the residues, f_l, determine the corresponding oscillator strengths.[157] The transition energies may be obtained by solving a matrix eigenvalue problem:

$$\Omega F_l = \omega_l^2 F_l \tag{2.24}$$

where Ω is defined in Ref. 157 and Ref. 158 and the oscillator strengths, f_l, are obtained from eigenvectors F_l. For more information see Ref. 168 and Ref. 169.

2.3   Basis Sets

As mentioned previously, it is possible to solve the Schrödinger equation exactly only for hydrogen-like cases such as H, He^+ or Li^{2+}. The obtained hydrogen-like wavefunctions are formed by a spherical harmonic angular part ($Y_{l,m}$) and a radial part ($R_{n,l}$):

$$\phi = Y_{l,m} R_{n,l} \tag{2.25}$$

being the radial part of Slater type. The Slater Type Functions (STF) have the following form:

$$\phi^{STF} = Ar^l e^{-\alpha(r-R)} \tag{2.26}$$

where A is the normalization constant, r the electron position, l an integer, α a nucleus charge-dependent constant and R the position of the nucleus. These functions are also denoted as Slater Type Orbitals (STO), since their form is similar to that of the hydrogen-like orbitals. Nevertheless, the three- and four-center two-electron integrals involving STOs cannot be evaluated analytically. In order to avoid this problem, Gaussian Type Orbitals (GTO) are employed:

$$\phi^{GTO} = Ar^l e^{-\alpha(r-R)^2} \tag{2.27}$$

Due to the square dependence in the exponential part, GTOs present problems to properly describe the behavior near the nucleus, due to a too rapidly decay. Therefore, more GTOs are needed to obtain the accuracy of a STO and the current basis sets consist of contractions of GTOs mimicking STOs. Yet, it is easier to manipulate mathematically several GTOs than one STO.

$$\phi_\mu^{CGO} = \sum_{i=1}^{L} c_{i\mu} \phi_i^{GTO} \approx \phi_\mu^{STO} \tag{2.28}$$

A minimal basis set containing one basis function for each occupied atomic orbital is defined as a basis set of single-ζ quality. In order to improve this minimal description of the orbitals, the basis set can be split and all basis functions doubled. Therefore, the basis set would have a double-ζ quality. Likewise, further splittings involves triple-ζ and quadruple-ζ types. In order to further improve the basis set, polarization functions can be added, which consist on higher angular momentum functions and are essential to describe electron correlation. Also, diffuse functions are needed for a better description of the charge distribution.

2.4   Analysis of the Lewis acidity and basicity

In this section, the different methodologies used to analyze the Lewis acidity and basicity are explained.

2.4.1   Hydride and proton affinity

The first criterion to analyze the Lewis acidity is the hydride affinity (HA), which is defined as the energy released when the molecule reacts with a hydride anion (H^-) in the gas phase, as follows:

$$A + H^- \rightarrow AH^- \qquad HA = \Delta H \tag{2.29}$$
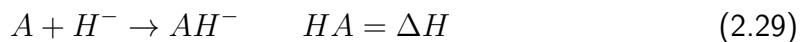
Hence, the hydride affinity of an ion or a neutral compound is the enthalpy change in the reaction between an acid and a hydride atom in gas phase.

In the same way, the Lewis basicity is calculated by the proton affinity (PA), which is defined as the negative of the enthalpy change of the following reaction:

$$B + H^+ \rightarrow BH^+ \qquad PA = -\Delta H \tag{2.30}$$
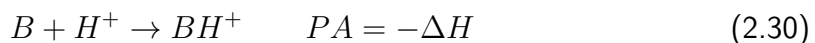
taking into account the correction for the thermal energy of a proton (H^+) as: $\frac{5}{2}RT$

2.4.2   Electrodonating and electroaccepting power

Parr et al. have defined the electrophilicity as the stabilization energy of a chemical species when it acquires an additional fraction of electronic charge from the environment.[170] The global electrophilicity index (ω) is defined as:

$$\omega = \frac{\mu^2}{2\eta} \tag{2.31}$$

where μ is the chemical potential and η the chemical hardness, which can be calculated using the vertical ionization energy (I) and the electron affinity (A). Gázquez and coworkers have defined the electrodonating (ω^-) and electroaccepting (ω^+) power as:[171,172]

$$\omega^- = \frac{(\mu^-)^2}{2\eta^-} = \frac{I^2}{2(I - A)} \tag{2.32}$$

$$\omega^+ = \frac{(\mu^+)^2}{2\eta^+} = \frac{A^2}{2(I - A)} \tag{2.33}$$

Therefore, higher ω^+ values correspond to better electroaccepting power, while lower ω^- correspond to better electrodonating power. In order to use the general notion of *more is better*, Pratihar and Roy have defined the nucleophilicity as the inverse of electrodonating power:[172,173]

$$N = \frac{10}{\omega^-} \tag{2.34}$$

These criteria allow to easily determine if a system is electrophilic (acid) or nucleophilic (base).

2.4.3 Gutmann-Beckett method

Another common technique to assess relative Lewis acidity employs spectroscopic techniques, such as infrared (IR) and nuclear magnetic resonance (NMR). The Gutmann-Beckett method[174] is a procedure to measure the Lewis acidity by making use of NMR. In particular, this method is based in the variation of the ^{31}P-NMR chemical shift ($\Delta\delta$) between free triethylphosphine oxide (Et_3PO) and the Et_3PO-LA adduct (see Fig. 2.1). The shift is caused by the interaction of the oxygen of Et_3PO with the Lewis acid causing a dishielding of the adjacent P atom. Thus, the larger is this shift, the greater is the Lewis acidity.
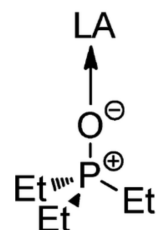
Figure 2.1: Interaction between Et_3PO and the Lewis acid (LA).

2.5 Analysis of bonding interactions

The following two methodologies have been used to analyze the nature of the intermolecular interactions: Natural Bond Orbital (NBO) and Energy Decomposition Analysis (EDA), which are summarized in the next subsections.

2.5.1   Natural Bond Orbital analysis (NBO)

The Natural Bond Orbital analysis[175,176] consists in a transformation of the wavefunction into localized natural atomic orbitals (NAO), hybrid orbitals (NHO), bonding orbitals (NBO) and localized molecular orbitals (NLMO) that form an orthonormal set related to the basis atomic orbitals.[177] Within the NBO analysis, the orbitals are classified as: i) core orbitals (occupancy $\geq$ 1.999), ii) lone-pair orbitals located in one atom (occupancy $\geq$ 1.900) and iii) bond orbitals, developed between two atoms (occupancy $\geq$ 1.900).

In this way, more intuitive Lewis-like structures are generated. Besides, corrections to these Lewis structures may be described as second order perturbations. The interaction of an occupied orbital (σ) of the normal Lewis structure with an antibonding orbital (σ^*) is defined as follows:

$$\Delta E_{\sigma\sigma^*}^2 = -2\frac{\langle\sigma|\,\hat{F}\,|\sigma^*\rangle^2}{\epsilon_{\sigma^*} - \epsilon_\sigma} \tag{2.35}$$

where $\hat{F}$ is the Fock operator and ϵ_{σ^*} and ϵ_σ are the NBO orbital energies. The non-covalent interaction is related with the $\sigma \to \sigma^*$ interaction, therefore, occupied orbitals are called donors (Lewis base) and empty orbitals acceptors (Lewis acids). For further information about NBO and its applications, see the review article by Reed, Curtiss and Weinhold.[175]

2.5.2   Energy Decomposition Analysis (EDA)

The energy decomposition analysis is a powerful method for the qualitative and quantitative analysis of the chemical bond.[178] It is considered as a bridge between the heuristic bonding models and the numerical results of accurate quantum chemical calculations. This analysis, based on the energy partition of Morokuma,[179] consists in partitioning the instantaneous interaction energy (ΔE_{int}) between two fragments A and B in a molecule (A-B) in the following three terms:

$$\Delta E_{int} = \Delta E_{elstat} + \Delta E_{Pauli} + \Delta E_{orb} \tag{2.36}$$

where ΔE_{elstat} is the quasi-classical electrostatic interaction, ΔE_{Pauli} is the repulsive exchange (Pauli) interaction between electrons of two fragments having the same spin and ΔE_{orb} is the orbital (covalent) interaction, which comes from the orbital relaxation and the orbital mixing between the fragments. This term can be further decomposed into contributions depending on the symmetry of the system.

The interaction energy, ΔE_{int}, is defined as the difference between the energy of the molecule and the energies of the fragments:

$$\Delta E_{int} = E_{AB} - E_A - E_B \tag{2.37}$$

In order to get the three contributions of the interaction energy (Equation 2.36), three steps corresponding to the bond formation process must be followed. In the first step, the

A and B fragments are brought from infinite separation to the position in the molecule. These fragments have frozen charge densities and the interaction between them at the equilibrium geometry of AB gives the quasi-classical Coulomb interaction, ΔE_{estat}. The product wavefunction $(\psi_A\psi_B)$ is normalized but violates the Pauli exclusion principle. Thus, in the second step, this product wavefunction is antisymmetrized and renormalized to provide an intermediate state ψ^0 and the corresponding energy E^0. Therefore, the energy difference between E^0_{AB} and E^0 gives the exchange Pauli repulsion term ΔE_{Pauli}. The third and last step is to relax the previously obtained intermediate state (ψ^0) to define a final state (ψ_{AB}) of the molecule A-B with E_{AB} energy. The energy lowering of this step is related to the mixing of orbitals and is regarded as the covalent contribution to the chemical bond formation ΔE_{orb}. This last term is always attractive, ΔE_{Pauli} is always repulsive and ΔE_{estat} is usually attractive.[180]

The numerical result obtained in this analysis depends on the DFT functional employed. It must be taken into account that, if an explicit correction term for dispersion interaction is used as it is suggested in some articles,[181,182] the EDA results remain unchanged and the dispersion correction appears as an extra term, but if the dispersion correction is part of the DFT functional, the EDA results will be changed.

2.5.3 Quantum Theory of Atoms in Molecules (QTAIM)

Another method to obtain information about the bond is the Quantum Theory of Atoms in Molecules (QTAIM) method, which is a tool to extract chemical information from the electron density $(\rho(\vec{r}))$.

Analyzing the gradient of electron density $(\nabla\rho(\vec{r}))$, it is possible to define an atom within a molecule through the zero flux surface condition. Furthermore, critical points $(\nabla\rho(\vec{r_c}) = 0)$ analysis provides a way to define the molecular structure. QTAIM identifies critical points based on the sign of the Laplacian of the electron density (the second derivative, $\nabla^2\rho(\vec{r_c})$), allowing for differentiation between various critical points. The bond critical point (BCP) between two atoms is situated where the electron density has its minimum value along the path linking these two atoms. The electron density and Laplacian at the BCP $(\rho(\vec{r_{cBCP}})$ and $\nabla^2\rho(\vec{r_{cBCP}}))$ can be used to determine the nature of the corresponding bond using the following equations:

$$H(\vec{r}) = G(\vec{r}) + V(\vec{r}) \tag{2.38}$$

$$\frac{1}{4}\nabla^2\rho(\vec{r}) = 2G(\vec{r}) + V(\vec{r}) \tag{2.39}$$

where $G(\vec{r})$ is the kinetic energy density, $V(\vec{r})$ stands for the potential energy density and, hence, $H(\vec{r})$ refers to the total electron energy density, all of them at the BCP.

Combining equations 2.38 and 2.39, the following is obtained:

$$H(\vec{r}) = \frac{1}{4}\nabla^2 \rho(\vec{r}) - G(\vec{r}) \tag{2.40}$$

Since $G(\vec{r})$ is always positive and $V(\vec{r})$ is always negative, when $|V(\vec{r})| > 2G(\vec{r})$, the Laplacian is negative, $\nabla^2\rho(\vec{r}) > 0$, meaning the interaction is covalent. In addition, if $|V(\vec{r})| > G(\vec{r})$, the Laplacian is positive ($\nabla^2\rho(\vec{r}) > 0$) but the total energy density is negative ($H(\vec{r}) < 0$), which denotes a partially covalent interaction. Moreover, if $|V(\vec{r})| < G(\vec{r})$, both the Laplacian and the total energy density are positive ($\nabla^2\rho(\vec{r})$ and $H(\vec{r}) > 0$), indicating a non-covalent interaction.[183–186] Lastly, if $\rho(\vec{r})$ is large enough (more than 0.03) and $H(\vec{r}) < 0$, the interaction is partially covalent.

Chapter 3

Theoretical characterization of new frustrated Lewis pairs for responsive materials

In this chapter, a computational study of the interaction between a set of frustrated Lewis pairs with the small molecule (diethyl azodicarboxylate, DEAD) is performed. Concretely, Lewis acids and bases based on triphenylborane (TPB) and triphenylphosphine (TPP) derivatives, including both electron donating (EDG) and electron withdrawing (EWG) substituents in *ortho* and *para* positions of the phenyl rings have been considered. Hence, the main goal of this work is to achieve a better comprehension of the interactions between the mentioned species and unveil the relevant parameters to design and suggest new improved candidates for self-healing materials.

3.1   Introduction

In the last years, responsive materials including dynamic bonds have been widely acclaimed due to their expectation to pilot advanced materials. Within these materials, synthetic polymers have shown to be good candidates. Recently, the frustrated Lewis pairs (FLP) have been used to create responsive materials. Concretely, the activation of diethyl azodicarboxylate (DEAD, see Figure 3.1, top-right panel) by a triphenylborane (TPB) and triphenylphosphine (TPP) based FLP has been recently exploited for the production of dynamic cross-links.[67,72] In this chapter, we explore computationally the underlying dynamic chemistry in these materials, in order to understand the nature and reversibility of the interaction between FLPs and DEAD. With this goal in mind, we first characterize the acidity and basicity of several TPB and TPP derivatives using different substituents, such as electron donating and electron withdrawing groups. Our results show that strong electron donating groups increase the acidity of TPB, while decrease the basicity of TPP. However, the FLP-DEAD interaction is not dominated by the in-

fluence of these substituents in the acidity or basicity of TPB or TPP, but by attractive
or repulsive forces between substituents such as hydrogen bonds or steric effects. Based
on these results, a new FLP-DEAD complex is proposed as a candidate for an improved
self-healing polymer.
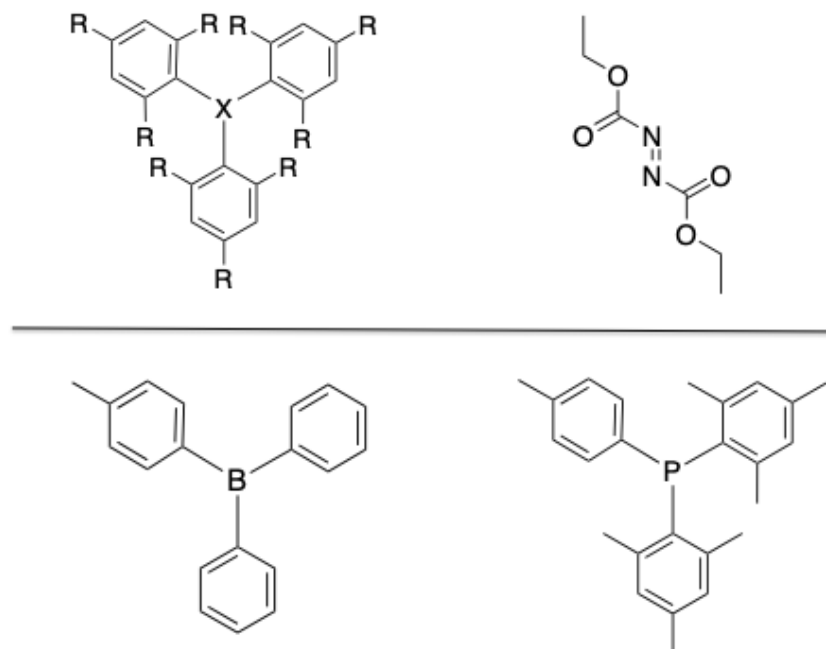
Figure 3.1: Top: Molecular models of the Lewis acids ($X = B$) and bases ($X = P$) sub-
stituted by electron-donating ($R = CH_3$, NH_2, OH, OCH_3 and $OCOCH_3$) and electron-
withdrawing ($R = F$, CF_3, CN, NO_2 and SO_3H) functional groups (left), and the linker
molecule, DEAD (right). Bottom: Reference Lewis acid and base from the experimental
work.[67]

3.2   Computational details

All geometry optimizations and vibrational frequency calculations were carried out within
Density Functional Theory (DFT)[146,147] using the Gaussian 16 program package.[187]
Concretely, geometries were optimized in gas phase using the TPSS exchange-correlation
functional,[188] combined with the def2-TZVP basis set.[189,190] Dispersion interactions were
considered using the empirical D3 version of Grimme's dispersion with Becke-Johnson
damping.[191] This level of theory was proposed by Schrimer and Grimme as the most
appropriate for weak acid-base interactions, such as those existing in frustrated Lewis
pairs.[192] After geometry optimizations, harmonic vibrational frequencies were obtained
by analytical differentiation of gradients, at the same level of theory, to identify if the
characterized structures were true minima. Such frequencies were then used to evaluate
the zero-point vibrational energy (ZPVE) and the thermal ($T = 298$ K) vibrational

corrections to the enthalpy. The interaction energies include the correction of the basis set superposition error (BSSE) by means of the Counterpoise method.[193,194]

Finally, the nature of the interaction has been analyzed using the Natural Bonding Orbital (NBO)[175,195,196] and the Energy Decomposition Analysis (EDA)[197,198] methodologies. The EDA calculations have been performed using the BP86 functional[199,200] with a triple-ζ quality basis set (ADF basis set TZP), using the program package ADF2017.[201]

3.3 Results and discussion

First of all, in subsection 3.3.1, the acidity and basicity of the TPB and TPP derivatives will be evaluated using different parameters. Afterwards, in subsection 3.3.2, the interaction energies between these species and the DEAD linker molecule will be computed and analyzed.

3.3.1 Acidity of TPB derivatives and basicity of TPP derivatives

In order to evaluate the acidity of the TPB and the basicity of the TPP derivatives, several parameters have been considered. Concretely, four parameters have been used to calculate the acidity, namely, hydride affinity (HA), electroaccepting power (ω^+), variation of the ^{31}P-NMR chemical shift ($\Delta\delta$) and the boron empty orbital energy (ε_B). Similarly, the basicity of TPP derivatives have been calculated by means of three parameters: proton affinity (PA), electrodonating power (ω^-) and phosphorous lone-pair orbital energy (ε_P). The results are gathered in Table 3.1 and depicted in Figure 3.2.

First of all, the hydride affinity of TPB derivatives and proton affinity of TPP derivatives will be analyzed, as a function of the substituents. As it has been explained in the Computational Methods section, hydride affinity is defined as the enthalpy change (ΔH) in the reaction between an acid (A) and a hydride anion (H$^-$) in gas phase. Similarly, proton affinity is defined as the negative of enthalpy change (PA = -ΔH) in the reaction of a base (B) with a proton (see Equations 2.29 and 2.30). The numerical results are represented in Figure 3.2a.

Regarding the hydride affinity, it can be observed that EDG-containing molecules show lower values than those with EWG substituents, while the reference molecule from the experimental work (see Fig. 3.1) shows an intermediate behavior. Since higher values of HA correspond to stronger acids, it can be concluded that EWG groups increase the acidity, while EDGs reduce it. Thus, the strongest acid is the CN-substituted TPB (HA = -150.90 kcal/mol). For R = SO$_3$H, the most stable structure presents an intramolecular interaction between the empty orbital of boron with an oxygen of one of the SO$_3$ groups, losing its acidic nature. It is remarkable the acidity of the TPB including acetoxy groups (OCOCH$_3$), HA = -126.32 kcal/mol, in the same range of several EWG groups and

Table 3.1: Acidity of triphenylborane (TPB) and basicity of triphenylphosphine (TPP)
substituted with electron donating (EDG) and electron withdrawing (EWG) groups (R).
Acidity is estimated by hydride affinity (HA), in kcal/mol, electroaccepting power (ω^+),
in eV, variation of the ^{31}P-NMR chemical shift ($\Delta\delta$), in ppm, and boron empty or-
bital energy (ε_B), in a.u. Basicity is estimated by proton affinity (PA), in kcal/mol,
electrodonating power (ω^-), in eV, and phosphorus lone-pair orbital energy (ε_P), in a.u.

R		TPB acidity				TPP basicity		
		HA	ω^+	$\Delta\delta$	ε_B	PA	ω^-	ε_P
EDG	H	-90.48	0.049	35.28	-0.0948	240.27	3.293	-0.1925
	CH_3	-87.42	0.056	16.04	-0.0885	253.88	2.957	-0.1690
	NH_2	-77.66	0.007	20.15	-0.0610	274.43	3.792	-0.1435
	OH	-74.67	0.002	16.39	-0.0602	267.92	2.555	-0.1504
	OCH_3	-73.89	0.003	25.35	-0.0547	274.94	2.944	-0.1421
	$OCOCH_3$	-126.32	0.321	43.85	-0.1385	232.98	2.847	-0.2160
EWG	F	-109.56	0.130	32.10	-0.1195	228.16	3.360	-0.2130
	5F[a]	-125.43	0.248	36.34	-0.1452	212.87	3.364	-0.2363
	CF_3	-127.89	0.337	44.21	-0.1595	218.54	2.992	-0.2321
	CN	-150.90	0.542	47.56	-0.1935	199.95	3.126	-0.2636
	NO_2	-138.57	—	—	-0.1229	202.58	—	-0.2562
	SO_3H	—	—	—	—	212.11	2.810	-0.2517
Reference		-89.45	0.034	35.13	-0.0913	252.13	3.132	-0.1736

[a]5F stands for fluorine substitution in all carbons of the aromatic ring.

even larger than that of the fluorine-containing TPB. The balance between σ-donor and
π-acceptor character, as well as the coplanarity with the phenyl rings, makes $OCOCH_3$
moiety a moderate EDG group, while fluorine can be considered both as a very weak
EWG or a weak EDG group when is in *para* position.

Contrary to hydride affinities, higher proton affinities are obtained for EDG sub-
stituents. Thus, the strongest Lewis bases correspond to TPP including amino (NH_2)
and methoxy (OCH_3) groups (PA = 274.43 and 274.94 kcal/mol, respectively). These
groups yielded the weakest TPB-based acids. The lowest value corresponds to CN group
(199.95 kcal/mol) and, therefore, is the weakest base. Hence, according to hydride
affinities of TPB and proton affinities of TPP, EWG lead to stronger acids and weaker
bases, while EDGs behave in the opposite way.
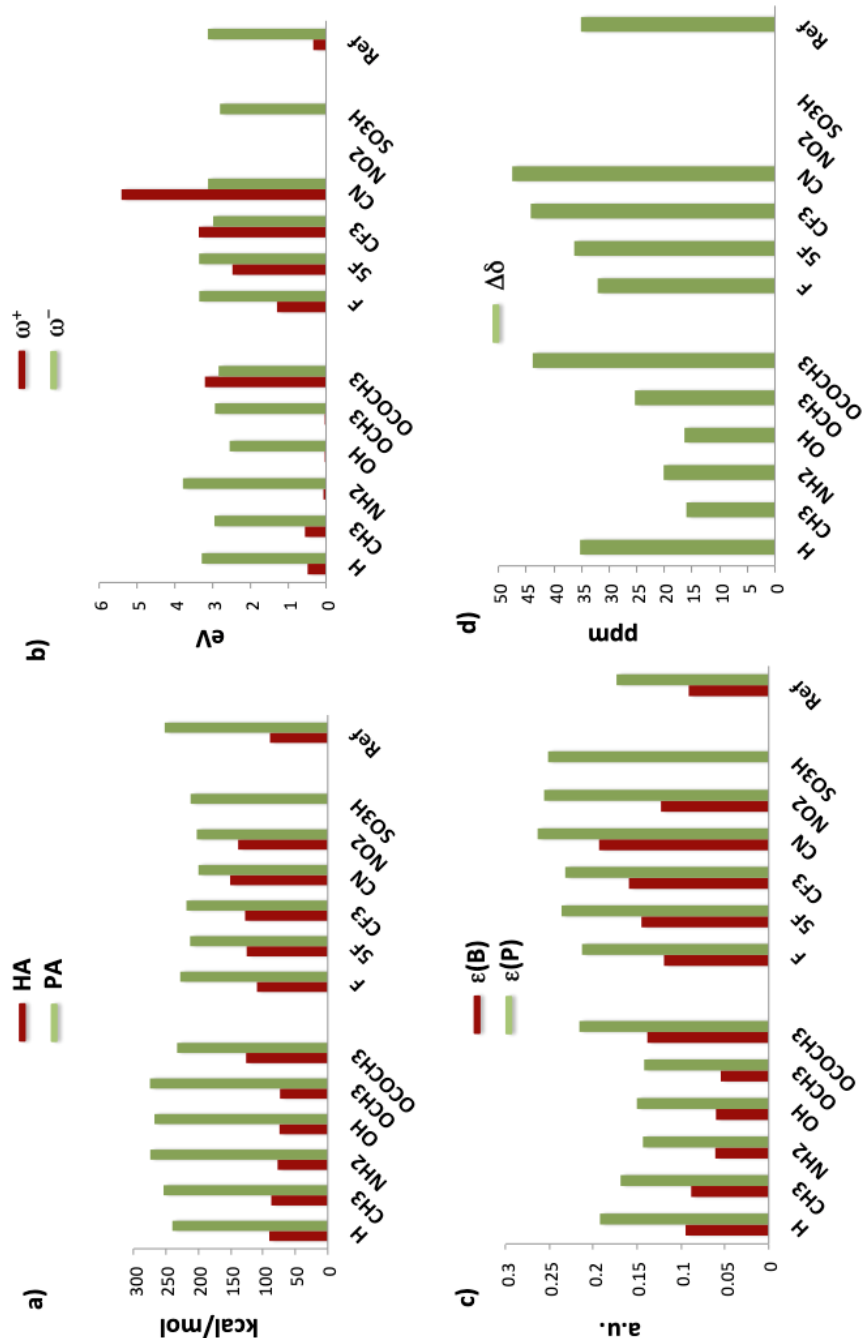
Figure 3.2: (a) Hydride affinity (HA, red bars, absolute values) and proton affinity (PA, green bars), in kcal/mol; (b) electroaccepting power ($\omega^+ \cdot 10$, red bars) and electrodonating power (ω^-, green bars), in eV; (c) boron empty orbital energy ($\varepsilon(B)$, red bars) and phosphorous lone-pair orbital energy ($\varepsilon(P)$, green bars), in a.u. (absolute values); (d) variation of the ^{31}P-NMR chemical shift ($\Delta\delta$), in ppm.

The acidity and basicity power may also be evaluated by means of the electroaccepting power (ω^+) and electrodonating power (ω^-), defined in Equations 2.32 and 2.33.[171,172] Larger ω^+ values correspond to better electroaccepting power, which can be related to stronger acidity. Similarly, lower values of ω^- correspond to stronger basicity. The calculated values are represented in Figure 3.2b. Focusing on the electroaccepting power of TPB derivatives, one may observe that EWG substituents provide larger values than EDG substituents, in agreement with the hydride affinity. In the case of the TPB including NO_2 groups, the calculation of the cation resulted in a molecule where one of the NO_2 oxygens is attached to boron. Again, the strongest acid is the molecule substituted with CN groups. Regarding electrodonating power of TPP derivatives, it is observed that EDG groups present, in general, lower values, in agreement with the previously calculated proton affinities. However, the NH_2-containing derivative shows a remarkably high value (3.792 eV), the largest value among all the calculated in this work, which is in disagreement with the trend observed in the proton affinity.

A third manner of considering the acidity and basicity power of different TPB and TPP derivatives is comparing their molecular orbital energies. Concretely, the acidity power may be related to the boron empty orbital energy that may accept electron density from a Lewis base. Lower energy values imply a more stable orbital and, therefore, better ability to accept electron density (stronger acidity). Besides, in TPP derivatives, the energy of the phosphorous lone-pair orbital (ε_P) may provide with an insight of the basicity of these species. In Figure 3.2c, it is observed that, for boron orbital energies, EWG substitutents yield to more negative values than EDG substitutents, following the same trend as the other parameters. Meanwhile, more positive phosphorus orbital energies values are observed for EDGs, which means that this orbital is more favorable to donate electron density and, therefore, these compounds are stronger electron donors (Lewis bases). One of the highest values corresponds to the amino group. Among the EWGs, the lowest value corresponds to cyanide, which would provide the weakest Lewis base, giving a similar picture as other previously considered parameters.

Finally, the acidity of TPB derivatives has also been calculated by means of the Gutmann-Beckett method,[174] which is based in the variation of the ^{31}P-NMR chemical shift ($\Delta\delta$) between free triethylphosphine oxide (Et_3PO) and the adduct formed with a Lewis acid. The variation is caused by the interaction of the oxygen, which behaves as a Lewis base, with the Lewis acid, inducing a deshielding of the phosphorous atom and shifting $\Delta\delta$ to larger values. Thus, the larger is the shift, the greater is the Lewis acidity. The calculated values of $\Delta\delta$ are represented in Figure 3.2d. As expected, the same trend as in HA and ω^+ is found, namely, EWG groups show larger variations of $\Delta\delta$ than the EDGs, and the largest shift is calculated for the CN-containing TBP. No stable Et_3PO-LA adduct was found for the NO_2 derivative.

Based on all these data, we may conclude that strong EDG groups would lead to stronger TPP Lewis basis and weaker TPB Lewis acid, while strong EWD would behave in the contrary way.

3.3.2 Interaction of frustrated Lewis pairs with DEAD

Once the acidity and basicity of the TBP and TPP derivatives have been evaluated, a set of frustrated Lewis pairs will be defined to analyze, firstly, the LA-LB interaction and, secondly, the interaction with the DEAD molecule. In order to do so, first the interaction enthalpies will be calculated, and then the interaction nature will be analyzed by means of Natural Bond Orbital (NBO) and Energy Decomposition Analysis (EDA). In particular, seventeen FLPs will be studied, generated by the combination of five acids and five bases including the following substituents: CN and CF_3 (strong acids and weak bases), H (moderate acid and base) and finally NH_2 and OCH_3 (weak acids and strong bases). See Figure 3.3. We are aware that the nucleophilic nitrogen of CN and the hydrogens of NH_2 may react with Lewis acids and bases respectively, destroying the FLP. Hence, the FLP's derived from the combination of these two substituents have been calculated just for analysis purposes. Finally, the FLP used in the experimental material will also be studied.
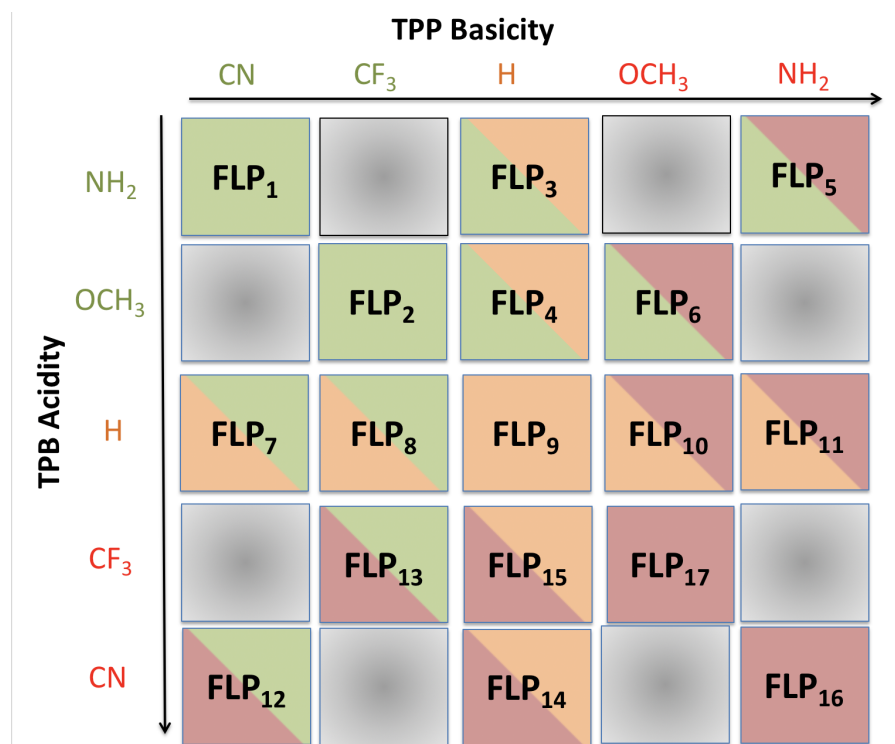
Figure 3.3: Combinations of the TPB- and TPP-derivatives to generate the 17 FLPs. Green, orange and red colors state for weak, moderate and strong acids and bases.

Interaction energies between FLPs and DEAD

In this subsection, both the interaction energy between the acids and bases to form the FLP (ΔH_1) and between each FLP and the DEAD molecule (ΔH_2) will be studied.

These interaction energies are defined as in Equation 3.1:

$$A + B \rightarrow AB \quad \Delta H_1$$
$$A + B + L \rightarrow ALB \quad \Delta H_2$$

(3.1)
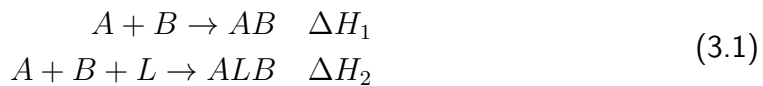
where ΔH_1 = H_{AB} - (H_A + H_B) and ΔH_2 = H_{ALB} - (H_A + H_B + H_L). H_A, H_B and H_L correspond to the enthalpies of the acid, base and DEAD molecules isolated, H_{AB} is the enthalpy of the FLP and H_{ALB} is the enthalpy of the FLP-DEAD complex. The obtained results are collected in Table 3.2.

Table 3.2: Interaction energies between Lewis acids and bases to form the FLPs (ΔH_1) and between the FLPs and DEAD molecule (ΔH_2), in kcal/mol. Bond distances (R_e), in Å. Red, orange and green groups stand for strong, moderate and weak acids or bases, respectively.

	Acid	Base	FLP		FLP-DEAD			
			ΔH_1	R_e(B-P)	ΔH_2	R_e(B-N)	R_e(N-N)	R_e(N-P)
FLP_1	NH_2	CN	-8.27	5.691	—	—	—	—
FLP_2	OCH_3	CF_3	-9.33	6.396	—	—	—	—
FLP_3	NH_2	H	-10.81	5.861	-43.54	3.586	1.416	1.703
FLP_4	OCH_3	H	-15.74	3.430	-32.37	1.700	1.414	1.721
FLP_5	NH_2	NH_2	-21.41	5.687	-48.58	4.176	1.432	1.731
FLP_6	OCH_3	OCH_3	-11.40	5.860	-4.95	1.709	1.436	1.763
FLP_7	H	CN	-9.23	5.455	-6.25	1.702	1.421	1.718
FLP_8	H	CF_3	-6.09	5.689	28.18	1.723	1.425	1.722
FLP_9	H	H	-18.90[a]	2.112	—	—	—	—
FLP_{10}	H	OCH_3	-14.95[a]	2.267	—	—	—	—
FLP_{11}	H	NH_2	-10.80	5.418	-57.47	1.694	1.428	1.789
FLP_{12}	CN	CN	-9.58	7.171	0.39	1.663	1.450	1.786
FLP_{13}	CF_3	CF_3	-8.95	7.820	—	—	—	—
FLP_{14}	CN	H	-9.31	5.686	-56.72	1.647	1.433	1.752
FLP_{15}	CF_3	H	-9.25	6.123	14.13	1.654	1.437	1.814
FLP_{16}	CN	NH_2	—	—	-50.87	1.646	1.446	1.879
FLP_{17}	CF_3	OCH_3	-9.29	6.212	26.17	1.687	1.448	1.877
	Reference		-13.09	3.811	-43.45	1.678	1.425	1.743

[a]Regular acid-base pair (not FLP)

Let us focus first in the FLP interaction. In principle, frustrated Lewis pairs would show weak interactions and B-P distances longer than those corresponding to covalent bonds. Inspecting the reference system, it is observed that the B-P distance is 3.811 Å, with an interaction energy of -13.09 kcal/mol. Having these values as reference, it is observed that all ΔH_1 values are in the range of -6 and -21 kcal/mol. Values larger than that of the reference correspond to FLP_4, FLP_5, FLP_9 and FLP_{10}. The last two show short bond distances similar to those of covalent bonds. Hence, larger ΔH_1 values (between -15 and -19 kcal/mol, approximately) are due to a low steric hindrance that allows an acid-base interaction, leading to a regular, non-frustrated, LA-LB pair. FLP_5 shows by far the largest ΔH_1 value, -21.41 kcal/mol, but with long B-P bond of 5.687 Å. This strong interaction is related to hydrogen bond interactions between the amine

groups of TPB and TPP derivatives. In FLP_4, the B-P bond distance is slightly shorter and ΔH_1 slightly larger than the reference, being the most similar FLP compared to our reference. The remaining FLPs show much larger B-P distances and smaller interaction energies, ranging between -6 and -11 kcal/mol, corresponding to weak non-covalent interactions between the bulky substituents and functional groups, indicative of very weakly interacting B-P pairs. Finally, it should be pointed out that we were not able to obtain the optimized structure of FLP_{16}, despite different attempts have been done. Based on these results, we can conclude that the FLP interaction energy is not directly related to the EDG or EWG nature of the substituent, but to attractive or repulsive interactions between these substituents. It should be noted that NH_2 and CN groups may not only interact with neighboring groups, but also with B and P centers from another LAs or LBs, which would prevent their experimental use.

Regarding the interaction of the FLPs with DEAD molecule, we will first focus on the reference model. According to the geometrical parameters given in Table 3.2, the linker molecule is located in between the Lewis acid and the Lewis base, leading to short B-N and P-N bond distances of 1.678 and 1.743 Å, respectively. These bond lengths suggest the formation of dative covalent bonds between the linker and both Lewis acid and base. Moreover, the N-N bond length in the isolated linker is 1.243 Å, which is elongated to 1.425 Å in the complex, suggesting a change from double N=N to single N-N bond in the complex. The nature of these bonds will be analyzed by means of NBO and EDA methods in the next subsection. The formation of the dative covalent bonds between the linker and the acid and base leads to an interaction energy, ΔH_2 of -43.45 kcal/mol. Notice that this interaction energy is similar to others found in self-healing materials, like those based on diphenyl disulfide bonds.[35]

Having a look to the results given in Table 3.2, we observe that several FLP-DEAD complexes are not formed. FLP_9-DEAD and FLP_{10}-DEAD have not been considered, since they are not frustrated Lewis pairs, as explained above. The combination of strong acids and strong bases, FLP_1-DEAD and FLP_2-DEAD, respectively, do not lead to converged structures. Finally, FLP_{13}-DEAD optimized structure was not found. All attempts to minimize the optimal geometries of the mentioned FLP-linker complexes eventually failed, probably because of the combination of strong acids and bases is not favored in FLP_1-DEAD and FLP_2-DEAD complexes, and due to steric repulsions in FLP_{13}-DEAD. Hence, hereafter only the remaining FLP-DEAD structures will be considered for discussion.

Inspecting the B-N and P-N interatomic distances of optimized complexes provided in Table 3.2, apparently dative covalent bonds are formed between Lewis acids and Lewis bases with the linker, with the exception of FLP_3-DEAD and FLP_5-DEAD complexes. In these two cases, B-N distances are too long for covalent bonds. The reason for this long interatomic distance is that the amine groups of the acid form hydrogen bonds with the DEAD linker, which are more favorable compared to the strong B-N interaction. Amine groups in the base are also able to form hydrogen bonds with DEAD, but in this case the formation of such bonds do not prevent the formation of B-N or P-N bonds. Finally, in the rest of FLP-DEAD complexes B-N, P-N and N-N distances similar to our reference

species are found. Hence, the optimized complexes may be classified in three type of structures: i) FLP-DEAD with only P-N covalent bond, and hydrogen bonds due to amine groups in the weak acid case, such as FLP_3-DEAD and FLP_5-DEAD complexes; ii) FLP-DEAD with B-N and P-N covalent bonds and hydrogen bonds, such as FLP_{11}-DEAD and FLP_{16}-DEAD complexes; iii) FLP-DEAD with B-N and P-N covalent bonds but without hydrogen bonds, similar to the reference system bond pattern, for the remaining 8 cases. Namely: FLP_n-DEAD, $n = 4, 6, 7, 8, 12, 14, 15, 17$.

Interaction energies of structures of type i and ii, which have hydrogen bonds between the amine substituents with the linker, are larger than the reference value. The formation of such hydrogen bonds is not desired in these materials, since they may prevent the correct performance of the linker molecule, DEAD. Hence, they should be discarded for the development of self healing materials. Hence, let us focus on the FLP-DEAD complexes of type iii, with the desired FLP-DEAD bond pattern. Among these complexes, we find the complexes with cyano groups. FLP_{14}-DEAD complex, which contains the cyano group in the Lewis acid, is the strongest one, with ΔH_2 value of -56.72 kcal/mol. This interaction energy is reduced drastically to -6.25 kcal/mol and 0.39 kcal/mol in the cases of FLP_7-DEAD and FLP_{12}-DEAD complexes, respectively, where the cyano group is found in the Lewis base (or in both like in FLP_{12}-DEAD complex). Clearly, the influence of the EDG is very different in the Lewis acid or in the Lewis base, as expected from the results of subsection 3.3.1. However, in addition to this influence, the lone pairs of cyano groups may lead to other non-desired interactions, such as the interaction with the empty orbital of the Lewis base, preventing in this way the proper interaction between the FLP and the linker. Hence, they will not be further considered hereafter. Among the remaining five complexes, only those containing methoxy groups as substituents in the Lewis acid have favorable ΔH_2 values. FLP_4-DEAD complex is the most promising one, with interaction energy of around -32 kcal/mol. The other remaining FLP-DEAD complexes have very weak or repulsive interactions, and hence must be discarded for the development of self-healing materials.

In the next subsection, the bonding patterns of these five FLP-DEAD complexes will be analyzed, in order to understand the electronic reasons for such different behaviour.

Natural Bond Orbital (NBO) and Energy Decomposition Analysis (EDA)

In this subsection, a detailed analysis of the bonding pattern in FLP pairs, isolated DEAD linker and the bonding between these FLPs and DEAD molecule is carried out by means of the NBO methodology. In Table 3.3, the calculated occupation numbers of key bonding orbitals and lone-pairs are given for FLPs, and FLP-DEAD complexes. In addition, the EDA method, based on the energy decomposition scheme of Morokuma,[179] has been used to provide further information about the nature of the interactions between the FLPs and DEAD, in particular the acid-DEAD (B-N) and base-DEAD (P-N) interactions. As it was explained in the Computational Methods section, with this methodology it is possible to obtain the electrostatic (ΔE_{elstat}), exchange (ΔE_{Pauli}) and covalent (ΔE_{orb})

contributions to the total bonding energy for a specific interaction. Besides, the steric energy, or Heitler-London interaction energy, is defined as the sum of the Pauli repulsion and electrostatic attraction terms: $\Delta E_{steric} = \Delta E_{Pauli} + \Delta E_{elstat}$. A positive value of ΔE_{steric} is related to a covalent character of the interaction.[186,202] The results are collected in Table 3.4.

Table 3.3: Orbital occupancies of empty boron (LP_σ^B) and phosphorous lone-pair (LP_σ^P) orbitals of the FLPs. In addition, occupancies of selected bonding orbitals of the FLP-DEAD complexes (σ_{B-N} and σ_{N-P}), along with selected lone pairs of boron (LP_σ^B) and nitrogen atom bonded to boron ($LP_\sigma^{N(B)}$, $LP_\pi^{N(B)}$) and phosphorous ($LP_\pi^{N(P)}$). Red, orange and green groups stand for strong, moderate and weak acids or bases, respectively.

	Acid	Base	FLP		FLP-DEAD			
			LP_σ^B	LP_σ^P	σ_{BN}	σ_{NP}	$LP_\pi^{N(B)}$	$LP_\pi^{N(P)}$
FLP_4	OCH$_3$	H	0.302	1.774	1.958	1.965	1.666	1.722
FLP_6	OCH$_3$	OCH$_3$	0.283	1.844	1.955	1.959	1.667	1.729
FLP_8	H	CF$_3$	0.271	1.781	1.949	1.959	1.630	1.732
FLP_{15}	CF$_3$	H	0.212	1.870	1.964	1.948	1.690	1.774
FLP_{17}	CF$_3$	OCH$_3$	0.235	1.855	1.953	1.937	1.690	1.776
	Reference		0.282	1.810	1.933	1.962	1.690	1.740

NBO analysis provides localized orbitals that help in rationalizing the bonding within molecules and the interaction between different molecules. According to the Lewis acid and base nature, one would expect an empty orbital located at boron in the Lewis acid, and a lone-pair located at phosphorus, in the Lewis base. Inspecting the occupation numbers given in Table 3.3 for the FLPs, it is observed that the occupation of the empty boron orbital, LP_σ^B, and of the lone-pair orbital in phosphorous, LP_σ^P, are slightly affected by the nature of the substituent in the phenyl rings. These electronic configurations lead to an almost trigonal planar geometry for the Lewis acid and a trigonal pyramidal geometry for the Lewis base. As expected, no σ_{B-P} bond is found between the acid and the base and, therefore, weak interaction energies are calculated for the FLPs.

Let us focus now on the electronic structure of the isolated DEAD species. The schematic representation of the electronic structure provided by NBO is depicted in the top of Figure 3.4. The isolated molecule shows a conjugated π system with 6 electrons in 6 centers. The carbonyl (C=O) and azo (N=N) groups possess a double bond, according to the localized bonds and orbitals provided by NBO. In addition, both nitrogens have lone pairs of σ symmetry perpendicular to the π system, in the directions where the Lewis acid and base should interact to form the complex.

This electronic structure favors the interaction with the Lewis acid, via a dative bond between the nitrogen lone pair and the boron empty orbital, but hinders the interaction with the lone pair of phosphorous. Hence, in order to form a stable complex, the electronic structure of the linker must be reorganized. The NBO analysis of the FLP-DEAD interactions show that, in this reorganization process, the two electrons of the
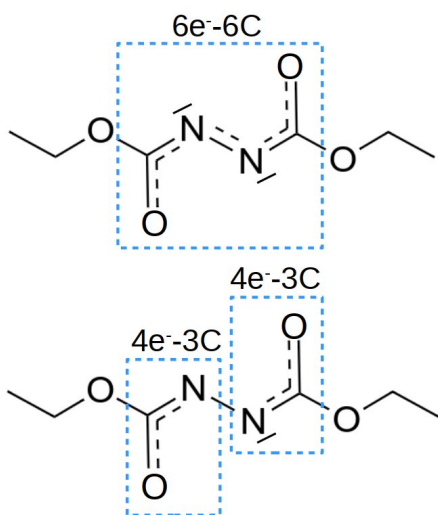
Figure 3.4: Electronic Lewis structure of the DEAD molecule isolated (top) and after complexation with the FLP (bottom).

nitrogen σ lone pair directed towards the phosphorous lone pair moves to the π system, in such a way that this σ orbital now is empty and able to accept electron density from the P atom. The π system, therefore, now contains 8 electrons and, as a consequence, the double bond in the azo group is broken, producing two 3-center 4-electron (3c-4e) systems which resemble peptidic bonds (see Figure 3.4 bottom), and stabilizing the complex. This feature is clearly observed both in the elongation of the N-N bond distance from the isolated molecule, $R_e = 1.254$ Å, to the complex, in the range of $1.400 - 1.450$ Å, and in the formation of B-N and N-P bonds, with bond distances between 1.600 and 1.800 Å (see Table 3.2).

According to this electronic reorganization, the interpretation of the interaction of Lewis acids and bases with DEAD molecule may be carried out. The occupation numbers of the formed B-N and P-N bonds, along with other relevant lone pairs is collected in Table 3.3. Focusing on the reference case, where both fragments show moderate acidity and basicity, the formation of covalent bonds is observed according to the occupation numbers of the bonding orbitals. No σ lone-pair orbitals are found for B and P. On the other hand, the π lone pairs are occupied in both N atoms. These orbitals are interacting with the carbonyl π system, leading to (3c-4e) bonds. The occupation numbers of all studied cases are very similar and are in agreement with calculated B-N, N-N and N-P bond distances in all complexes (see Table 3.2), which suggest that the type of bond in all cases is similar. Hence, from the NBO results we can conclude that, in general, the bonding interactions between the Lewis acid and Lewis bases and DEAD molecule are polar covalent bonds, with no clear influence of the substituents in the calculated occupation numbers that could explain the calculated differences in the interaction energies.

Energy Decomposition Analysis provides an alternative way to analyze the interaction

of FLP-DEAD species. In Table 3.4, it is observed that all ΔE_{steric} values are positive and, therefore, all the interactions can be regarded as covalent. Inspecting the percentage contributions to the total attractive interactions ($\Delta E_{elstat} + \Delta E_{orb} + \Delta E_{disp}$) for the B-N bond, both the term related to the mixing of the orbitals (covalent character), ΔE_{orb}, and the term corresponding to the electrostatic interaction, ΔE_{elstat}, show similar values of around 40%. This means that the B-N bond is a polarized covalent bond in all complexes. Considering the P-N bond, remarkably higher values of the ΔE_{steric} term are calculated. This may indicate a larger covalent character of the P-N bond. Inspecting the percentage contributions to the total attractive interactions, the contribution of the ΔE_{orb} is also notably larger than the ΔE_{elstat} term in all cases, around 55% and 35%, respectively. Besides, the dispersion term is also lower. This suggests that the P-N bond is a less polarized covalent bond than B-N.

Table 3.4: Interaction energy (ΔE_{int}), Pauli repulsion (ΔE_{Pauli}), electrostatic interaction (ΔE_{elstat}), steric energy (ΔE_{st}), orbital attraction (ΔE_{orb}) and dispersion energy (ΔE_{disp}), in kcal/mol, for the B-N (acid-DEAD) and P-N (base-DEAD) bonds. Values in brackets are the percentage contributions to the total attractive interactions: $\Delta E_{elstat} + \Delta E_{orb} + \Delta E_{disp}$. Red, orange and green groups stand for strong, moderate and weak acids or bases, respectively.

	Acid	Base	ΔE_{int}	ΔE_{Pauli}	ΔE_{elstat}	ΔE_{st}[a]	ΔE_{orb}	ΔE_{disp}
					Acid (B-N)			
FLP_4	OCH_3	H	-68.05	215.88	-118.41 (41.7%)	97.47	-114.11 (40.2%)	-51.44 (18.2%)
FLP_6	OCH_3	OCH_3	-67.68	211.41	-109.07 (39.1%)	102.34	-116.10 (41.6%)	-53.95 (19.3%)
FLP_8	H	CF_3	-55.75	161.49	-92.39 (42.5%)	69.10	-88.28 (40.6%)	-36.58 (16.8%)
FLP_{15}	CF_3	H	-96.11	229.26	-139.18 (42.8%)	90.08	-138.56 (42.6%)	-47.64 (14.6%)
FLP_{17}	CF_3	OCH_3	-107.17	216.50	-133.17 (41.1%)	83.34	-138.50 (42.8%)	-52.02 (16.1%)
Reference			-73.34	175.17	-107.01 (43.1%)	68.16	-105.35 (42.4%)	-36.16 (14.6%)
					Base (P-N)			
FLP_4	OCH_3	H	-119.91	592.84	-282.42 (39.6%)	310.43	-393.95 (55.2%)	-36.39 (5.1%)
FLP_6	OCH_3	OCH_3	-86.04	521.46	-235.17 (38.7%)	286.29	-327.17 (53.9%)	-45.19 (7.4%)
FLP_8	H	CF_3	-86.68	636.17	-303.47 (41.9%)	332.70	-376.63 (52.1%)	-42.77 (5.9%)
FLP_{15}	CF_3	H	-134.95	485.87	-230.11 (37.1%)	255.76	-357.59 (57.6%)	-33.13 (5.4%)
FLP_{17}	CF_3	OCH_3	-109.05	408.32	-188.80 (36.5%)	219.51	-283.62 (54.8%)	-44.97 (8.7%)
Reference			-139.90	549.10	-256.80 (37.3%)	292.30	-396.57 (57.6%)	-35.65 (5.2%)

$$^{a}\Delta E_{st} = \Delta E_{Pauli} + \Delta E_{elstat}$$

3.4 Conclusions

In this chapter, we have studied computationally complexes of several frustrated Lewis pairs with a small molecule (diethyl azodicarboxylate, DEAD) as potential candidates for new dynamic bonds useful in self-healing materials. Inspired by the experimental work of Shaver and coworkers,[67] we have designed a set of FLPs using Lewis acids and bases based on triphenylborane (TPB) and triphenylphosphine (TPP), in order to understand the nature of the interaction with the DEAD molecule and the influence of the substituents in the acid and the base.

First of all, the acidity and basicity of the isolated TPB and TPP derivatives have been analyzed by means of different parameters. For Lewis acids, hydride affinity (HA), electroaccepting power (ω^+), variation of the ^{31}P-NMR chemical shift ($\Delta\delta$) and boron empty orbital energy (ε_B) were analyzed, while for Lewis bases the studied criteria were proton affinity (PA), electrodonating power (ω^-) and phosphorous lone-pair orbital energy (ε_P). For the acids, all criteria show that electron withdrawing substituents in the phenyl rings lead to stronger Lewis acids, while for bases electron donating groups were those leading to stronger Lewis bases.

From the previous set, three TPB and TPP derivatives corresponding to strong, moderate and weak acids and bases were chosen and combined to generate 17 FLPs, including the reference from the experimental work. The acid-base interaction energy to form the FLP (ΔH_1) as well as the interaction of all the FLPs with DEAD (ΔH_2) were calculated. Based on the obtained structures and interaction energies, substituents with the capacity to form hydrogen bonds or donor-acceptor bonds should be discarded, since they can easily hinder the proper FLP-DEAD interaction.

Finally, both NBO and EDA analyses provide complementary pictures of the interaction within FLP-DEAD patterns. According to NBO, the DEAD species undergoes an electronic configuration rearrangement, so that dative covalent bonds are formed between TPB-DEAD and TPP-DEAD fragments, leading to polar covalent bonds. The polarity of these bonds is observed to be larger for the B-N bond than for the P-N bond. Compared to the reference system, similar bond natures are observed for the rest of the systems. These small differences between these complexes cannot explain the large calculated differences in FLP-DEAD interaction energies. Hence, these differences may be attributed to the steric repulsion between substituents, and not to substantial changes in the bond patterns.

To conclude, in this part of the work the FLP$_4$-DEAD system is proposed as a promising candidate to develop new self-healing polymers. Other alternatives, such as different linker molecules or the use of FLPs including different acidic and basic centers (such as Al, Ga, N, etc.) should be considered for further improvements.

Chapter 4

Computational insight into the metal-ligand interaction in self-healing metallopolymers

In this chapter, a computational study of the interaction between pincer ligands, based on terpyridine (TPY) and terphosphinine (TPPh), and different transition metals is performed. The main objective is to achieve a better understanding of this interaction and identify the key parameters that could be used to design new candidates for self-healing materials. A detailed analysis of the bond is carried out, and the influence of both the ligand and the metal is investigated.

4.1   Introduction

Over the past few years, synthetic metallopolymers have emerged as promising candidates to create advanced materials. In this context, different metal-ligand complexes have been explored in the pursuit of new self-healing materials. The use of multidentate ligands such as terpyridine (TPY) enhances the binding affinity to a wider range of metals due to the chelating effect[100] and the metal-ligand $d\pi$-$p\pi$ back bonding.[101] As a result, TPY-containing polymers have been developed using transition metals such as Fe(II),[103] Cd(II),[103,104] Zn(II),[105,106] and Co(II).[107] This includes the self-healing metallopolymer developed by Rowan and Weder based on the interaction between Zn(II) and La(III) with a pyridyl-based tridentate ligand.[53]

This bonding interaction can be modified by changing both the ligand and the transition metal. The phosphorus analogue of terpyridine (terphosphinine, TPPh) has not yet been used, to our knowledge, as a pincer ligand for metallopolymers. The electronic features of phosphinines notably differ from those of pyridines, showing a strong π-acceptor character.

In this chapter, we employ computational methods to explore the dynamic chemistry in these metallopolymers. Concretely, the models employed to represent these cross-linkers are depicted in Figure 4.1, i.e., complexes containing one pincer ligand (left panel) or two pincer ligands (right panel), where X = N corresponds to TPY and X = P states for TPPh. Electron donating (EDG) and electron withdrawing (EWG) groups in the ligands have been included (R), as well as different metal cations (M).
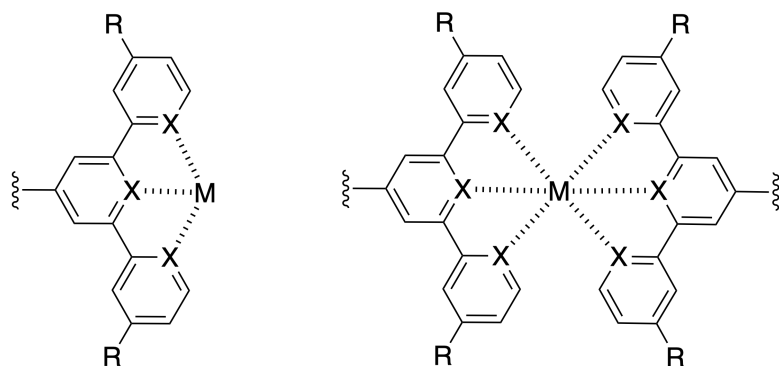
Figure 4.1: Molecular model of the studied systems containing one pincer ligand (left panel) and two pincer ligands (right panel). For X = N, the ligand is terpyridine (TPY) and for X = P is terphosphinine (TPPh). The ligands are substituted with an electron-donating (EDG, R = NH_2) and an electron-withdrawing (EWG, R = CN) group. The complexed metal ions are M = Fe(II), Cu(I), Zn(II), Ru(II), Cd(II), Sc(I), Sc(II) and Sc(III).

Based on these models, we will be able to identify some key electronic features of metal-ligand interactions in order to help in the design of more efficient self-healing materials. Concretely, we will study the influence of the transition metal in TPY-containing metallopolymers. Then, an electron-withdrawing and an electron-donating group in the phenyl rings of TPY ligands will be included to modify the σ-donating character of nitrogen and, finally, we will explore the effect of changing nitrogen by phosphorus using the TPPh ligand. Our findings indicate that transition metals positioned on the left side of a series lead to stronger interactions compared to those located on the right side. Additionally, introducing substituents in the pincer ligand may have a slight impact on the interaction; however, the presence of these substitutes does not solely determine the metal-ligand interaction. Alternatively, substituting TPY with TPPh ligand results in a decrease in interaction energies. Based on these results, certain complexes are proposed as potential candidates for an enhanced self-healing polymer.

4.2   Computational details

All geometry optimizations have been performed within density functional theory (DFT) using the ωB97XD functional[203] combined with the 6-31+G(d,p) basis set.[204] In order

to confirm that the optimized structures were minima or transition states in the potential energy surfaces, frequency calculations have been carried out at the same level of theory. These frequencies have been then used to evaluate the zero-point vibrational energy (ZPVE) and the thermal correction to the enthalpy (T = 298.15 K) in the harmonic oscillator approximation. Finally, single-point calculations with the 6-311++G(2df,2p) basis set[205] have been performed on the optimized structures to refine the electronic energy.

The nature of the interaction has been analyzed using the natural bonding orbital (NBO)[175,195,196] and the quantum theory of atoms in molecules (QTAIM)[206,207] methodologies. QTAIM identify critical points, i.e., points of the space where the gradient of the electron density ($\nabla\rho$) vanishes. The critical points are identified depending on the sign of the Laplacian of the electron density ($\nabla^2\rho$). The bond critical point (BCP) between two atoms is located where the electron density has its minimum value along the path that links those two atoms. The electron density and the Laplacian at the BCP (ρ_{BCP} and $\nabla^2\rho_{BCP}$) can be used to identify the nature of the corresponding bond using the following relationships:

$$\frac{1}{4}\nabla^2\rho = 2G + V \tag{4.1}$$

$$H = G + V \tag{4.2}$$

where G, V and H are the kinetic, potential and total electron energy densities at the BCP. Since G is positive and V is negative, if $|V| > 2G$, then the Laplacian is negative ($\nabla^2\rho < 0$) and the interaction is covalent. If $|V| > G$, the Laplacian is positive ($\nabla^2\rho > 0$) but the total energy density is negative (H < 0), which implies a partially covalent interaction. Finally, if $|V| < G$, both the Laplacian and the total energy density are positive ($\nabla^2\rho$, H > 0), denoting a non-covalent interaction.[183–186] Also, if ρ is large ($\rho > 0.03$) and H < 0, then the interaction can be represented as partially covalent.

All calculations have been performed using the Gaussian 16[187] and AIMAII suite of programs.[208]

4.3   Results and discussion

In this section, the nature of the metal-ligand interaction in complexes present in metallopolymers has been analyzed in detail. In the first subsection, the effect of the transition metal will be discussed, including early, medium and late transition metals, metals from different series as well as different oxidation states, using terpyridine as ligand. Then, the effect of functional groups in the phenyl rings of terpyridine will be studied and, finally, terpyridine will be substituted by terphosphinine to get insight into the role of the ligand in the interaction.

4.3.1   Effect of the transition metal

In this subsection, the interaction of one and two TPY ligands (X = N and R = H) with the following transition metals has been studied: Fe(II), Cd(II), Ru(II), Cu(I), Zn(II) and Sc(III). Besides, Sc(I) and Sc(II) have been included to see the effect of the oxidation state. Although the electronic ground state in several isolated metal ions is not a singlet, no magnetic information has been reported in the experimental works, therefore, we assume that the ground state multiplicity of the complex with the pincer ligand will be singlet.

The interaction energies are defined as the enthalpy change in the following reactions, where M stands for the metal ion and L stands for ligands:

$$
\begin{aligned}
M^{n+} + L &\rightarrow [M - L]^{n+} \quad \Delta H_1 \\
M^{n+} + 2L &\rightarrow [L - M - L]^{n+} \quad \Delta H_2
\end{aligned}
\tag{4.3}
$$
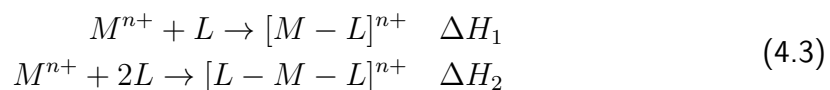
The results are depicted in Figure 4.2 and the numerical results are collected in Table 4.1. The strength of the interaction follows the trend: Sc(III) > Ru(II) > Fe(II) > Zn(II) > Cd(II) > Cu(I). This trend can be understood by means of different parameters, like the charge and acidity of the metal, and the ligand-to-metal electron transfer. Highly charged ions are expected to show large ion-dipole interaction energies. Thus, the interaction energy calculated for the Sc(III) complex is the largest of all the complexes studied (499.8 and 719.1 kcal/mol for one and two TPY ligands, respectively).
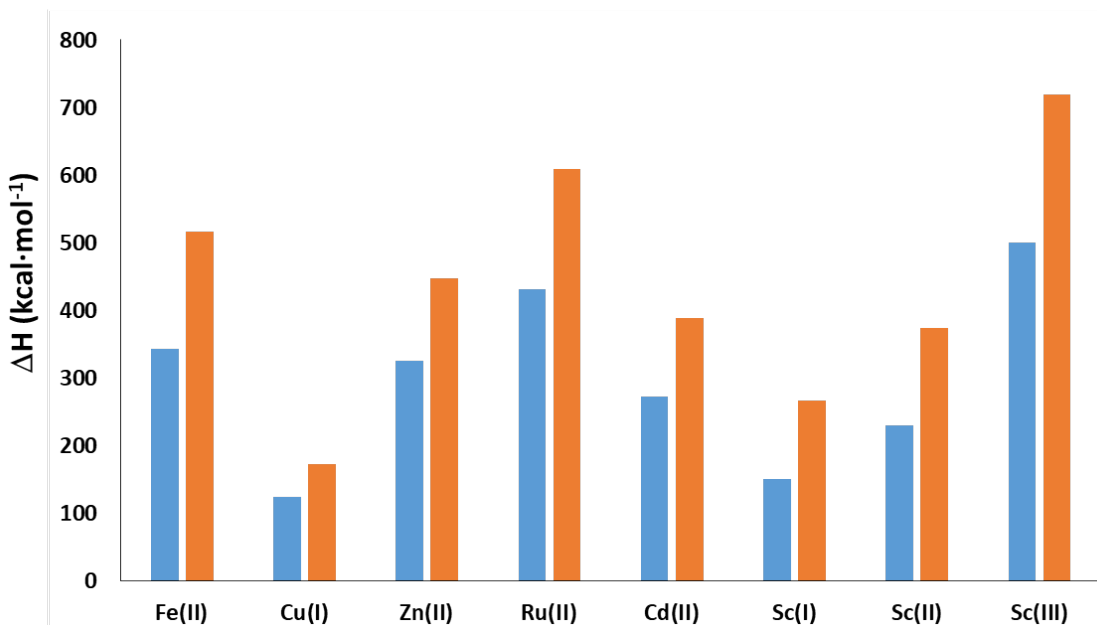
Figure 4.2: Interaction energy, in kcal/mol, of different transition metals with one (ΔH_1, blue bars) and two TPY (ΔH_2, orange bars) ligands.

The effect of the metal oxidation state can also be observed comparing the calculated values for Sc(II) (229.5 and 374.3 kcal/mol, for one and two TPY ligands, respectively) and Sc(I) (150.1 and 265.7kcal/mol, for one and two TPY ligands, respectively) complexes. This behavior is also supported by the hard and soft Lewis acids and bases concept (HSAB),[209] since Sc(III) is a hard acid, Ru(II), Fe(II) and Zn(II) are borderline acids, while Cu(I) are Cd(II) are soft acids.

Table 4.1: Interaction energies in kcal/mol for various transition metals with one (ΔH_1) and two (ΔH_2) TPY ligands.

	Fe(II)	Cu(I)	Zn(II)	Ru(II)	Cd(II)	Sc(I)	Sc(II)	Sc(III)
ΔH_1	342.6	123.6	324.8	430.9	271.5	150.1	229.5	499.8
ΔH_2	516.0	172.0	447.8	608.5	388.4	265.7	374.3	719.1

The metal-nitrogen bond distances of the $[\text{TPY-M}]^{n+}$ and $[\text{TPY-M-TPY}]^{n+}$ complexes are depicted in Figure 4.3 and the numerical values are collected in Table 4.2. The nitrogen-metal distances in $[\text{TPY-M}]^{n+}$ complexes are approximately in the range of 1.850-2.200 Å, while those in $[\text{TPY-M-TPY}]^{n+}$ complexes fall within the range of 1.900-2.400 Å. The large distances observed in $[\text{TPY-M-TPY}]^{n+}$ complexes may be attributed to steric hindrance, which increases the distances to achieve a more stable configuration and minimize steric strain. In $[\text{TPY-M}]^{n+}$ complexes, Cu(I) and Cd(II) exhibit nitrogen-metal distances that are longer than those observed in other complexes, which may indicate weaker metal-ligand interactions. Sc(III), on the other hand, displays unexpectedly long nitrogen-metal bond distances, considering the large interaction energy observed in these complexes. This feature will be further investigated in the bonding analysis. In the $[\text{TPY-M-TPY}]^{n+}$ complexes, the same trend is observed and the longest nitrogen-metal bond distances are calculated for Cd(II) and Cu(I) metals. Again, Sc(III) exhibits unexpectedly long nitrogen-metal bond distances.

Regarding the dihedral angles, Zn(II), Cd(II) and Cu(I) complexes with one TPY show planar or almost planar geometries (see Table 4.2) due to their fully filled d and empty s and p valence shells, which minimizes electronic repulsion. However, Cd(II) and Cu(I) complexes with two pincers lose planarity (104.5° and 106.4°, respectively) due to steric hindrance caused by electron density, while the Zn(II) complex with two pincers remains planar (179.9°). In contrast, Fe(II) and Ru(II) complexes have a partially filled d and empty s and p valence shells, allowing for greater flexibility in coordination. Regarding these metals, complexes with one pincer are non-planar (24.6° and 34.8°, respectively) due to the distribution of the electron density mainly in the d-shell, but in systems with two pincers, the increased electron density causes more repulsion, and the electronic density is distributed in the d, s and p orbitals, creating planar structures (179.9° and 179.8°, respectively). Additionally, scandium complexes also contain a partially filled d-shell and empty s and p valence shells. Despite this, Sc(II) and Sc(III) complexes with one TPY show planar or almost planar geometries (0.5° and 0°, respectively), while with two pincers the planarity is lost (114.8° and 168.2°, respectively). Besides, Sc(I) complex does not show planarity neither with one pincer (21.0°) nor with two (79.8°). In essence, this behaviour may be attributed to the relationship between the electronic

structure, the size of the metals and the geometry of the complexes in the space. It can be observed how metals that have partially filled d orbitals undergo from non-planar (1 TPY) to planar (2 TPY) geometries, being scandium metal a exception, while those that have fully filled d orbitals do the opposite, being Zn(II) metal a exception due to the relation mentioned before.

Table 4.2: Geometrical parameters for $[M\text{-}TPY]^{n+}$ and $[TPY\text{-}M\text{-}TPY]^{n+}$ complexes. Distances in Å and dihedral angles in degrees.

	Fe(II)	Cu(I)	Zn(II)	Ru(II)	Cd(II)	Sc(I)	Sc(II)	Sc(III)
				$[M\text{-}TPY]^{n+}$				
M-N$_1$	1.936	2.039	1.992	2.001	2.200	2.172	2.247	2.121
M-N$_2$	1.846	2.048	1.947	1.943	2.174	1.967	2.184	2.070
M-N$_3$	1.936	2.039	1.993	2.001	2.200	2.172	2.247	2.121
dihedral	24.6	1.3	0.0	34.8	0.0	21.0	0.5	0.0
				$[TPY\text{-}M\text{-}TPY]^{n+}$				
M-N$_1$	2.008	2.312	2.190	2.093	2.363	2.222	2.208	2.225
M-N$_2$	1.910	2.200	2.106	1.995	2.340	2.160	2.104	2.232
M-N$_3$	2.008	2.260	2.190	2.093	2.354	2.285	2.215	2.226
M-N$_4$	2.008	2.260	2.190	2.093	2.355	2.222	2.262	2.225
M-N$_5$	1.910	2.200	2.106	1.995	2.340	2.160	2.284	2.232
M-N$_6$	2.008	2.313	2.190	2.093	2.361	2.285	2.266	2.225
dihedral	179.9	106.4	179.9	179.8	104.5	79.8	114.8	168.2

In order to understand the nature of the interaction, we use the natural bond orbital methodology (NBO). In table 4.3 are collected the results for the complexes with one TPY ligand. The results corresponding to the complexes with two TPY ligands are in Table 4.4.

The NBO analysis for $[M\text{-}TPY]^{n+}$ complexes indicates that no metal-ligand covalent bond is formed, and instead, the interaction between the metal and the ligand is mainly electrostatic. The occupation of the nitrogen lone pairs, which donate electron density to the empty orbitals of the metal, provides an idea of the strength of the interaction. The electron transfer is denoted by Δ_{occ}. The largest electron transfer occurs with Ru(II), where more than one electron is effectively transferred to the $4d$ orbitals. Fe(II) also exhibits a significant electron transfer. However, in Cu(I), Zn(II), and Cd(II), the filled d orbitals lead to less electron density transfer, which must happen in the more energetic $(n + 1)s$ and $(n + 1)p$ orbitals, resulting in weaker interactions. These trends are consistent with the interaction energies. In the case of Sc(III), a remarkable charge transfer (0.711) from the nitrogens is observed, but the orbitals receiving electron density are virtual and more energetic than the other metals' $3d$ orbitals. Besides, the second-order interaction energy between the nitrogen and the empty Sc orbitals is almost the lowest (233.5 kcal/mol). As a consequence, in this metal the interaction energy is large due to the ion-dipole interactions, but the Sc-N distances are long because of the charge transfer occurring in energetic orbitals. Comparing the latter with +1 and +2 oxidation states, it can be seen that Sc(I) shows lower electron transfer (0.549) and second-order
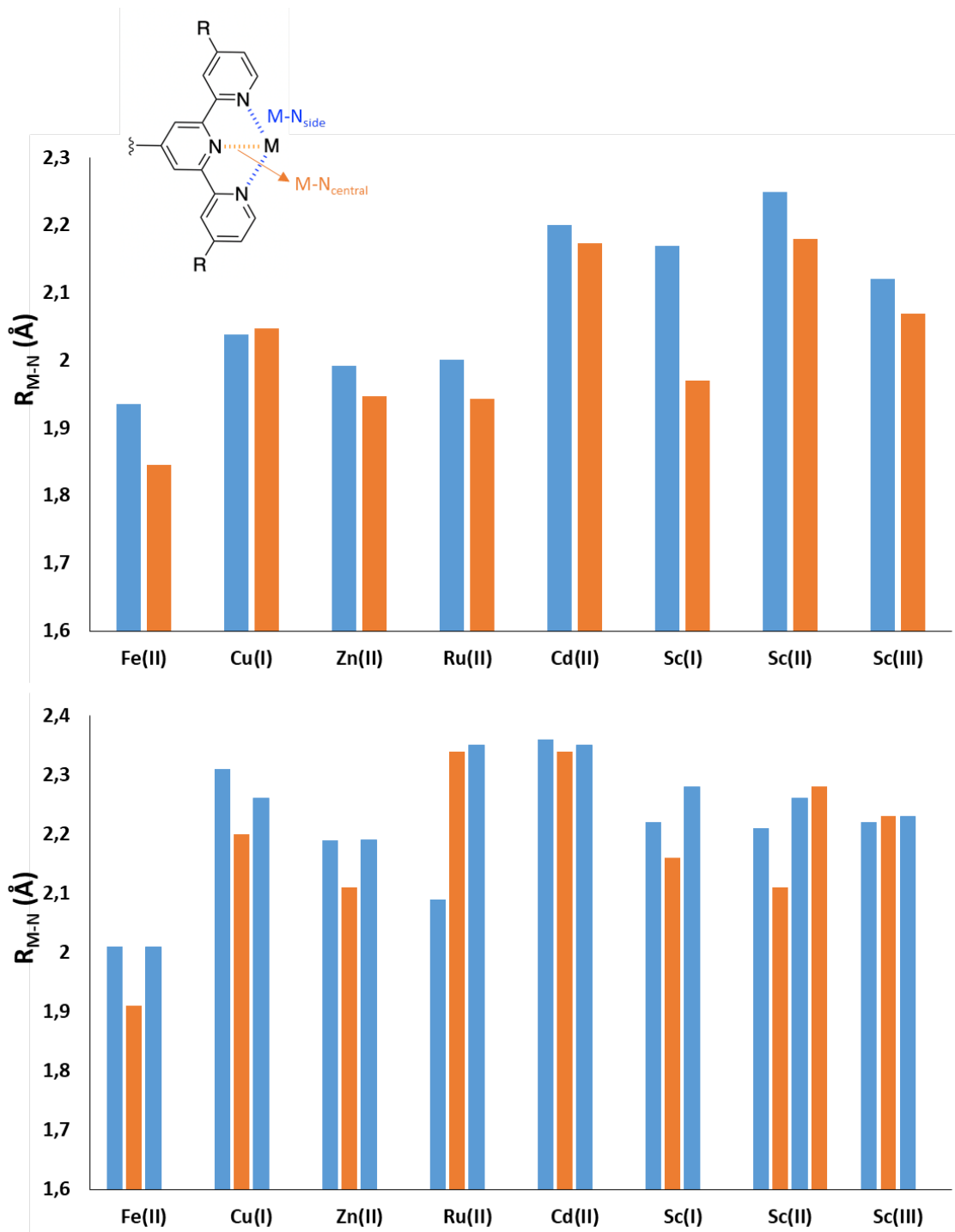
Figure 4.3: Bond distances, in Å, for the M-N$_{side}$ (blue bars) and M-N$_{central}$ bonds (orange bars) in the [M-TPY]$^{n+}$ complexes (top) and [TPY-M-TPY]$^{n+}$ complexes (bottom).

Table 4.3: Natural bond orbital (NBO) analysis for the $[M\text{-}TPY]^{n+}$ complexes. Orbital occupancies of the nitrogen lone pair (LP_{N_i}) and the metal atomic orbitals (LP_{nd}, $LP_{(n+1)s}$ and $LP_{(n+1)p}$); variation of the occupation after and before the complexation (Δ_{occ}), and second-order interaction energies ($E^{(2)}$), in kcal/mol.

	Fe(II)	Cu(I)	Zn(II)	Ru(II)	Cd(II)	Sc(I)	Sc(II)	Sc(III)
LP_{N_1}	1.701	1.827	1.772	1.593	1.785	1.838	1.998	1.817
LP_{N_2}	1.615	1.866	1.830	1.543	1.842	1.788	1.925	1.782
LP_{N_3}	1.701	1.827	1.771	1.593	1.785	1.838	1.933	1.817
Total	5.017	5.520	5.373	4.729	5.412	5.464	5.856	5.416
Δ_{occ}	-0.983	-0.480	-0.627	-1.271	-0.588	-0.536	-0.144	-0.584
LP_{nd}	6.664	9.939	9.985	6.926	9.988	0.392	1.004	0.530
$LP_{(n+1)s}$	0.223	0.240	0.368	0.201	0.361	0.140	0.054	0.152
$LP_{(n+1)p}$	0.061	0.124	0.197	0.042	0.143	0.017	0.043	0.029
Total	6.948	10.303	10.550	7.169	10.492	0.549	1.101	0.711
Δ_{occ}	0.948	0.303	0.550	1.169	0.492	0.549	0.101	0.711
$E^{(2)}$	457.7	186.6	302.2	642.2	457.0	227.6	77.3	233.5

interaction energy (227.6 kcal/mol). The main electron density donation occurs in d and s orbitals, as in Sc(III), however, the M-N distances are quite elongated than in Sc(III). On the other hand, Sc(II) shows very little electron transfer (0.101) and very low second-order interaction energy (77.3 kcal/mol). In this case, electron density transfers mainly to d orbitals and the M-N distances are even more elongated than Sc(I). Hence, this confirms the assumption made before, i.e., there is a relation between the electronic structure, the size of the metal and the complex geometry.

When examining $[TPY\text{-}M\text{-}TPY]^{n+}$ complexes, the same trend is observed. Fe(II) and Ru(II) exhibit the largest electron transfer, with nearly one electron being transferred to the corresponding nd orbital. In contrast, Cu(I), Zn(II), and Cd(II) have fully filled d orbitals, causing the electron density to distribute to the more energetic $(n + 1)s$ and $(n + 1)p$ orbitals. This results in weaker interactions and lower interaction energies. Additionally, Sc(III) exhibits high electron transfer, as seen in the $[M\text{-}TPY]^{n+}$ complex. Comparing with one-pincer complexes, Fe(II), Ru(II), and Sc(III) show increased second-order interaction energies, whereas Cd(II), Zn(II), and Cu(I) display decreased energies. This phenomenon can be explained by the geometries adopted by the complexes to avoid steric hindrance. Furthermore, when looking at Sc(I) and Sc(II), the first shows even larger electron transfer than Sc(III), while Sc(II) shows lower, and same happens with second-orbital interaction energies. Hence, it is clear that above all the complexes try to minimize steric hindrance to maximize the interaction.

In order to further analyze these interactions, the quantum theory of atoms in molecules (QTAIM) methodology has been used. This analysis has been performed only for Fe(II), Ru(II) and Cd(II) (see Table 4.5). Within this methodology, an interaction can be considered as covalent if the Lapacian is negative ($\nabla^2\rho < 0$), which is not the case. Nevertheless, if large values of the density are calculated ($\rho > 0.03$) and H <

0, then the interaction can be considered as partially covalent. This is the case for all metal-nitrogen interactions in these complexes. It is found that Ru(II) shows the largest density values, while Cd(II) presents the lowest ones.

Table 4.4: Natural bond orbital (NBO) analysis for the $[\text{TPY-M-TPY}]^{n+}$ complexes. Orbital occupancies of the nitrogen lone pair (LP_{N_i}) and the metal atomic orbitals (LP_{nd}, $\text{LP}_{(n+1)s}$ and $\text{LP}_{(n+1)p}$); variation of the occupation after and before the complexation (Δ_{occ}), and second-order interaction energies ($\text{E}^{(2)}$), in kcal/mol.

	Fe(II)	Cu(I)	Zn(II)	Ru(II)	Cd(II)	Sc(I)	Sc(II)	Sc(III)
LP_{N_1}	1.656	1.849	1.823	1.634	1.840	1.822	1.908	1.808
LP_{N_2}	1.650	1.849	1.822	1.621	1.840	1.822	1.912	1.815
LP_{N_3}	1.656	1.850	1.823	1.634	1.842	1.814	1.908	1.808
total occ	4.962	5.548	5.468	4.889	5.522	5.458	5.728	5.431
Δ_{occ}	-1.038	-0.453	-0.532	-1.111	-0.478	-0.542	-0.272	-0.569
$\text{E}^{(2)}$	773.1	167.1	250.8	1352.6	369.1	283.7	137.2	294.5
LP_{N_4}	1.656	1.851	1.823	1.634	1.842	1.814	1.905	1.808
LP_{N_5}	1.650	1.849	1.822	1.621	1.841	1.822	1.905	1.815
LP_{N_6}	1.660	1.849	1.823	1.634	1.840	1.822	1.905	1.808
Total	4.966	5.549	5.468	4.889	5.523	5.458	5.715	5.431
Δ_{occ}	-1.034	-0.453	-0.532	-1.111	-0.477	-0.542	-0.285	-0.569
$\text{E}^{(2)}$	534.4	167.1	250.3	1089.1	335.2	283.3	155.6	294.5
LP_{nd}	6.900	9.874	9.981	6.950	9.980	0.781	0.416	0.576
$\text{LP}_{(n+1)s}$	0.277	0.265	0.385	0.257	0.342	0.202	0.111	0.228
$\text{LP}_{(n+1)p}$	0.539	0.348	0.464	0.488	0.390	0.428	0.214	0.439
Total	7.716	10.487	10.830	7.695	10.712	1.411	0.741	1.243
Δ_{occ}	1.716	0.487	0.830	1.695	0.712	1.411	0.741	1.243

Table 4.5: Electron density (ρ), kinetic (G), potential (V) and total (H) electron energy densities, and Laplacian of the electron density ($\nabla^2\rho$) at the bond critical points, in a.u., for the $[\text{M-TPY}]^{n+}$ and $[\text{TPY-M-TPY}]^{n+}$ complexes, with M = Fe(II), Ru(II) and Cd(II).

	$[\text{M-TPY}]^{n+}$			$[\text{TPY-M-TPY}]^{n+}$					
	N_1	N_2	N_3	N_1	N_2	N_3	N_4	N_5	N_6
				Fe(II)					
ρ	0.110	0.110	0.132	0.083	0.083	0.0102	0.083	0.1026	0.083
$\nabla^2\rho$	0.448	0.448	0.670	0.447	0.447	0.690	0.447	0.690	0.447
G	0.137	0.137	0.199	0.121	0.121	0.184	0.121	0.184	0.121
V	-0.162	-0.162	-0.231	-0.130	-0.130	-0.196	-0.130	-0.916	-0.130
H	-0.025	-0.025	-0.032	-0.009	-0.009	-0.012	-0.009	-0.012	-0.009
				Ru(II)					
ρ	0.132	0.148	0.132	0.099	0.120	0.099	0.120	0.099	0.099
$\nabla^2\rho$	0.362	0.464	0.362	0.383	0.564	0.383	0.564	0.0383	0.383
G	0.144	0.180	0.144	0.124	0.179	0.124	0.179	0.124	0.124
V	-0.200	-0.246	-0.200	-0.153	-0.220	-0.153	-0.220	-0.153	-0.153
H	-0.056	-0.067	-0.056	-0.029	-0.041	-0.029	-0.041	-0.029	-0.029
				Cd(II)					
ρ	0.081	0.084	0.081	0.055	0.0057	0.055	0.057	0.054	0.054
$\nabla^2\rho$	0.257	0.309	0.257	0.201	0.208	0.200	0.207	0.197	0.198
G	0.084	0.098	0.084	0.057	0.059	0.057	0.059	0.055	0.056
V	-0.103	-0.119	-0.103	-0.064	-0.067	-0.063	-0.067	-0.062	-0.062
H	-0.020	-0.021	-0.020	-0.007	-0.007	-0.006	-0.007	-0.006	-0.006

4.3.2 Effect of including substituents in TPY

In this subsection, we have studied the effect exerted by functional groups (R) in the phenyl rings of TPY (see Figure 4.1). For that purpose, the complexes of Fe(II) with one and two TPY ligands have been studied. Two functional groups have been elected as representative for electron withdrawing (CN) and electron donating (NH_2) ligands. In Figure 4.4 are depicted the interaction energies and in Figure 4.5 the geometrical parameters. The numerical results are gathered in Table 4.6 and Table 4.7.

It is observed in Figure 4.4 that the presence of an EDG group (NH_2) increases the interaction energy, while the presence of an EWG (CN) has the opposite effect. This can be explained by the inductive and resonance effects accomplished by the substituents in the aromatic ring. Thus, CN group removes charge from the N atom by both inductive and resonance effects, while NH_2 group promotes the basicity of N by resonance. Nevertheless, these effects slightly change the interaction energy, from 346 kcal/mol in the unsubstituted complex to 371 and 323 kcal/mol for the NH_2 and CN derivatives, respectively. This trend is the same for $[\text{Fe-TPY}]^{2+}$ and $[\text{TPY-Fe-TPY}]^{2+}$ complexes.

Table 4.6: Interaction energies in kcal/mol of $[Fe\text{-}TPY]^{2+}$ (ΔH_1) and $[TPY\text{-}Fe\text{-}TPY]^{2+}$ (ΔH_2) complexes substituted with R = H, NH_2 and CN.

	H	NH_2	CN
ΔH_1	342.6	371.2	323.4
ΔH_2	516.0	542.4	478.1

Upon examining the geometrical parameters, it is found that all distances fall within the range of 1.800-2.000 Å in $[Fe\text{-}TPY]^{2+}$ complexes and between 1.900-2.010 Å in $[TPY\text{-}Fe\text{-}TPY]^{2+}$ complexes. As expected, $[TPY\text{-}Fe\text{-}TPY]^{2+}$ complexes exhibit longer distances due to steric hindrance. However, the effect of substituents on the geometrical parameters is almost negligible. Moreover, $[Fe\text{-}TPY]^{2+}$ complexes are non-planar, while $[TPY\text{-}Fe\text{-}TPY]^{2+}$ complexes exhibit planarity. This feature is not due to the substituent, but rather the electronic structure, as discussed in the previous section (4.3.1).
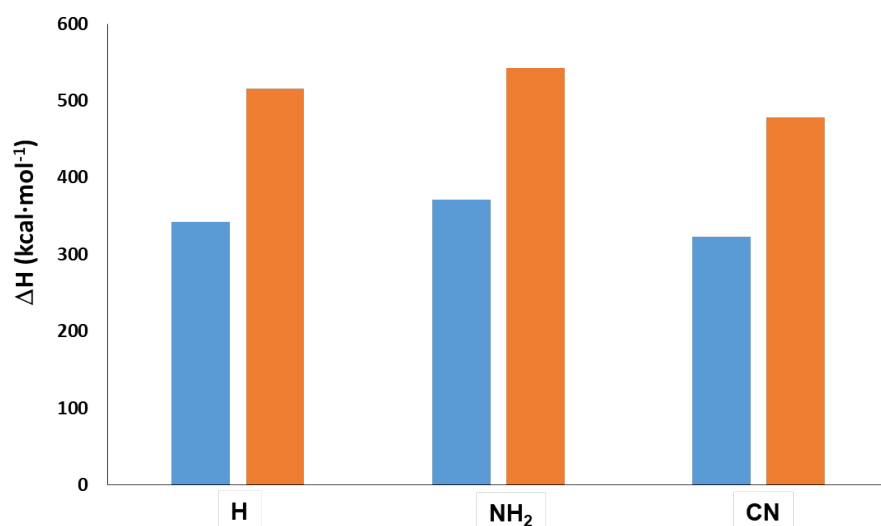
Figure 4.4: Interaction energy of $[Fe\text{-}TPY]^{2+}$ (ΔH_1, blue bars) and $[TPY\text{-}Fe\text{-}TPY]^{2+}$ complexes (ΔH_2, orange bars), in kcal/mol, substituted with R = H, NH_2 and CN.

The analysis of the bond by NBO (Table 4.8 and Table 4.9) and QTAIM (Table 4.10) methodologies show a little impact of the substitution in the interaction with the metal. Thus, the nature of the interaction remains unchanged, meaning that the strength of the interaction is mainly determined by the metal and the ligand itself, rather than by the presence or absence of EDGs and EWGs.
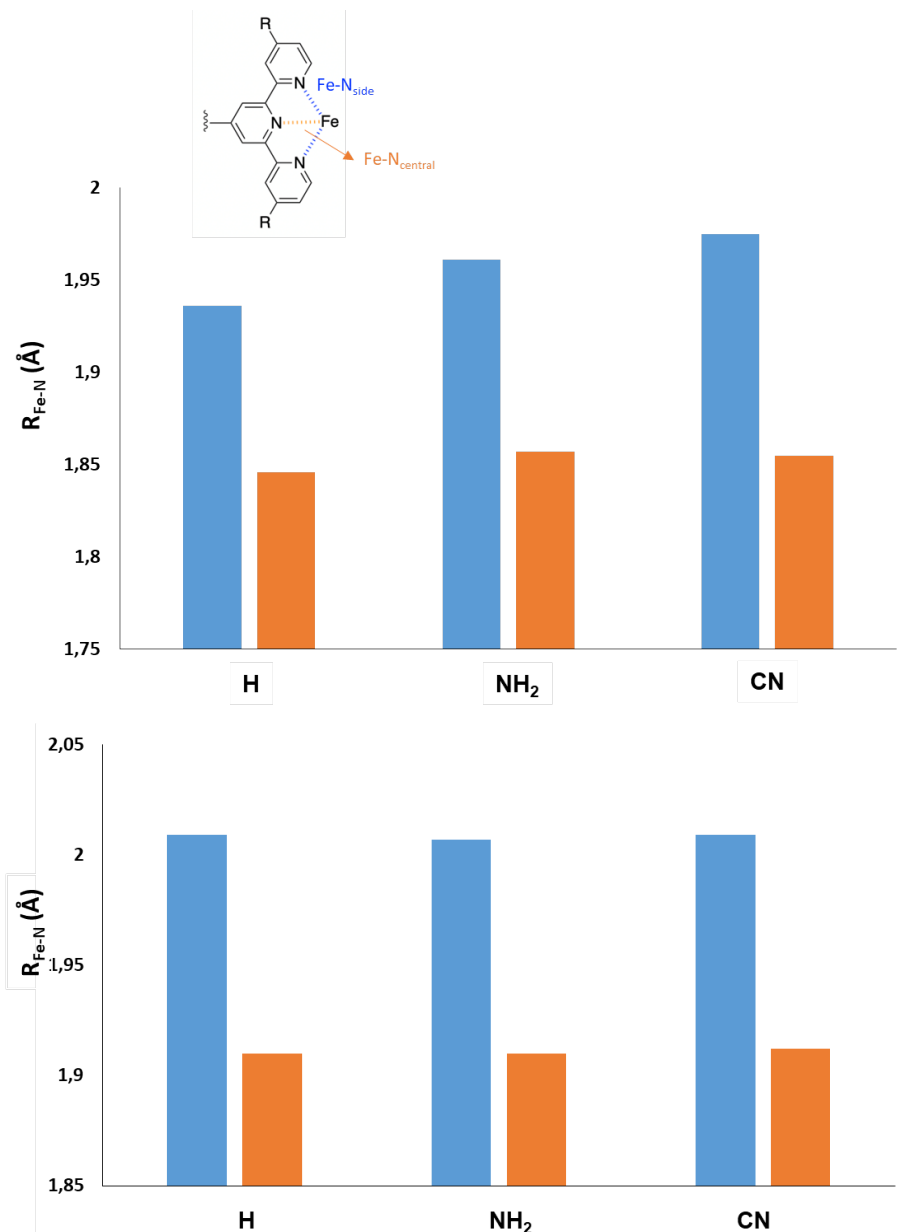
Figure 4.5: Bond distances, in Å, for the Fe(II)-N$_{side}$ (blue bars) and Fe(II)-N$_{central}$ bonds (orange bars) in the [Fe-TPY]$^{2+}$ complexes (top) and [TPY-Fe-TPY]$^{2+}$ complexes (bottom).

Table 4.7: Geometrical parameters in [Fe-TPY]$^{2+}$ and [TPY-Fe-TPY]$^{2+}$ complexes substituted with R = H, NH$_2$ and CN. Distances in Å and dihedral angles in degrees.

	H	NH$_2$	CN
	[Fe-TPY]$^{2+}$		
Fe-N$_1$	1.936	1.961	1.975
Fe-N$_2$	1.846	1.857	1.855
Fe-N$_3$	1.936	1.961	1.975
dihedral	24.6	0.0	0.0
	[TPY-Fe-TPY]$^{2+}$		
Fe-N$_1$	2.008	2.007	2.009
Fe-N$_2$	1.910	1.910	1.912
Fe-N$_3$	2.008	2.007	2.009
Fe-N$_4$	2.008	2.007	2.009
Fe-N$_5$	1.910	1.910	1.912
Fe-N$_6$	2.008	2.007	2.009
dihedral	179.9	180.0	180.0

Table 4.9: Natural bond orbital (NBO) analysis for the [TPY-Fe-TPY]$^{2+}$ complexes with R = H, NH$_2$ and CN substituents. Orbital occupancies of the nitrogen lone pair (LP$_{N_i}$) and the metal atomic orbitals (LP$_{3d}$, LP$_{4s}$ and LP$_{4p}$); variation of the occupation after and before the complexation (Δ_{occ}), and second-order interaction energies (E$^{(2)}$), in kcal/mol.

	H	NH$_2$	CN
LP$_{N_1}$	1.656	1.652	1.658
LP$_{N_2}$	1.650	1.654	1.650
LP$_{N_3}$	1.656	1.652	1.658
Total	4.962	4.958	4.966
Δ_{occ}	-1.038	-1.042	-1.034
E$^{(2)}$	773.1	628.0	634.7
LP$_{N_4}$	1.656	1.652	1.658
LP$_{N_5}$	1.650	1.654	1.650
LP$_{N_6}$	1.660	1.652	1.658
Total	4.966	4.958	4.966
Δ_{occ}	-1.034	-1.042	-1.034
E$^{(2)}$	534.4	627.9	450.5
LP$_{3d}$	6.900	6.892	6.900
LP$_{4s}$	0.277	0.281	0.277
LP$_{4p}$	0.539	0.545	0.054
Total	7.716	7.718	7.231
Δ_{occ}	1.716	1.718	1.231

Table 4.8: Natural bond orbital (NBO) analysis for the $[Fe-TPY]^{2+}$ complexes with R = H, NH_2 and CN substituents. Orbital occupancies of the nitrogen lone pair (LP_{N_i}) and the metal atomic orbitals (LP_{3d}, LP_{4s} and LP_{4p}); variation of the occupation after and before the complexation (Δ_{occ}), and second-order interaction energies ($E^{(2)}$), in kcal/mol.

	H	NH_2	CN
LP_{N_1}	1.701	1.737	1.737
LP_{N_2}	1.615	1.672	1.970
LP_{N_1}	1.701	1.737	1.737
Total	5.017	5.146	5.444
Δ_{occ}	-0.983	-0.854	-0.556
LP_{3d}	6.664	6.675	6.673
LP_{4s}	0.223	0.079	0.077
LP_{4p}	0.061	0.007	0.030
Total	6.948	6.761	6.780
Δ_{occ}	0.948	0.761	0.780
$E^{(2)}$	457.7	424.3	401.2

Table 4.10: Electron density (ρ), kinetic (G), potential (V) and total (H) electron energy densities, and Laplacian of the electron density ($\nabla^2\rho$) at the bond critical points, in a.u., for the $[Fe-TPY]^{2+}$ and $[TPY-Fe-TPY]^{2+}$ complexes, with R = H, NH_2 and CN substituents.

	$[Fe-TPY]^{2+}$			$[TPY-Fe-TPY]^{2+}$					
	N_1	N_2	N_3	N_1	N_2	N_3	N_4	N_5	N_6
				H					
ρ	0.110	0.110	0.132	0.083	0.083	0.0102	0.083	0.0102	0.083
$\nabla^2\rho$	0.448	0.448	0.670	0.447	0.447	0.690	0.447	0.690	0.447
G	0.137	0.137	0.199	0.121	0.121	0.184	0.121	0.184	0.121
V	-0.162	-0.162	-0.231	-0.130	-0.130	-0.196	-0.130	-0.196	-0.130
H	-0.025	-0.025	-0.032	-0.009	-0.009	-0.012	-0.009	-0.012	-0.009
				NH_2					
ρ	0.105	0.105	0.127	0.083	0.102	0.083	0.083	0.102	0.083
$\nabla^2\rho$	0.413	0.413	0.664	0.445	0.696	0.445	0.445	0.696	0.445
G	0.127	0.127	0.194	0.120	0.185	0.120	0.120	0.185	0.120
V	-0.150	-0.150	-0.223	-0.130	-0.197	-0.130	-0.130	-0.197	-0.130
H	-0.023	-0.023	-0.028	-0.009	-0.012	-0.009	-0.009	-0.012	-0.009
				CN					
ρ	0.092	0.127	0.092	0.082	0.102	0.082	0.082	0.102	0.082
$\nabla^2\rho$	0.519	0.676	0.519	0.445	0.685	0.445	0.445	0.685	0.445
G	0.142	0.198	0.142	0.120	0.183	0.120	0.120	0.183	0.120
V	-0.154	-0.227	-0.154	-0.129	-0.194	-0.129	-0.129	-0.194	-0.129
H	-0.012	-0.029	-0.012	-0.009	-0.011	-0.009	-0.009	-0.011	-0.009

4.3.3 Effect of the ligand

In this subsection, the impact of ligand, e.g. the coordinating atom (X), on the interaction is studied. For that purpose, TPY will be substituted by the phosphorus analogous, TPPh (see Figure 4.1).

Phosphinines are aromatic phosphorus heterocycles that possess a distinctive electronic configuration.[210] This unique configuration leads to a weak σ-donor (the lone pair is HOMO-2) and strong π-acceptor character (the LUMO is at low energies, notably lower than that of pyridine).[110] When it comes to coordination with metals, σ-coordination is observed for late transition metals and low oxidation states such as 0 or $+1$. This is because there is a pronounced π back donation from the metal to the phosphinine. Some examples of metals that exhibit σ-coordination with phosphinines include Rh(I),[211] Ru(II),[212,213] and Os(II).[213] However, complexes containing metals in medium-to-high oxidation states are scarce.[214,215] To achieve coordination with metals in medium-to-high oxidation states, one strategy is to use chelating polydentate phosphinines.[110] Thus, hybrid pincer ligands including sulfur (SPS) have been used to synthesize complexes with Group 10 metals such as Ni(II), Pd(II) and Pt(II).[216] Additionally, complexes with pincer ligands including nitrogen (PNP) have also been described in the literature.[217] Overall, phosphinines are a versatile class of ligands with a unique electronic structure that makes them attractive for a variety of metal coordination chemistry.

In this part of the work, different complexes of TPPh with Fe(II) will be studied and compared with the TPY-containing complexes. In Figure 4.6 and Figure 4.7, interaction energies and geometrical parameters are represented, respectively. The numerical values are gathered in Tables 4.11 and 4.12.

Table 4.11: Interaction energies in kcal/mol for the complexes [Fe-TPPh]$^{2+}$ (ΔH_1) and [TPPh-Fe-TPPh]$^{2+}$ (ΔH_2) substituted with R = H, NH$_2$ and CN.

	H	NH$_2$	CN
ΔH_1	294.4	314.9	270.5
ΔH_2	439.6	457.8	414.6

It is observed that the interaction energies of [Fe-TPPh]$^{2+}$ complexes (see Fig. 4.6, orange bars) are lower than those of [Fe-TPY]$^{2+}$ complexes (see Fig. 4.6, blue bars). In addition, the effect of EWG and EDG on TPPh follows the same trend as in TPY ligands, as expected. This trend is also observed when comparing [TPPh-Fe-TPPh]$^{2+}$ and [TPY-Fe-TPY]$^{2+}$ systems.

Examining Figure 4.7, it can be seen that replacing N with P in the ligand results in a significant increase in the metal-ligand distance. When TPY is replaced with TPPh, the electronic structure of the ligand changes and affects the interaction between the iron d-orbitals and the ligand orbitals. TPPh shows lower σ-donor character than TPY, since the lone pair of phosphorus is not the HOMO and, besides, this sp^2 orbital shows greater $3s$ character than that of nitrogen, leading to a poorer overlap with the $3d$
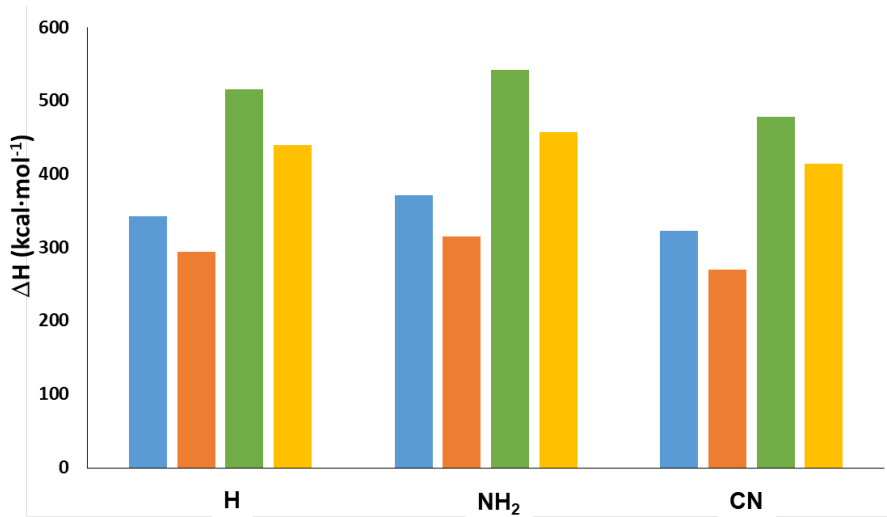
Figure 4.6: Interaction energy of $[Fe(II)-TPY]^{2+}$ (blue bars), $[Fe(II)-TPPh]^{2+}$ (orange bars), $[TPY-Fe(II)-TPY]^{2+}$ (green bars) and $[TPPh-Fe(II)-TPPh]^{2+}$ (yellow bars) complexes, in kcal/mol, substituted with R = H, NH_2 and CN.

orbitals. Thus, comparing the NBO results of $[Fe-TPY]^{2+}$ and $[Fe-TPPh]^{2+}$ complexes with R = H (see Tables 4.8 and 4.13), the electron transfer from P to Fe (0.712) is lower than that from N to Fe (0.948), as well as the second-order interaction between the lone pairs and the unoccupied orbitals of Fe (457 and 420 kcal/mol for TPY and TPPh, respectively). The lower occupation of the Fe orbitals may be also ascribed to a $d\pi$-$p\pi$ retrodonation from Fe to P. Nevertheless, this π-acceptor of phosphinine character may not be strong enough to shorten the bond and increase the interaction energy.

Table 4.12: Geometrical parameters in $[Fe-TPPh]^{2+}$ and $[TPPh-Fe-TPPh]^{2+}$ complexes substituted with R = NH_2 and CN. Distances in Å and dihedral angles in degrees.

	H	NH_2	CN
	$[Fe-TPPh]^{2+}$		
Fe-P$_1$	2.333	2.265	2.309
Fe-P$_2$	2.240	2.175	2.234
Fe-P$_3$	2.333	2.265	2.309
dihedral	6.817	19.694	35.091
	$[TPPh-Fe-TPPh]^{2+}$		
Fe-P$_1$	2.285	2.298	2.286
Fe-P$_2$	2.139	2.155	2.145
Fe-P$_3$	2.285	2.293	2.286
Fe-P$_4$	2.285	2.293	2.286
Fe-P$_5$	2.139	2.154	2.145
Fe-P$_6$	2.285	2.298	2.286
dihedral	180.0	169.1	180.0

Interestingly, the NBO analysis also indicates that a Fe-P covalent bond is formed when TPPh is substituted with NH_2. In this case, the lone pair of P shows a clear sp^2 character (less contribution of the $3s$ orbital), increasing the σ-donation capacity. As a result, the interaction energy is increased and the bond length is shortened (see Figures 4.6 and 4.7).
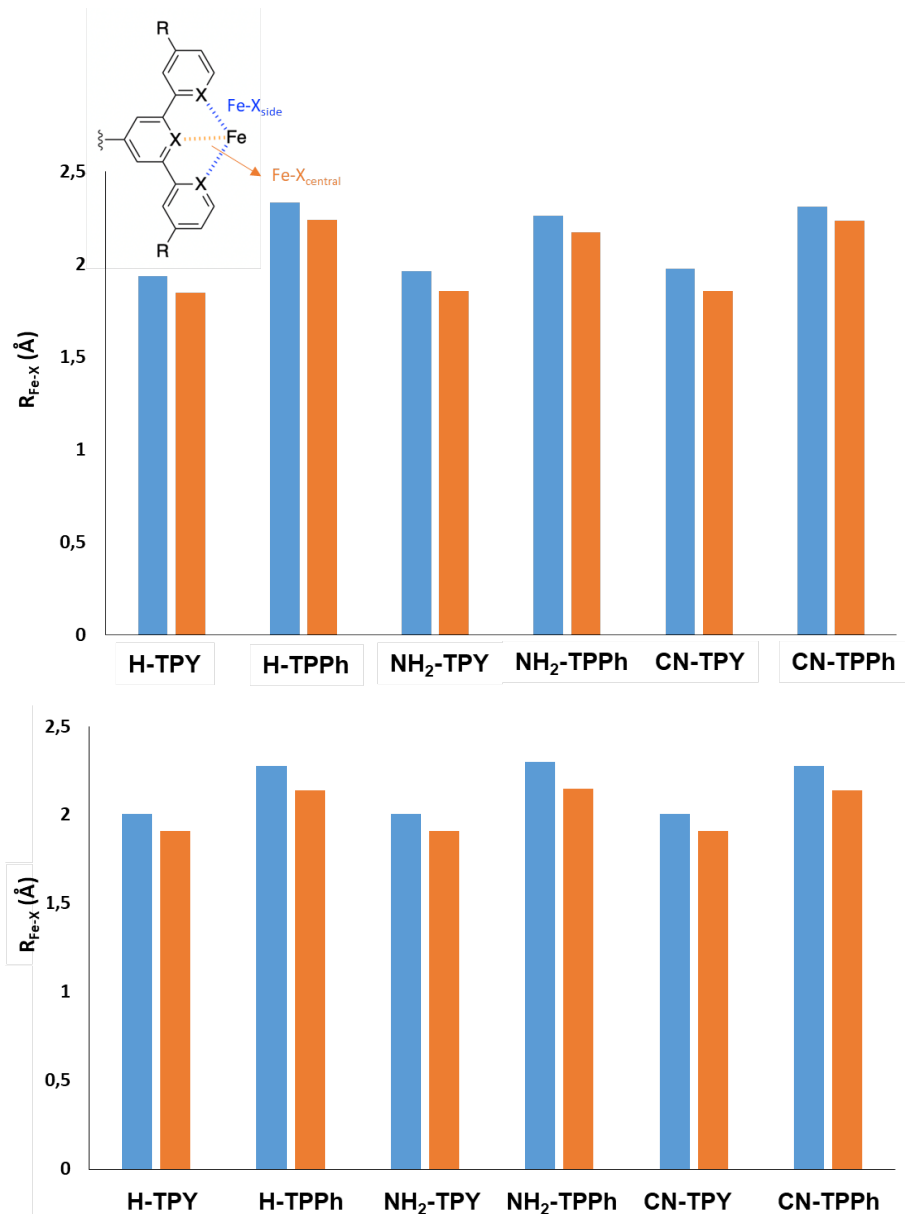
Figure 4.7: Bond distances, in Å, for the Fe(II)-X_{side} (blue bars) and Fe(II)-$X_{central}$ bonds (orange bars) in the [Fe-TPY]$^{2+}$ and [Fe-TPPh]$^{2+}$ complexes (top) and [TPY-Fe-TPY]$^{2+}$ and [TPPh-Fe-TPPh]$^{2+}$ complexes (bottom).

Table 4.13: Natural bonding orbital (NBO) analysis for the $[\text{Fe-TPPh}]^{2+}$ complexes with R = H, NH_2 and CN substituents. Orbital occupancies of the phosphorus lone pair (LP_{P_i}) and the metal atomic orbitals (LP_{3d}, LP_{4s} and LP_{4p}); variation of the occupation after and before the complexation (Δ_{occ}), and second-order interaction energies ($E^{(2)}$), in kcal/mol.

	H	NH_2	CN
LP_{P_1}	1.564	1.568	1.536
LP_{P_2}	1.564	1.568	1.531
LP_{P_3}	1.583	*bond*	1.536
Total	4.711	3.136	4.603
Δ_{occ}	-1.289	-0.864	-1.397
LP_{3d}	6.647	6.097	6.770
LP_{4s}	0.048	0.010	0.051
LP_{4p}	0.017	—	0.054
Total	6.712	6.107	6.875
Δ_{occ}	0.712	0.107	0.875
$E^{(2)}$	420.0	95.31	501.6

Table 4.14: Natural bonding orbital (NBO) analysis for the $[\text{TPPh-Fe-TPPh}]^{2+}$ complexes with R = H, NH_2 and CN substituents. Orbital occupancies of the phosphorus lone pair (LP_{P_i}) and the metal atomic orbitals (LP_{3d}, LP_{4s} and LP_{4p}); variation of the occupation after and before the complexation (Δ_{occ}), and second-order interaction energies ($E^{(2)}$), in kcal/mol.

	H	NH_2	CN
LP_{P_1}	1.057	1.163	1.045
LP_{P_2}	*bond*	1.132	*bond*
LP_{P_3}	*bond*	*bond*	*bond*
Total	1.057	2.295	1.045
Δ_{occ}	-0.943	-1.705	-0.955
$E^{(2)}$	4.48	9.47	4.61
LP_{P_4}	*bond*	1.162	*bond*
LP_{P_5}	*bond*	1.163	*bond*
LP_{P_6}	*bond*	*bond*	*bond*
Total	0	2.325	0
Δ_{occ}	0	-1.675	0
$E^{(2)}$	0	9.48	0
LP_{3d}	5.756	5.782	5.758
LP_{4s}	—	—	—
LP_{4p}	—	—	—
Total	5.756	5.782	5.758
Δ_{occ}	-0.244	-0.218	-0.242

When the TPPh ligand is substituted with the CN group, the NBO analysis shows that there is a greater transfer of electron density to the Fe $3d$ orbitals, which may be related to a weaker $d\pi$-$p\pi$ retrodonation. Inspecting the [TPPh-Fe-TPPh]$^{2+}$ systems, several Fe-P bonds are formed.

The results of the QTAIM analysis for the [Fe-TPPh]$^{2+}$ and [TPPh-Fe-TPPh]$^{2+}$ (R = H) complexes are presented in Table 4.15. Since $\nabla^2\rho > 0$ in all cases, no covalent bond is formed between Fe and P, which indicates that the predicted NBO bonds correspond to an electrostatic interaction with partially covalent nature.

Table 4.15: Electron density (ρ), kinetic (G), potential (V) and total (H) electron energy densities, and Laplacian of the electron density ($\nabla^2\rho$) at the bond critical points, in a.u., for the [Fe-TPPh]$^{2+}$ and [TPPh-Fe-TPPh]$^{2+}$ complexes.

	[Fe-TPPh]$^{2+}$			[TPPh-Fe-TPPh]$^{2+}$					
	N_1	N_2	N_3	N_1	N_2	N_3	N_4	N_5	N_6
ρ	0.073	0.091	0.073	0.104	0.079	0.079	0.079	0.079	0.104
$\nabla^2\rho$	0.156	0.148	0.156	0.234	0.155	0.155	0.0155	0.155	0.234
G	0.064	0.073	0.064	0.099	0.068	0.068	0.068	0.068	0.099
V	-0.090	-0.109	-0.090	-0.140	-0.097	-0.097	-0.097	-0.097	-0.140
H	-0.025	-0.036	-0.025	-0.041	-0.029	-0.029	-0.029	-0.029	-0.041

4.4 Conclusions

In this chapter, we have studied computationally complexes of terpyridine (TPY) and terphosphinine (TPPh) pincers with various transition metals such as Cd(II), Zn(II), Cu(I), Fe(II), Ru(II) and Sc(III), as potential candidates for new dynamic bonds useful in self-healing materials, in order to understand the nature of the interaction.

Firstly, the effect of the transition metal was analyzed. For this purpose, the dissociation energies were analyzed. It was found that there is a decreasing trend of the dissociation energy from left to right in the series, that may correspond to a larger ligand-to-metal charge transfer, due to vacant d orbitals, and resulting in stronger bonds. This trend is in agreement with the variation of the N-M bond distance, which is larger for Cu(I), Cd(II) and Zn(II), and shorter for Fe(II) and Ru(II). Sc(III) is a special case, since the charge transfer takes place in virtual, more energetic orbitals and the large interaction energy is due to the high ionic charge, leading to strong ion-dipole interactions. The steric hindrance may also increase the M-N bond length. The analysis of the bonding reveals partially covalent electrostatic interactions.

Secondly, the impact of electron donating and withdrawing functional groups in the phenyl rings of the ligand was analysed. To do so, both TPY and TPPh ligands were subtituted with EDG (NH$_2$) and EWG (CN) groups. In general, it is found that the

presence of an electron donating group leads to an increase in interaction energy, while an electron withdrawing group results in a decrease. However, the effect on interaction energy is minimal and the geometrical parameters are largely unaffected, indicating that the bond strength is mainly determined by the nature of the metal and the ligand rather than the presence of EDGs and EWGs.

Finally, the impact of the coordinating atom (X) in the ligand is discussed, by comparing Fe(II)-TPY and Fe(II)-TPPh complexes. Additionally, TPPh was also substituted with NH_2 and CN. It was found that the dissociation energies of the complexes with TPPh are lower than those with TPY due to the influence of the ligand's electronic structure on the interaction between the iron d-orbitals and the ligand orbitals. Thus, the phosphorus lone pair is not the HOMO orbital and shows a larger $3s$ character (less sp^2 character) than the nitrogen lone pair, lowering the σ-donor capacity and leading to weaker interactions. Although $d\pi$-$p\pi$ retrodonation is observed, revealing the π-acceptor ability of TPPh, it does not appear to be enough to compensate the weak σ-donor capacity. For TPPh ligands substituted with NH_2 (EDG), higher dissociation energies were found than for TPPh ligands with CN (EWG), in accordance with the results obtained for the TPY ligand.

In conclusion, due to the unusually large interaction energies caused by high charges, proposing a complex to achieve the self-healing property is challenging. Self-healing materials at near-room temperatures commonly show interaction energies ranging from 40-60 kcal/mol, which shows the importance of the counter-ions. The effect of counter-ions, should, hence, be taken into account to reproduce quantitative accurate interaction energies in these materials. Nevertheless, it is very difficult to address the real metal-ion - counter-ion structure in these metallopolymers, since the experiments are usually carried out in bulk and probably metal-counter ion clusters may be formed (see further work for more details). However, we expect that the trends observed based on metal-cation models will be similar to those obtained when including the counter-ions. Based on our results, we believe that it would be interesting to explore the combination of certain aspects to obtain the desired interaction. For instance, combining the pincer ligand with a transition metal located on the right of a series would result in a weaker interaction compared to using a transition metal positioned on the left. On the other hand, introducing substitutes in the pincer ligand could slightly affect the interaction. Alternatively, using the TPPh ligand could be an option to decrease these high interaction energies. Consequently, it can be speculated that $[TPY\text{-}Fe\text{-}TPY]^{+2}$, $[TPPh\text{-}Fe\text{-}TPPh]^{+2}$ and $[TPY\text{-}Zn\text{-}TPY]^{+2}$ complexes could exhibit the self-healing property. Nevertheless, further investigation into the TPPh ligand is needed as part of future work.

Chapter 5

Photophysical properties of metal-ligand based metallopolymers

In this chapter we study how several metal-ligand complexes used as cross-linkers in metallopolymers, similar to those studied in Chapter 4 interact with light. Hence, the main goal in this chapter is to understand the photophysical properties such as absorption and emission processes that may take place in these complexes, which would provide polymeric structures with interesting fluorescent or phosphorescent properties, in addition to the self-healing capacity.

5.1 Introduction

The interaction between light and matter involves both photochemical (chemical reactions triggered by light) and photophysical processes (excitation and deactivation processes with or without light emission). In the latter, in principle, no chemical reactions are involved, and comprise the processes we intend to study in our target materials. Concretely, in photoexcitation, molecules are promoted from the electronic ground state to electronic excited states by photon absorption. This process leads to the absorption spectra in molecules, usually known as UV/Vis spectra. During the absorption process, the excited state and the ground state are of the same spin, due to the selection rules. Once the absorption takes place, the evolution of these electronic excited states may be very different. The main processes may be collected in four different categories, as collected in Figure 5.1 in a Jablonski diagram. The electronic excited state may stay in the same spin state, and may irradiate from the lowest excited state, leading to fluorescence, or may go back to the ground state through internal conversion (IC). In addition to this, the excited state may cross to a state with a different spin state through an intersystem crossing process (ISC). Once there, it may decay to the electronic state through light emission leading to phosphorescence, or without emitting through a second ISC process with the ground state. In summary, there are non-radiative processes, and emitting

ones such as fluorescence and phosphorescence. Our interest is focused on studying the possibility of such emitting properties in the systems under study.
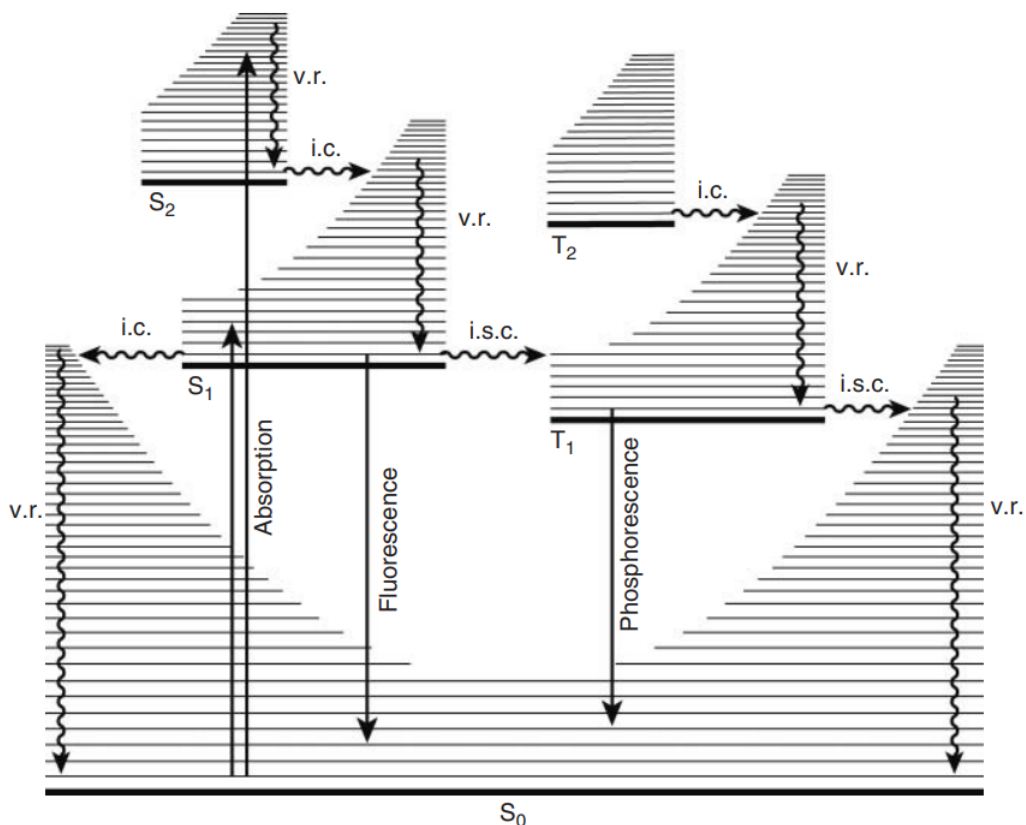

Figure 5.1: Jablonski diagram, representing the ground (S_0) and excited states (S_1, S_2 and T_1) of a molecule and the photophysical processes involved, i.e., absorption, fluorescence, phosphorescence, vibrational relaxation (v.r.), internal conversion (i.c.) and intersystem crossing (i.s.c.). Image taken from Ref. 218.

It is well known that transition metals can absorb and emit photons with several different wavelengths due to their electronic structure. Among inorganic molecules, transition metal complexes are one of the most important in terms of photochemistry and photophysics. Usually, these complexes are highly symmetrical and the transition metal exhibits open-shell d orbital configurations, with different ground-state multiplicities. Additionally, the presence of heavy atoms can induce a significant degree of spin-orbit coupling, particularly in metals from the second and third transition series, which facilitates the ISC processes. For instance, platinum complexes display a formally spin-forbidden absorption band that is similar in intensity to a formally spin-allowed absorption band. In such cases, for complexes with a singlet ground state (S_0), the $S_1 \rightarrow T_1$ intersystem crossing efficiency is usually close to unity and the fluorescence quantum yield is close to zero.[219,220] In the case of ruthenium, for instance, Ru(II)-polypyridine and Ru(II)-2,2'-bipyridine complexes exhibit luminescence, concretely, phosphorescence. In these complexes, the nature of the lowest excited state can be altered by selecting the appropriate metal and/or ligand. Thus, the excited state energy can be greatly modified by changing the ligands involved in metal-to-ligand charge transfer processes (MLCT), and

the energy can be finely tuned by modifying the ligand structure. Substituting ligands that do not participate in MLCT transitions can also result in significant changes in excited state energies.[221,222]

Regarding self-healing materials, it is evident that photophysical processes play a crucial role in the development of innovative materials. These two aspects may be closely related, as seen in the Introduction. Rowan and Weder demonstrated that the self-healing process in metallopolymers was assisted by the release of heat by internal conversion after exposure to ultraviolet light, resulting in low-yield fluorescence.[53] Nevertheless, no further information was provided, to our knowledge, regarding the electronic structure of the complex and the origin of the observed fluorescence. Therefore, a detailed knowledge of the electronic states and the photophysical processes that take place in these complexes is essential to understand the self-healing processes in these materials. Hence, the aim of this chapter is to explore the photophysical properties of several of the complexes studied in the previous chapter of this thesis, e.g., $[\text{TPY-M-TPY}]^{n+}$ for Fe(II), Ru(II), Cd(II), Zn(II) and Ir(III). The latter has been included due to the interesting luminescent properties that their complexes exhibit.[223] Besides, the $[\text{TPPh-Fe-TPPh}]^{2+}$ complex has also been investigated to examine the role of the ligand.

5.2   Computational details

All geometry optimizations have been carried out using the ωB97XD functional[203] within the framework of density functional theory (DFT)[144,145], combined with the 6-31+G(d,p) basis set[204]. To confirm that the optimized structures were minima or transition states in the potential energy surfaces, harmonic frequency calculations have been performed using the same level of theory. Once the ground state geometries were optimized and electronic structures were properly characterized, photophysical properties were calculated by means of TDDFT,[156] at the same level of theory used for the ground state calculations. In order to study absorption properties, the lowest-lying twenty vertical transition energies and their corresponding oscillator strengths were computed to identify the most probable transitions. Then, the evolution of the lowest singlet and triplet excited states were calculated by optimizing their geometries, and analyzing the state crossing and oscillator strengths to predict in this way emission properties such as fluorescence and phosphorescence. All calculations have been performed using the Gaussian 16[187] program.

5.3   Results and discussion

In this section, the photophysical properties of $[\text{XXX-M-XXX}]^{n+}$ and $[\text{M-XXX}]^{n+}$ complexes have been studied for M = Cd(II), Zn(II), Fe(II), Ru(II) and Ir(III), with XXX = TPY and TPPh (terpyridine and terphosphinine). First of all, in subsection 5.3.1, the

absorption properties of TPY complexes (with one and two ligands) are studied. In order to see the influence of the ligand, the $[TPPh\text{-}Fe\text{-}TPPh]^{2+}$ and $[Fe\text{-}TPPh]^{2+}$ complexes are analysed. Afterwards, the emission properties of the same complexes are studied in 5.3.2 subsection.

5.3.1 Absorption spectra

To assess the absorption characteristics, vertical transition states have been calculated at the ground state geometries for each mentioned system. The calculated spectra are depicted in Figure 5.2 and numerical data collected in Table 5.1 for single pincer ligands, and in Figure 5.3 and Table 5.2 for two pincer ligands, respectively. It should be pointed out that although up to twenty singlet states and ten triplet states were calculated, only the lowest excited states with non-zero oscillator strengths are collected in the Tables. Figures display the absorption spectra in the range of the near UV/vis regions. All the remaining data are given in Appendix A.1.
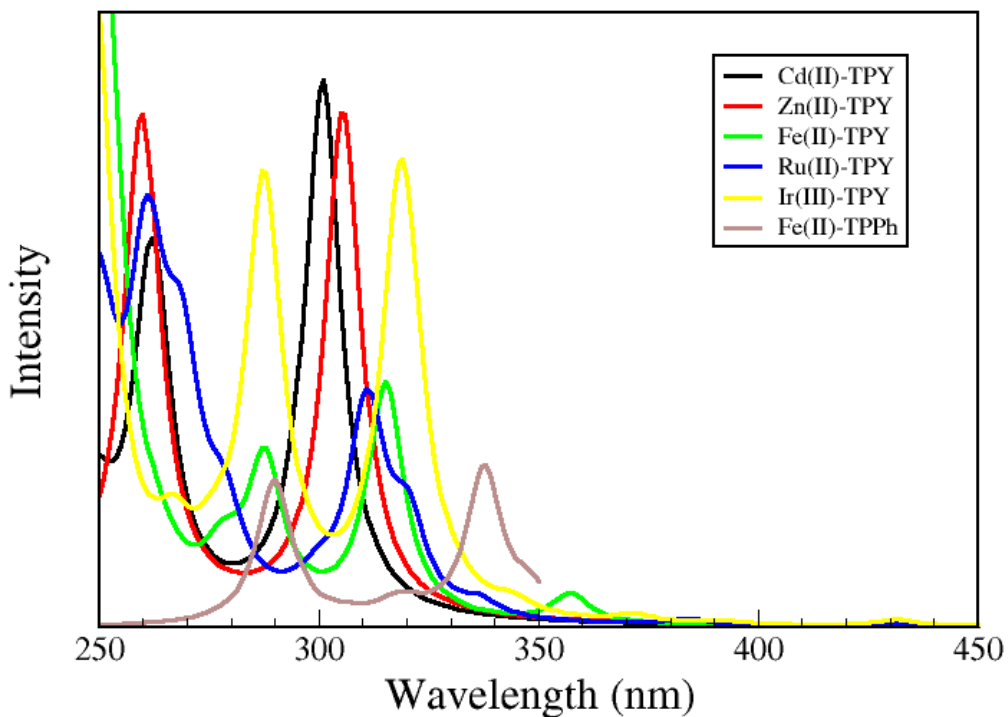

Figure 5.2: Calculated absorption spectra of $[Cd\text{-}TPY]^{2+}$, $[Zn\text{-}TPY]^{2+}$, $[Fe\text{-}TPY]^{2+}$, $[Ru\text{-}TPY]^{2+}$, $[Ir\text{-}TPY]^{3+}$ and $[Fe\text{-}TPPh]^{2+}$ complexes in the range of 250 nm - 450 nm.

First of all, we will focus on the absorption properties of single pincer ligand com-

plexes. As can be seen in Figure 5.2, [Zn-TPY]$^{2+}$ and [Cd-TPY]$^{2+}$ systems exhibit similar spectra, as expected since both have the same valence electronic configuration (nd^{10}). This first peak is located around 300 nm. [Fe-TPY]$^{2+}$ and [Ru-TPY]$^{2+}$ complexes, whose metals are isovalent (nd^6), show similar intense peaks around 310 nm. [Ir-TPY]$^{3+}$ system also exhibits a peak at 320 nm, notably more intense than those of [Fe-TPY]$^{2+}$ and [Ru-TPY]$^{2+}$. For [Fe-TPPh]$^{2+}$ system, the first peak is observed at around 340 nm, indicating a redshift in the spectrum due to the change of the ligand, compared to the [Fe-TPY]$^{2+}$ case.

The numerical details of the above mentioned peaks for [M-XXX]$^{n+}$ complexes are collected in Table 5.1. Concretely, the excited state the transition occurs to, the excitation energies and photon wavelengths, oscillator strengths, and the nature of the transition are given. Focusing first on [Cd-TPY]$^{2+}$ and [Zn-TPY]$^{2+}$, whose metals have closed shell configurations, the vertical transitions take place to the S$_2$ and S$_1$ states, respectively. The excitation energies are around 4.1 eV, which correspond to photons with wavelengths of 301 nm and 306 nm, respectively. Note that oscillator strengths are also similar, around 0.3. Hence, both transitions are very similar in these complexes. The analysis of the nature of the transition shows that, while in [Cd-TPY]$^{2+}$ the transition corresponds to HOMO (H) $\to$ LUMO (L)+1, in the case of [Zn-TPY]$^{2+}$ it corresponds to H $\to$ L transition, being in both cases a ligand (P) to metal (M) transition.

Table 5.1: Calculated absorption properties of the lowest-lying singlet states of [M-XXX]$^{n+}$ complexes. The final state (State, S$_i$), transition energy (ΔE) in eV, and the corresponding photon wavelength (λ values in parenthesis) in nm and oscillator strength (f) are given. Orbitals involved in the transition are denoted as H for HOMO and L for LUMO, and X for multiple transitions. Different parts of the complex are denoted as P for ligand and M for metal to summarize the nature of the transition.

	State	ΔE (λ)	f	Transition	Nature
		[M-TPY]$^{n+}$			
Cd(II)	S$_2$	4.12 (301)	0.306	H $\to$ L+1	P $\to$ M
Zn(II)	S$_1$	4.06 (306)	0.289	H $\to$ L	P $\to$ M
Fe(II)	S$_8$	3.93 (315)	0.133	H $\to$ L+1	P $\to$ M
Ru(II)	S$_{10}$	3.99 (311)	0.117	H-2 $\to$ L+1	P $\to$ M
Ir(III)	S$_{11}$	3.87 (321)	0.087	X $\to$ X	P $\to$ M
		[M-TPPh]$^{n+}$			
Fe(II)	S$_{14}$	3.67 (338)	0.084	X $\to$ X	P $\to$ M

The results obtained for [Fe-TPY]$^{2+}$ and [Ru-TPY]$^{2+}$ complexes show some similarities. On one hand, the absorption energies are slightly smaller than those obtained for [Cd-TPY]$^{2+}$ and [Zn-TPY]$^{2+}$ complexes. Concretely, the calculated values are 3.93 eV and 3.99 eV, corresponding to absorbed photons of 315 and 311 nm, respectively. The oscillator strengths are similar for [Fe-TPY]$^{2+}$ and [Ru-TPY]$^{2+}$ complexes, with values around 0.1, which are much smaller than those obtained for [Cd-TPY]$^{2+}$ and [Zn-TPY]$^{2+}$ complexes. Regarding the orbitals involved in the transitions, in [Fe-TPY]$^{2+}$ complex the

transition corresponds to H $\to$ L+1, while for [Ru-TPY]$^{2+}$ the transition corresponds to H-2 $\to$ L+1. In both cases, the nature of the transition is similar to [Cd-TPY]$^{2+}$ and [Zn-TPY]$^{2+}$ complexes, namely, P $\to$ M transition. The main difference between [Fe-TPY]$^{2+}$/[Ru-TPY]$^{2+}$ complexes and [Cd-TPY]$^{2+}$/[Zn-TPY]$^{2+}$ complexes is that in the former the transitions in the UV region are up to the S$_8$ and S$_{10}$ states, respectively. This is probably due to the fact that the open-shell electronic configuration of the metal allow for other lower transitions, as may be seen in the Appendix A.1.

This effect is even more noticeable in the case of [Ir-TPY]$^{3+}$ complex, where the orbitals involved in the transition show multielectronic transition influence. Due to this influence, the excitation energies and oscillator strengths differ slightly from other medium TM systems, with an absorption energy of 3.87 eV, corresponding to a photon of 321 nm and a lower oscillator strength. Nevertheless, as in other cases, the transition nature is clearly a metal to ligand transition, like in other cases. Finally, the values obtained for [Fe-TPPh]$^{2+}$ show similar trends, but with a red-sift and lower intensities in comparison to its TPY counterpart.
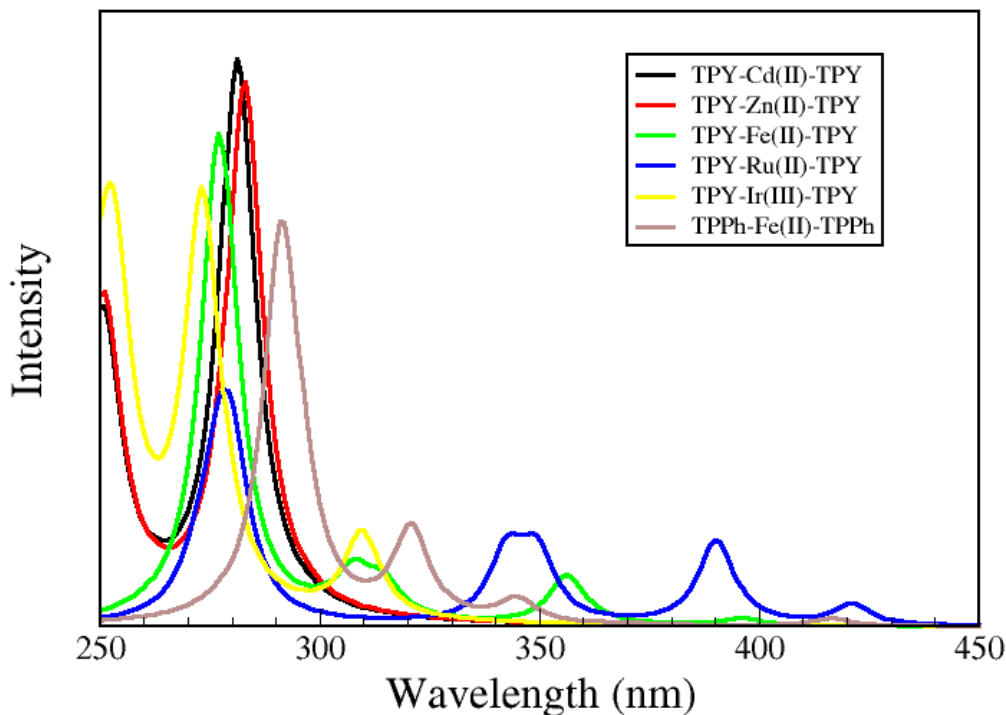

Figure 5.3: Calculated absorption spectra of [TPY-Cd-TPY]$^{2+}$, [TPY-Zn-TPY]$^{2+}$, [TPY-Fe-TPY]$^{2+}$, [TPY-Ru-TPY]$^{2+}$, [TPY-Ir-TPY]$^{3+}$ and [TPPh-Fe-TPPh]$^{2+}$ complexes, in the range of 250 nm - 450 nm.

The optical absorption properties of two pincer ligands will be examined by study-

ing [XXX-M-XXX]$^{n+}$ systems. Figure 5.3 displays the absorption spectra of [XXX-M-XXX]$^{n+}$ complexes in the near UV range (250-450 nm). It can be observed that [TPY-Zn-TPY]$^{2+}$ and [TPY-Cd-TPY]$^{2+}$ systems exhibit similar peaks, both showing an intense peak around 280 nm, which is expected for late TM species. For the middle TM complexes, [TPY-Fe-TPY]$^{2+}$, [TPY-Ru-TPY]$^{2+}$ and [TPY-Ir-TPY]$^{3+}$ the most intense peaks are around 280 nm as well, but there are some other less intense peaks at larger wavelengths. [TPY-Ru-TPY]$^{2+}$ complex is the one having the peak most red-shifted at around 425 nm, while [TPY-Ir-TPY]$^{3+}$ behaves in the opposite way and its first peak appears at around 330 nm. [TPY-Fe-TPY]$^{2+}$ complex show a variety of low intensity peaks at wavelengths larger than 300 nm as well, in addition to the most intense peak at around 280 nm. The first peak appear at around 390 nm, with very small intensity. The change of the ligand affects the absorption spectra as in the one-pincer complexes. The [TPPh-Fe-TPPh]$^{2+}$ complex exhibits the most intense peak around 280 nm as well, and others at larger wavelengths, being the first one at 416 nm. Compared to the [TPY-Fe-TPY]$^{2+}$ case, it can be seen that the spectrum is similar but for [TPPh-Fe-TPPh]$^{2+}$ is red-shifted towards larger wavelengths. Hence, based on the results of one and two-pincer complexes, TPPh ligand provokes a red-shift in the spectra.

The numerical results regarding the most important features of absorption for [XXX-M-XXX]$^{n+}$ systems are summarized in Table 5.2, which includes the excited state the transition occurs to, the excitation energies and photon wave lengths, oscillator strengths, and the nature of the transition. The results for late TM systems show a consistency between [TPY-Cd-TPY]$^{2+}$ and [TPY-Zn-TPY]$^{2+}$ complexes. In both cases, the vertical transitions to singlet states are degenerate, with S_1 and S_2 states being degenerate for both species. Furthermore, the absorption energy is nearly identical, around 4.4 eV with [TPY-Cd-TPY]$^{2+}$ exhibiting a transition from H-1 $\rightarrow$ L+1, while [TPY-Zn-TPY]$^{2+}$ shows a transition from H $\rightarrow$ L. In both cases, no metal contribution is observed in these orbitals, and hence it can be concluded that the nature of the transition is mainly ligand to ligand.

When considering earlier TM systems, [TPY-Fe-TPY]$^{2+}$ complex shows three significant transitions with non zero oscillator strength in the near UV region. The first two, to S_4 and S_5, are degenerate, with excitation energies of 3.13 eV. In both cases, the transition occurs from the same orbital to different ones, namely H-1 $\rightarrow$ L+6 and L+7, respectively. The excitation with the largest oscillator strength happens to S_{10} state, with an excitation energy of 3.47 eV. In this case the transition occurs from H $\rightarrow$ L. In all cases, the transition may be considered as being ligand to metal. [TPY-Ru-TPY]$^{2+}$ complex shows a more intense peak at 390 nm, having a less intense peak to S_1 at 2.94 eV (421 nm). The most intense peak occurs for S_5, being also a metal-to-ligand transition like in the Fe(II) case. For [TPY-Ir-TPY]$^{3+}$ complex, there are four transitions in the near UV. The first two, to S_1 and S_2 states, are degenerate (310 nm) and the transition is from H-1 and H $\rightarrow$ L, respectively. The latter two are also degenerate and occur to S_6 and S_7 states, happening at 273 nm. The transitions occurs from H-2 $\rightarrow$ L and L+1, respectively. Taking into account these results, the main difference between earlier and late TM is that for the former the transitions are likely M $\rightarrow$ P, while for the latter they occur in the ligand. Finally, the results obtained for the [TPPh-Fe-TPPh]$^{2+}$

show a red-shift in comparison to the $[\text{TPY-Fe-TPY}]^{2+}$ case. The lowest-lying transition occurs to S_2 state, which happens at 416 nm. Notice that the effect of the ligand change is that excitation energies occur at lower energies, and that the involved orbitals have more mix than in TPY complexes.

Table 5.2: Calculated absorption properties of the lowest-lying singlet states of $[\text{XXX-M-XXX}]^{n+}$ complexes. The final state (State, S_i; S_i - S_j for degenerate states), transition energy (ΔE) in eV and the corresponding photon wavelength (λ values in parenthesis) in nm and oscillator strength (f) are given. Orbitals involved in the transition are denoted as H for HOMO and L for LUMO, and X for multiple transitions. Different parts of the complex are denoted as P for ligand and M for metal to summarize the nature of the transition.

	State	ΔE (λ)	f	Transition	Nature
		$[\text{TPY-M-TPY}]^{n+}$			
Cd(II)	S_1	4.41 (281)	0.363	H-1 → L+1	P → P
	S_2	4.41 (281)	0.363	H → L	P → P
Zn(II)	S_1	4.39 (283)	0.348	H → L	P → P
	S_2	4.39 (283)	0.348	H-1 → L	P → P
Fe(II)	S_1	2.09 (594)	0.000	H → L+1	M → P
	S_4 - S_5	3.13 (396)	0.005	H-1 → L+6	M → P
	S_{10}	3.48 (356)	0.064	H-1 → L	M → P
	S_{15}	4.03 (308)	0.056	H → L+3	M → P
	S_{19} - S_{20}	4.47 (277)	0.319	X → X	M → P
Ru(II)	S_1	2.94 (421)	0.014	H → L+1	M → P
	S_5	3.18 (390)	0.110	H-1 → L	M → P
Ir(III)	S_1	4.00 (310)	0.055	H-1 → L	M → P
	S_2	4.00 (310)	0.055	H → L	M → P
	S_6	4.54 (273)	0.265	H-2 → L	M → P
	S_7	4.54 (273)	0.265	H-2 → L+1	M → P
		$[\text{TPPh-Fe-TPPh}]^{2+}$			
Fe(II)	S_1	2.27 (547)	0.000	X → X	P → M
	S_2	2.98 (416)	0.005	X → X	P → M
	S_9 - S_{10}	3.60 (345)	0.015	X → X	P → M
	S_{11} - S_{12}	3.87 (320)	0.059	X → X	P → M
	S_{14} - S_{15}	4.20 (296)	0.023	X → X	M → P
	S_{17}	4.26 (291)	0.496	X → X	M → P

Therefore, in conclusion, apparently all the systems under study would have absorption properties within the ultraviolet range, and the replacement of the pincer ligand from TPY to TPPh results in the shift of the absorption range towards lower energies, being in the visible region for the two-pincer complexes.

5.3.2 Emission spectra

Once the absorption properties of the studied complexes have been properly character-ized, the evolution of the excited states have been studied. In this vein, in order to check whether these complexes may have emitting properties or if the energy decays through internal conversion (IC) or intersystem crossing (ISC) processes, geometry opti-mization calculations have been carried out for both S_1 and T_1 electronic states of all the $[M\text{-}XXX]^{n+}$ and $[XXX\text{-}M\text{-}XXX]^{n+}$ complexes previously studied. Once these geometry optimizations are carried out, vertical excitations to singlet and triplet states have been calculated from such optimized geometries in order to characterize both fluorescent and phosphorescent properties. First, the possibility of fluorescence has been studied and the obtained results are summarized below.

Fluorescence of $[M\text{-}XXX]^{n+}$ and $[XXX\text{-}M\text{-}XXX]^{n+}$ complexes

First of all, the optimized geometries for the S_1 electronic excited states have been cal-culated by means of TDDFT. At this S_1 optimized geometry vertical excitation energies have been calculated for different singlet and triplet excited states. The obtained re-sults are summarized in Table 5.3 and Table 5.4 for $[M\text{-}XXX]^{n+}$ and $[XXX\text{-}M\text{-}XXX]^{n+}$ complexes, respectively.

Let us focus first on one-pincer complexes. Table 5.3 collects the most significant vertical transitions to S_0 at the optimized geometry of the S_1 electronic state. Concretely, the starting singlet states, transition energies and corresponding photon wavelengths and oscillator strengths are given, along with the orbitals involved in the transition and its nature. Regarding the late TM systems, such as $[Cd\text{-}TPY]^{2+}$ and $[Zn\text{-}TPY]^{2+}$, a clear difference may be seen at first glance. While the S_1 state of $[Zn\text{-}TPY]^{2+}$ complex is radiative in the UV region at 3.66 eV, the S_1 state of $[Cd\text{-}TPY]^{2+}$ complex is not. In addition, it is located much closer in energy, in the visible spectrum at 1.93 eV. For $[Cd\text{-}TPY]^{2+}$ complex, three radiative states have been characterized, concretely, S_3, S_4 and S_7 states. All of them are in the UV region, at 3.29 eV, 3.78 eV and 4.29 eV, respectively. However, the largest intensity is calculated for the latter, with an oscillator strength of 0.625. In both complexes, the lowest possible emitting transitions correspond to $P \rightarrow M$ transition. In the case of earlier TM systems, only the geometry of the S_1 for the $[Ru\text{-}TPY]^{2+}$ complex was optimized. For the remaining $[Fe\text{-}TPY]^{2+}$ and $[Ir\text{-}TPY]^{3+}$ complexes, we encountered many technical issues and we were not able to reach the optimal geometries. For $[Ru\text{-}TPY]^{2+}$, S_1 is not a radiative state, since the oscillator strength is 0.000. In addition to this, it is located in the IR region, which would allow for an IC process and getting back to the ground state by a non-radiative process. The higher S_9 and S_{10} states could be radiative states with low probability since the most probable evolution of excited states is to end up in the S_1 state. However, some few molecules might decay from these states emitting in the UV region at around 3.9 eV. A very similar pattern is found for $[Fe\text{-}TPPh]^{2+}$ complex, where the first excited state is non-radiative, and might undergo a non-radiative decay via internal conversion. Nevertheless, there are

some possible radiative states located higher in energy, which would emit in this case in the visible region at around 2.8 eV, in the blue region. In these last two complexes, the transitions evolve multielectronic excitations and it is not possible to determine properly the nature of the transition.

Table 5.3: Calculated TDDFT most significant vertical transitions to S_0 at the optimized geometry of S_1 electronic state for [M-XXX]$^{n+}$ complexes. For each system, the starting singlet states (State, S_i), transition energies (ΔE) in eV and corresponding photon wavelengths (λ values in parenthesis) in nm, and oscillator strengths (f) are given. Orbitals involved in the transition are denoted as H for HOMO, L for LUMO, and X for multiple transitions. Finally, different parts of the complex are denoted as P for the ligand and M for the metal to summarize the nature of the transition. C denotes that all complex is involved in the transition.

	State	ΔE (λ)	f	Transition	Nature
		[M-TPY]$^{n+}$			
	State	ΔE (λ)	f	Transition	Nature
Cd(II)	S_1	1.93 (645)	0.000	H → L	P → M
	S_3	3.29 (376)	0.002	X → X	P → M
	S_4	3.78 (328)	0.057	X → X	C → C
	S_7	4.29 (289)	0.625	X → X	C → C
Zn(II)	S_1	3.66 (339)	0.317	H → L	P → M
Fe(II)	—	—	—	—	—
Ru(II)	S_1	0.77 (1600)	0.000	X → X	C → C
	S_9	3.87 (320)	0.048	X → X	C → C
	S_{10}	3.99 (311)	0.117	X → X	C → C
Ir(III)	—	—	—	—	—
		[M-TPPh]$^{n+}$			
Fe(II)	S_1	0.07 (17979)	0.000	X → X	P → M
	S_8	2.73 (454)	0.088	X → X	C → C
	S_{10}	2.97 (417)	0.008	X → X	C → C

Based on these results, we could conclude that fluorescence in these one-pincer complexes is not very probable. Emission in the UV region would be possible mostly for late transition metal complexes, while for middle transition metal complexes internal conversion processes would end up in a non-radiative decay towards the ground state, and less probable emission from higher excited state would also be plausible but in the UV region, with the exception of TPPh containing complexes. As for absorption, apparently there is a red-shift also in the emission properties. However, for a complete picture of fluorescence activity we should analyze the two-pincer complexes as well. The electron distribution is closely linked to the chemical structure of the compound, and the inclusion of a new pincer ligand can alter the bonding and interactions between the metal ion and the ligands, leading to changes in the emission properties.

Hence, geometry optimizations were carried out for the first excited singlet states (S_1) for the [XXX-M-XXX]$^{n+}$ complexes, and vertical excitations from different singlet states

to the ground states were computed, as done for one-pincer complexes. All the results are collected in Table 5.4, which includes the starting singlet states, transition energies and corresponding photon wavelengths and oscillator strengths are given, along with the orbitals involved in the transition and its nature. According to the results obtained for late TM systems, both $[TPY-Cd-TPY]^{2+}$ and $[TPY-Zn-TPY]^{2+}$ complexes have radiative S_1 states, with large oscillator strengths in the UV region, emitting at 281 nm and 311 nm, respectively. Note that for the $[TPY-Cd-TPY]^{2+}$ complex, the absorption and emission for S_1 state is similar, indicating that the geometry of the excited state is very similar to that of the ground state. However, for $[TPY-Zn-TPY]^{2+}$ complex the emission occurs at lower energies, as expected, which indicates the relaxation of the S_1 state. The nature of the transition indicates a ligand to ligand transition, which shows that the nature of the transition is not affected by the relaxation of the excited state.

Table 5.4: Calculated TDDFT most significant vertical transitions to S_0 at the optimized geometry of S_1 electronic state for $[XXX-M-XXX]^{n+}$ complexes. For each system, the starting singlet states (State, S_i), transition energies (ΔE) in eV and corresponding photon wavelengths (λ values in parenthesis) in nm, and oscillator strengths (f) are given. Orbitals involved in the transition are denoted as H for HOMO, L for LUMO, and X for multiple transitions. Finally, different parts of the complex are denoted as P for the ligand and M for the metal to summarize the nature of the transition. C denotes that all complex is involved in the transition.

	State	ΔE (λ)	f	Transition	Nature
$[TPY-M-TPY]^{n+}$					
Cd(II)	S_1	4.41 (281)	0.363	X $\rightarrow$ X	P $\rightarrow$ P
Zn(II)	S_1	3.99 (311)	0.390	X $\rightarrow$ X	P $\rightarrow$ P
Fe(II)	S_1	1.45 (853)	0.000	X $\rightarrow$ X	P $\rightarrow$ M
	S_{10}	3.69 (336)	0.065	X $\rightarrow$ X	M $\rightarrow$ P
Ru(II)	S_1	2.61 (476)	0.011	H $\rightarrow$ L	M $\rightarrow$ P
	S_3	2.92 (425)	0.015	H $\rightarrow$ L+1	M $\rightarrow$ P
	S_4	3.00 (414)	0.057	X $\rightarrow$ X	M $\rightarrow$ P
Ir(III)	S_1	2.22 (557)	0.000	X $\rightarrow$ X	P $\rightarrow$ M
	S_6	4.15 (299)	0.085	X $\rightarrow$ X	C $\rightarrow$ C
	S_7	4.16 (298)	0.166	X $\rightarrow$ X	C $\rightarrow$ C
$[TPPh-M-TPPh]^{n+}$					
Fe(II)	S_1	1.32 (939)	0.000	X $\rightarrow$ X	P $\rightarrow$ M
	S_9-S_{10}	3.60 (344)	0.026	X $\rightarrow$ X	C $\rightarrow$ C

In the case of medium TM systems, the first excited state is a non-radiative state with a zero oscillator strength, with the exception of $[TPY-Ru-TPY]^{2+}$ complex, which shows a radiative state in the visible region at 476 nm. In all cases, the S_1 state is high enough above the ground state to prevent an internal conversion decay. Hence, irradiation from higher electronic states or intersystem crossing to other triplet states would be possible. This possibility will be studied in the next subsection. The irradiation from higher singlet electronic states would occur for $[TPY-Fe-TPY]^{2+}$ and $[TPY-Ir-TPY]^{3+}$ complexes in the

UV region, since the excited states with non-zero oscillator strengths are much higher than the lowest excited state, with wavelengths corresponding to the UV region. Focusing on the nature of the transition, with the exception of [TPY-Ru-TPY]$^{2+}$ complex, the transitions correspond to ligand to metal transitions or transitions involving the whole complex. For [TPY-Ru-TPY]$^{2+}$ complex, on the other hand, metal-to-ligand transitions appear to be the more significant, and might be the cause of the possible emission in the visible range. Finally, the calculated properties for the [TPPh-Fe-TPPh]$^{2+}$ complex are very similar to those of [TPY-Fe-TPY]$^{2+}$, and are red-shifted as in the previous cases.

In summary, we may distinguish a very different behavior between the late transition metal complexes and the middle transition metals, and between one- and two-pincer ligands. One-pincer middle transition metal complexes may undergo a non-radiative internal conversion process, while late transition metal complexes are prevented to this process by much higher location of the first excited state. For two-pincer ligands, on the contrary, no internal conversion processes are predicted. Late TM complexes may emit from the first excited state, while middle transition metal complexes, with the exception of the [TPY-Ru-TPY]$^{2+}$ complex, would emit from higher excited states in the UV region. The only complex which is predicted to emit from the first singlet state in the visible region is the [TPY-Ru-TPY]$^{2+}$ complex, which would be fluorescent according to our data. However, the possibility of crossing towards triplet states through an intersystem crossing process should also be considered. This possibility will be studied in some detail in the next subsection.

Phosphorescence of [XXX-M-XXX]$^{n+}$ complexes

In general, phosphorescence arises when light is emitted from a triplet electronic excited state to the singlet electronic ground state. In the complexes under study, where the ground and excited states are singlets, the first step to have phosphorescent properties is to locate an intersystem crossing that allows the spin state change to a triplet state, which eventually would end up in the T_1 excited state. If this step is possible, then the excited state geometry would be relaxed to the optimal geometry of the lowest triplet state, and would emit from that geometry. The study of intersystem crossing is very complicated because the geometry of the crossing point has to be located and the spin-orbit coupling evaluated. In this work, we have only carried out preliminary calculations on two selected cases, namely, [TPY-Zn-TPY]$^{2+}$ and [TPY-Ru-TPY]$^{2+}$. Concretely, the relative location of the lowest three triplet states have been calculated at the S_0 and S_1 optimal geometries, in order to check for the energy crossing between singlet and triplet states. Energy crossing could be seen as a first condition for intersystem crossing. Then, the geometry is optimized for the lowest triplet state and the energy with respect to S_0 is calculated at this point. The energy difference between these two states at such optimized geometry would be indicative of a possible emission in the visible range.

The obtained results are collected in Table 5.5. Focusing on the [TPY-Zn-TPY]$^{2+}$ case, the energy difference between singlet and triplet states decreases when the complex

is excited from S_0 to S_1 and the geometry is relaxed in this state. The same occurs for the [TPY-Ru-TPY]$^{2+}$ complex. According to this, the S_1 electronic state probably crosses other higher triplet states and could undergo a spin change through an intersystem crossing process. If this occurs, the complex geometry would relax to that of the optimal geometry of the T_1 state. We have carried out geometry optimizations for both the [TPY-Zn-TPY]$^{2+}$ and the [TPY-Ru-TPY]$^{2+}$ complexes, and in both cases the T_1 state is kept higher in energy by 2.38 eV and 1.63 eV, respectively. In both cases, the emission from the triplet would happen in the visible range. Hence, according to these preliminary results, at least in these two complexes, phosphorescence would be a possible evolution of the excited state. Nevertheless, we can not ensure that these complexes would be phosphorescent, and further calculations should be carried out in order to predict the most probable evolution of the excited state.

Table 5.5: Results of TDDFT calculations for emission properties of [XXX-M-XXX]$^{n+}$ complexes. For each system, transition energies (ΔE) in eV of the most significant singlet states (S_i) and the first three triplet states (T_1, T_2 and T_3) are collected. Note that S_0, S_1 and T_1 stands for the transition states optimized at those geometries.

	State	S_0	S_1	T_1
	S_1	4.39	3.99	
	T_1	2.74	2.73	2.38
Zn(II)	T_2	3.00	2.96	
	T_3	3.13	3.38	
	S_1	2.94	2.61	
	S_3	3.07	2.93	
Ru(II)	T_1	2.29	2.16	1.63
	T_2	2.38	2.32	
	T_3	2.50	2.52	

5.4 Conclusions

In this chapter, we have studied the optical properties of some metal-ligand complexes used in synthesized materials. Concretely, the absorption and emission properties of [M-XXX]$^{n+}$ and [XXX-M-XXX]$^{n+}$ complexes have been studied, being M transition metals such as Zn(II), Cd (II), Fe(II), Ru (II) and Ir(III), and XXX pincer ligands such as terpyridine (TPY) and terphosphinine (TPPh).

The absorption properties of these compounds show that the absorption occurs in the UV region, for both one- and two-pincer ligands. Late transition metals such as Cd(II) and Zn(II) show absorption peaks at higher energies. For both cases, regardless being one- or two- pincer ligands, the absorption energies are higher than 4.0 eV, being smaller for one-pincer complexes than for two-pincer ones. Earlier transition metal complexes are more versatile, with intense peaks similar to those of late transition metals, but

with other less intense peaks for transitions at lower energies (larger wavelengths). In general, these peaks are in the UV region, but are close to the visible range for Fe and Ru complexes. Finally, the substitution of TPY by TPPh ligand leads to a red-shift of the spectra.

In order to study the fluorescence properties, the geometry of the lowest-lying singlet electronic excited state have been optimized for all systems. As for absorption properties, late and middle transition metal complexes behave differently. Non-radiative internal conversion would be possible for one-pincer middle transition metal complexes, while this process would not happen for late transition metal complexes, in principle, because the lowest-lying singlet state is far more higher in energy. Focusing on two-pincer ligands, no internal conversion would occur in any complex, and all of them would emit in the UV region with the exception of the [TPY-Ru-TPY]$^{2+}$ complex, which would be fluorescent according to our data.

However, the evolution of the singlet states might end up in triplet states by intersystem crossing process. According to our very preliminary calculations on [TPY-Zn-TPY]$^{2+}$ and [TPY-Ru-TPY]$^{2+}$ complexes, we have observed that in the relaxation of the S_1 state it may cross other triplet states and eventually end up in the lowest lying T_1 state. In both cases, in the optimized geometry for such state the energy difference with respect to the ground state is in the visible region. Therefore, although we cannot conclude that these materials would be phosphorescent, we observe that phosphorescence is one of the possible evolutions of the excited state. Hence, the excited state evolution in these systems may be rather complex, moving from non-radiative decay via internal conversion to radiative decay like fluorescence or phosphorescence.

Chapter 6

Summary, General Conclusions and Future Work

In the present thesis, we have investigated different types of dynamic bonds such as FLP-linker and metal-ligand interactions with favorable mechanical properties for incorporation into polymeric materials. In addition to this, photophysical properties of metal-ligand complexes have been studied, in order to obtain materials with complementary properties in addition to the self-healing ones. In this way, we have been able to understand some key factors to further design more efficient self-healing materials which could have, in addition, interesting optical properties. Understanding the electronic structure and interactions of these bonds is crucial for the development of new dynamic bonds. Concretely, the research involves a detailed characterization of the dynamic interactions of cross-linkers in polymeric chains with a general structure as shown in Figure 6.1. In order to study these systems and reveal the underlying interaction mechanisms, we have employed computational methods, such as Density Functional Theory (DFT). Furthermore, we have investigated the photophysical features of selected metal-ligand based self-healing materials by means of Time Dependent Density Functional Theory (TDDFT), characterizing in this way their absorption and emission properties.

6.1   FLP-DEAD based materials

The first part of this Thesis (Chapter 3) has focused on the theoretical characterization of dynamic bonds based on Frustrated Lewis Pairs (FLP). Inspired by the experimental work of Shaver and colleagues, a set of FLPs have been designed using Lewis acids and bases based on triphenylborane (TPB) and triphenylphosphine (TPP) and derivatives to understand the interaction with DEAD linker molecule (See Figure 6.2 for a ball and stick representation). To start with, the acidity and basicity of substituted TPB and TPP have been characterized. Then, the interaction energies between acid and base fragments in the isolated frustrated Lewis pair and the frustrated Lewis pair with the

linker molecule have been studied.

   Concretely, the systems under study have been TPB and TPP substituted at the *ortho* and *para* positions with EDG groups (R = CH$_3$, NH$_2$, OH, OCH$_3$, OCOCH$_3$) or EWG groups (R = F, CF$_3$, CN, NO$_2$, SO$_3$H). Various parameters have been employed to analyze the acidity and basicity of these compounds. For the acids, the parameters used have been the hydride affinity (HA), electroaccepting power (ω^+), variation of the ^{31}P NMR chemical shift ($\Delta\delta$), lone-pair orbital energy (LP) and occupation numbers ($\eta(\sigma_B)$). Proton affinity (PA), electrodonating power (ω^-), nucleophilicity index (N), and lone-pair orbital energy (LP) and occupation numbers ($\eta(\sigma_P)$) have been employed to analyze the bases. Analyzing these results some conclusions have been achieved. Concerning the acids, HA, ω^+, $\Delta\delta$, and LP parameters have yielded the same outcome, indicating that EWG substituents lead to stronger Lewis acids than EDG substituents, while $\eta(\sigma_B)$ is not useful for measuring Lewis acidity. Regarding the bases, PA, ω^-, N, and LP parameters have showed a consistent pattern, confirming that EDG compounds result in stronger Lewis bases than EWG compounds, while $\eta(\sigma_P)$ is not effective for measuring Lewis basicity.
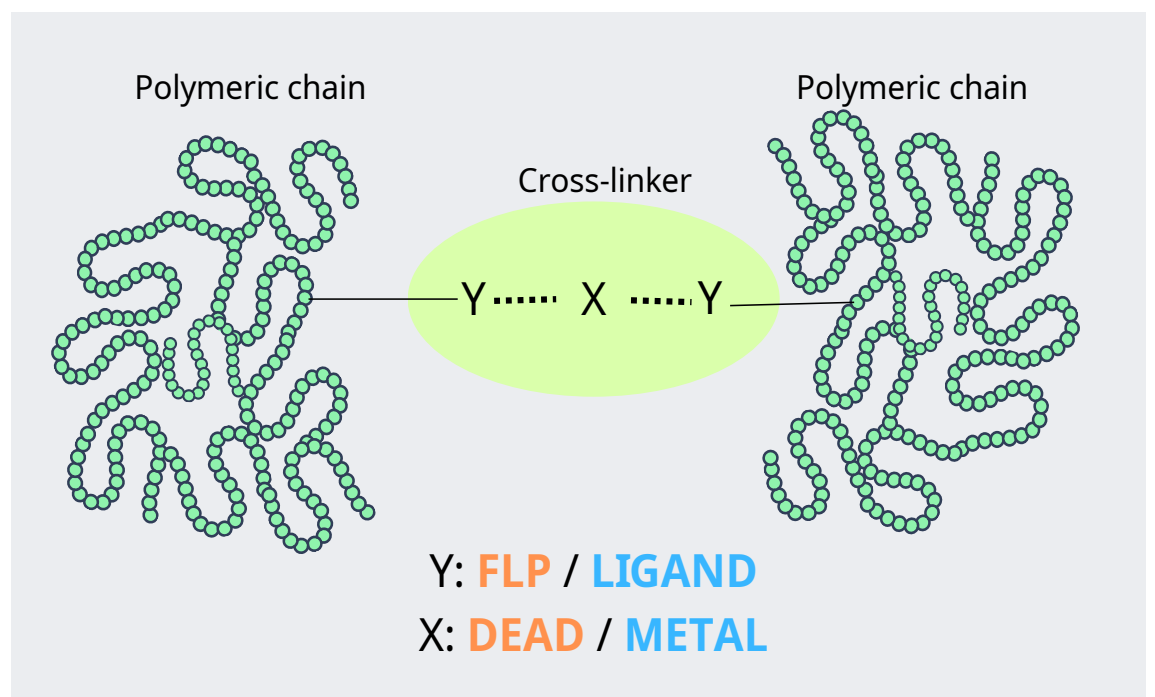
Figure 6.1: Schematic description of the systems studied in this thesis work. The cross-linker is represented as a Y-X-Y cluster, in which Y letter corresponds to either FLP or ligand compounds, whereas X letter corresponds to either DEAD molecule or a transition metal.

   Based on these results, different TPB and TPP derivatives have been chosen to study the interaction in the formation of FLPs and their interaction with DEAD molecule. Concretely, five TPB and TPP derivatives with varying acid and base strengths have been chosen and combined to create 17 FLPs, including the experimental system as reference.

Based on these results, we have concluded that substituents capable of forming hydrogen bonds or donor-acceptor bonds should be avoided because they can impede the proper interaction between FLP and DEAD. In addition, TPB and TPP with intermediate acid and base properties are the most proper ones to balance the interaction with DEAD molecule, and, hence, provide self-healing capacity to the materials.
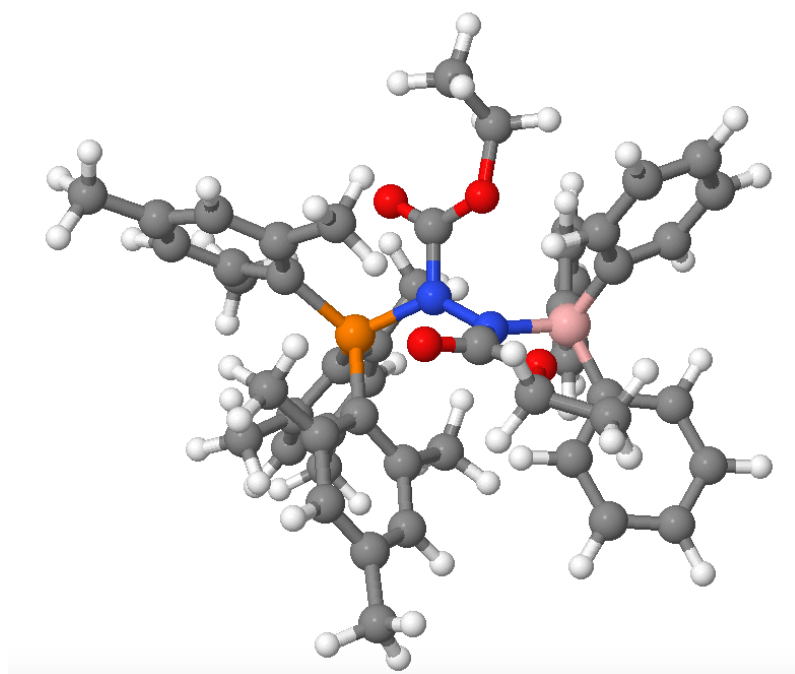
Figure 6.2: FLP-DEAD model for the experimental system developed by Shaver and coworkers.

NBO and EDA analyses have provided complementary insights into the nature of the interactions within FLP-DEAD systems. NBO has revealed that TPB-DEAD and TPP-DEAD fragments have formed dative covalent bonds, leading to polar covalent bonds. The polarity of these bonds has been greater for the B-N bond than for the P-N bond. These results have been confirmed by EDA analysis. The differences in the complexes' interaction energies may have been due to steric repulsion between substituents rather than substantial changes in bond patterns. Furthermore, with the help of NBO, it has been possible to understand the change in the electronic structure that occurs in the linker, where new bonds between B-N and N-P have been formed and the double bond between nitrogen atoms has been split into two lone-pair orbitals.

In conclusion, we propose the FLP_4-DEAD system as a promising candidate for developing new self-healing polymers. However, we suggest considering other alternatives, such as different linker molecules or FLPs with different acidic and basic centers (e.g., Al, Ga, N) for future improvements.

6.2   Metal-ligand based materials

The second part of this work has focused on materials based on transition metal and pincer ligands, both in their interactions and optical properties. Regarding the study of the interaction nature between transition metals and pincers, terpyridine (TPY) and ter-phosphinine (TPPh) based ligands and derivatives have been considered. The interaction of these pincer ligands with transition metals such as Cd(II), Zn(II), Cu(I), Fe(II), Ru(II) and Sc(III), have been fully discussed in Chapter 4. We calculated both the interaction energies, and carried out a systematic study of the nature of the interaction by means of NBO and QTAIM analysis, in order to understand the underlying physical aspects of the interaction and to identify the key parameters affecting the interaction that could help in the improvement of the self-healing capacity of polymeric materials containing these systems as cross-linkers. This part of the study has been inspired by the experimental research conducted by Rowan and Weder.[53]
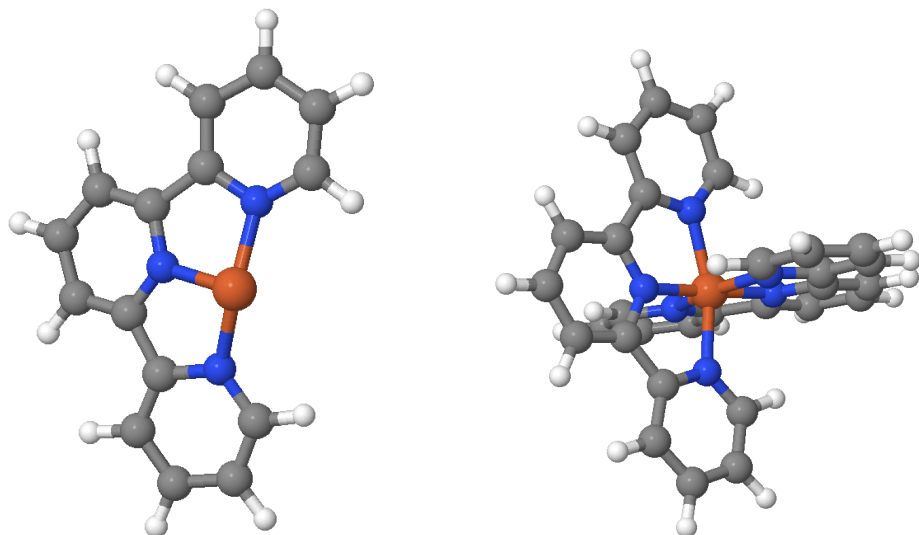
Figure 6.3: Optimized $[\text{Fe-TPY}]^{2+}$, left, and $[\text{TPY-Fe-TPY}]^{2+}$, right, complex structures.

First of all, the influence of transition metals in the interaction energy has been examined by calculating and analyzing the complexation energies of different metal-ligand complexes mentioned above. We have observed that the interaction energy is affected by the charge of the metal and the occupancy of the metal d orbitals, where metals with vacant d orbitals may accept electronic density from the nitrogen lone-pairs, thus enhancing the interaction. Regarding the M-N bond distances, we observe a clear agreement with the interaction energy and, in comparison between one- and two-ligand complexes, longer distances in $[\text{TPY-M-TPY}]^{n+}$ complexes are observed, possibly caused by steric hindrance. Sc(III) has been found to be a special case in this context, as the charge transfer occurs in virtual and more energetic orbitals. Its large interaction energy is a result of its high ionic charge, which leads to strong ion-dipole interactions.

In addition to the metal ion influence, the effects of EDG and EWG functional groups (R = H, NH_2 and CN) on the phenyl rings of the ligand have been further analyzed. Based on the obtained results, we may conclude that the presence of an EDG produces an increase in the interaction energy, while the presence of an EWG has the opposite effect. Nevertheless, the effect of these groups is much smaller than that exerted by the metal, and may be used to modulate the interaction once the proper metal is chosen. Hence, the bond strength is mainly determined by the nature of the metal and the ligand rather than by the presence of substituents in the phenyl rings.

Lastly, we have investigated the effect of substituting TPY ligand by the phosphorus analogous, TPPh. The dissociation energies of Fe(II) complexes with TPPh ligands have been found to be lower than those with TPY ligands due to a weaker phosphorous-metal interaction, as a result of a different electronic structure. The effects of EDGs and EWGs (R = H, NH_2 and CN) on TPPh ligands have also been calculated, with larger dissociation energies found for EDGs. NBO analysis has indicated that a bond is formed in [Fe-TPPh-NH_2]$^{2+}$ complex, while the interaction is mainly electrostatic for the other cases. Besides, several bonds have been formed in [TPPh-Fe-TPPh]$^{2+}$ (R = H, NH_2 and CN) systems. However, according to QTAIM analysis, the Fe-P interactions are electrostatic with partial covalent character.

Based on these results, we observe that the most important factors are the ligands (TPY and TPPh) and the metal ion. Nevertheless, the calculated interaction energies are too high to consider these interactions as dynamic bonds. Note that typical dynamic bonds, such as those based on disulfides or in FLP-DEAD system, range around 40-50 kcal/mol, and are an order of magnitude larger in these metal ion - pincer complexes. This apparent incongruency may arise from the fact that in experimental conditions the metallic salts do not dissociate completely, and the effect of salt clusters may be important, including the counter-ion effect. In this vein, preliminary calculations have been carried out with $FeCl_2$ salts. Concretely, the interaction of one and two TPY ligands with a small Fe_6Cl_{12} cluster have been calculated. In Figure 6.4, the optimized structures for the isolated cluster and the complex formed with two TPY ligands are depicted. The calculated interaction energies are roughly 50 kcal/mol for 1 pincer and 150 kcal/mol for two pincer ligands. These smaller values are indicative of the importance of a proper modelization of the experimental conditions. In the future, one should consider the fact that metal ions probably are not free species in the experimental conditions where these materials are synthesized. Hence, the importance of considering salt clusters and the effect of counter-ions is crucial. Anyway, we believe that the influence of the factors studied in this Thesis would be similar in these cases.
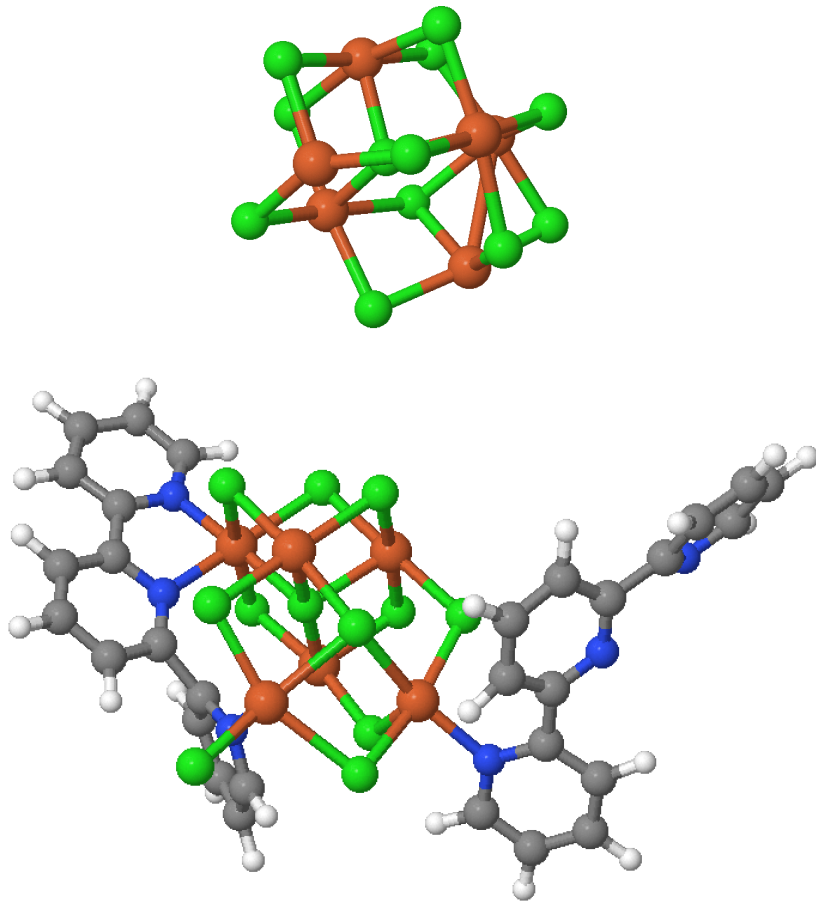
Figure 6.4: Top, the isolated Fe_6Cl_{12} cluster. Bottom, the interaction of this cluster with two TPY pincer ligands.

Once the nature of the interaction has been understood, we have studied the optical properties of related $[M\text{-}XXX]^{n+}$ and $[XXX\text{-}M\text{-}XXX]^{n+}$ complexes. Concretely, the optical properties have been studied for Zn(II), Cd (II), Fe(II), Ru (II) and Ir(III) metals, and terpyridine (TPY) and terphosphinine (TPPh) pincer ligands. These compounds were chosen due to their experimental use in these kind of materials. The studied optical properties have been, concretely, UV/Vis absorption and emission as fluorescence and phosphorescence.

According to our results, in general, late transition metals show absorption and fluorescent emission in the UV region, while preliminary calculations on the phosphorescent emission reveals that $[TPY\text{-}Zn\text{-}TPY]^{2+}$ complex could emit in the visible range. Middle transition metal complexes are more versatile. One-pincer ligands may undergo non-radiative internal conversion processes, and two-pincer ligands, on the contrary, are prevented to this non-radiative process by higher lowest-lying singlet excited states. In principle, they will emit in the near UV region, with the exception of $[TPY\text{-}Ru\text{-}TPY]^{2+}$ complex, which could emit in the visible range. In addition to this, preliminary results on the lowest-lying triplet state reveal that both $[TPY\text{-}Zn\text{-}TPY]^{2+}$ and $[TPY\text{-}Ru\text{-}TPY]^{2+}$

complexes might irradiate in the visible range from this state leading to phosphorescent properties. Comparing TPY and TPPh ligands, it was observed that TPPh ligands provoke a red-shift of the spectra.

In order to study the fluorescence properties, the geometry of the lowest-lying singlet electronic excited state have been optimized for all systems. As for absorption properties, late and middle transition metal complexes behave differently. Non-radiative internal conversion would be possible for one-pincer middle transition metal complexes, while this process would not happen for late transition metal complexes, in principle, because the lowest-lying singlet state is far more higher in energy. Focusing on two-pincer ligands, no internal conversion would occur in any complex, and all of them would emit in the UV region with the exception of the [TPY-Ru-TPY]$^{2+}$ complex, which would be fluorescent according to our data.

This study on the optical properties of these complexes may be seen as a first approach to study these properties. Indeed, there is plenty of work to be done in order to properly understand the optical properties of metallopolymeric materials. For instance, the influence of the counterions and the fact that not isolated metal ions are present in theses systems should be considered, as mentioned above. In addition to this, since the excited state evolution in these systems is very complex, the close study of internal conversion and intersystem crossing should be considered, in order to provide not only qualitative but also a quantitative prediction. Moreover, once these processes are better understood, the influence of other transition metals such as La(III), Co(II), or Pt(II), would also provide insights into their potential applications.

Kapitulua 7

Sarrera

Natur Zientziek hainbat diziplina biltzen dituzte bizi garen unibertsoa ulertzeko. Horiek bi kategoriatan bereiz daitezke: izaki bizidun gabeko sistemetan (materia, energia eta unibertsoa, esaterako) oinarritzen diren zientzia fisikoak (materia, energia eta unibertsoa, esaterako) eta izaki bizidunak eta horiek ingurumenarekin dituzten elkarreraginak aztertzen dituztenak. Kimika zientzia fisikoen adar bat da, eta materiaren konposizio, egitura, propietate eta erreakzioez arduratzen da. Dena den, beste adarrarekin ere lotura estua du, organismo bizidunen barruko prozesu kimikoak aztertzen ditu eta.

Kimika hainbat modutan defini daiteke. Oxford Hiztegiaren arabera, "Kimika zientziaren adarra da, materia osatzen duten substantziak, haren propietateak eta erreakzioak ikertzen dituena, eta erreakzio horiek substantzia berriak sortzeko erabiltzen dituena". Cambridgeko Hiztegiak ere antzera definitzen du; Entziklopedia Britainiarrak, berriz, definizioan prozesu kimikoetan askatutako edo xurgatutako energiaren kontzeptua ere badu. Horrek aukera ematen du materiaren eta argiaren arteko interakzioa ere kimikan sartzeko, eta argia prozesu fotokimiko edo fotofisikoetan parte har dezakeen energia-iturria da.

Kimikaren barruan sailkapen ezberdinak daude. Aztertutako molekula motetan oinarrituta, zenbait eremu bereiz daitezke, hala nola kimika organikoa, ez-organikoa eta biokimika. Bestalde, molekulak eta haien prozesuak aztertzeko moduari erreparatzen badiogu, beste arlo batzuk sortzen dira, hala nola kimika analitikoa edo kimika fisikoa. Azken horrek erreaktibotasun kimikoa aztertzeko aukera ematen du, bi irizpide nagusitan oinarrituta. Batetik, erreakzio jakin baten itzulgarritasuna edo itzulezintasuna, eta, bestetik, erreakzioaren abiadura. Testuinguru horretan, giro-tenperaturan (edo harengandik hurbil) gertatzen diren eta zinetikoki baimenduta dauden erreakzio itzulgarriek kimikaren adar berri bat ireki dute, *Kimika Dinamikoa* izenekoa, eta eragin handia du material berrien garapenean.

7.1   Kimika dinamikoa

Tradizionalki, konposatu organikoen sintesia zinetikoki kontrolatu izan da, eta lotura kobalenteen eraketa itzulezina lortu da. Lotura kobalentearen eraketa indartsu hori erreakzio kimikoaren biderik eraginkorrena bilatzean, oso kontu handiz hautatutako erreaktiboen eta baldintzen ondorio da. Hain zuzen, lotura kobalente itzulezinaren erreakzioa lortzeko, produktu jakin bat sortzeko energia aldetik bide egokiena bilatzen da. Beraz, trantsizio-egoera eta -egoeren ulermen zehatza behar da produktuaren banaketa kontrolatua lortzeko. Erreakzioaren izaera itzulezin horrek bermatzen du, produktua eratu ondoren, ezin dela ez hasierako erreaktiboa birsortu, ezta beste produktu batean bihurtu. Testuinguru horretan, kimikariek produktu naturalen eta ez-naturalen sintesi eraginkorrak eman dituzte.

Hala ere, azken urteetan kimika itzulgarria asko aintzatetsi da, horri esker materialen zientzian aurrerapen handiak lortzea espero baita. Lotura kobalente edo ez-kobalente batek orekan eratu, hautsi eta modu itzulgarrian birsortzeko duen ahalmenean oinarritzen da kimika itzulgarria.

Kimika dinamikoak gero eta garrantzi gehiago du polimeroen zientzian eta ingeniaritzan; izan ere, material asko lotura dinamikoari dagokion gaitasun bereziekin garatu dira, hala nola birprozesatze, birziklatze edo autokonpongarritasun gaitasuna dutenak.[4] Lotura dinamiko horiek haustura itzulgarri azkarra izan behar dute, egitura eta diseinu eraginkorrak disoziazio- eta aktibazio-energiak doitzeko. Horrek efektu esterikoak[5–7] eta elektronikoak[8,9] erabiltzea barne hartzen du. Itzulgarritasuna estimulu desberdinek eragin dezakete (kimikoek, biologikoek edo fisikoek), eta materialean propietate bat edo gehiago aldatu. Ikerketa-eremu horren garapenak dinamikoki kontrolatutako sistemak sor ditzake hainbat aplikaziotarako, sendagaietarako, robotikarako, (bio)sentsoreetarako eta material autokonpongarrietarako, esaterako.[10] Testuinguru horretan, polimero sintetikoak egokiak dira ezaugarri dinamikoak izateko, zeren eta kimikoki erraz alda daitezke, ondorioz, erraz manipula daitekeen erantzun-mekanismoa sortzen dute.

Laburbilduz, kimika dinamikoak aplikazio praktiko ugari ditu, ikusi 7.1 Irudia. Aplikazio horien artean daude, besteak beste, sendagaiak modu kontrolatuan askatzen dituzten sistemak, maila molekularrean zeregin mekanikoak egin ditzaketen makina molekularrak, ingurunean gertatzen diren aldaketak atzemateko eta horietara egokitzeko gai diren material sentikorrak, kanpoko estimuluei erantzunez konfigurazioa alda dezaketen memoria-materialak, seinale txikien anplifikazio edo aldaketa kimikoa detekzio zehatzagorako, kanpo-estimuluei erantzuten lotura kobalenteak sortzea eta deuseztatzea eragiten duen katalisia, eta kalteak jasan ondoren beren burua konpon dezaketen materialak. Beraz, kimika dinamikoko aurrerapenek medikuntza, materialen zientzia eta nanoteknologia bezalako eremuak eralda ditzakete.
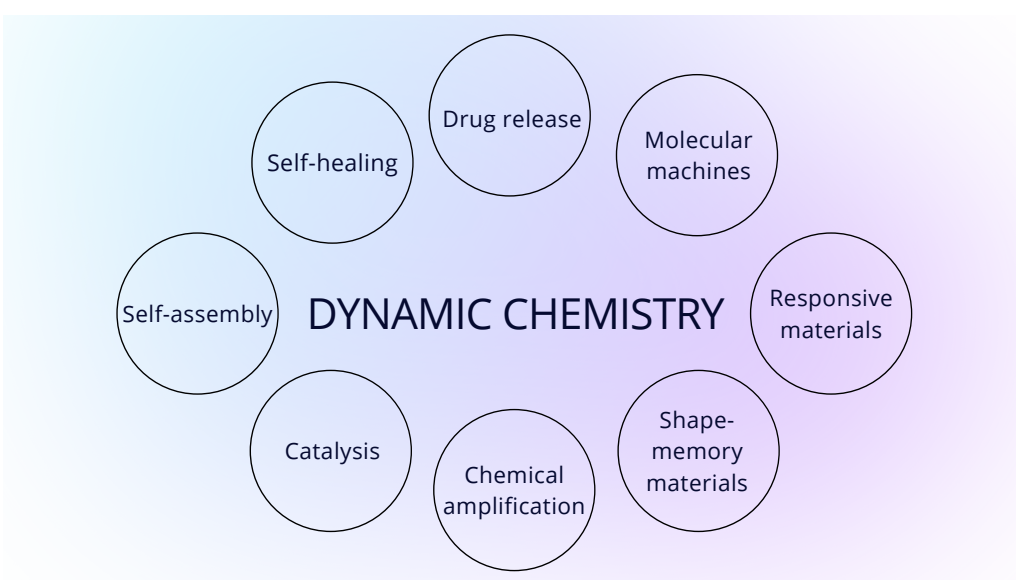
7.1. Irudia: Kimika dinamikoaren aplikazio batzuk.

7.2 Material autokonpongarriak

Material autokonpongarrien garapenerako inspirazioa naturan aurki daiteke, non organismo bizidun askok beren burua sendatzeko gaitasuna erakusten duten hainbat estrategia erabiliz. Horietako batzuk 7.2 irudian ageri dira. Arrabioek gorputzeko atal galduak birsor ditzakete, zelula-masa bat eratzen dute blastema izenekoa gorputz-adar bat moztu ondoren. Narrastiek larruazala jariatzen dute, errazago hazteko; izan ere, larruazal berria larruazal zaharraren azpian garatzen da, eta kanpoko geruza hil eta erori egiten da. Muskuiluen bizarrak beren kabuz konpontzen dira histidina-metal interakzioen eraginez, ozeanoan estres mekanikoaren eraginpean horri esker substratuei lotuta egoten dira. Zelulek DNA molekuletan gertatzen den edozein kalte detektatzeko eta konpontzeko gaitasuna dute. Hostoetan, zauria dagoen lekua airean jartzean, zelulak handitu eta ugaldu egiten dira, eta zauria ixten da. Zelula-seinalea funtsezkoa da plaketen koagulazio-jarduera, erantzun immunea, ehunen konponketa eta zauriak orbaintzen diren bitartean infekzioak ekiditeko. Oro har, argi dago naturan autokonpongarritasun prozesua aurki daitekeela bai maila molekularrean, baita makroskopikoan ere.

Adibide natural horietan oinarrituta, zientzialariek hainbat mekanismo diseinatu dituzte autokonpongarritasun gaitasuna duten material ez-biziak sintetizatzeko. Azken urteotan, konponketa automatikoaren bidez[11] edo kanpoko estimulu bati erantzunez (adibidez, beroa[12] edo presioa[13]) ingurumen estresa jasan dezaketen material funtzionalak interes teknologiko handikoak dira, eta azkar hedatzen ari den ikerketa eremua da.[14–17] Hala, polimero autokonpongarriak sakon aztertu dira, aplikazio ugari eta sendatzeko mekanismo ugari baitituzte.[18–21] Material inteligente horiek beren osotasun kimikoa edo funtzioa bermatzen duten produktuen bizitza luzatzeko sortzen dira, eta kimika itzulgarrian oinarritzen dira. Horrela, lotura kimikoak berrantolatzean, kaltetutako zatiak berriz elkartuko dira, eta, ondorioz, materiala partzialki edo osorik berreskuratuko da.

Self-healing in nature
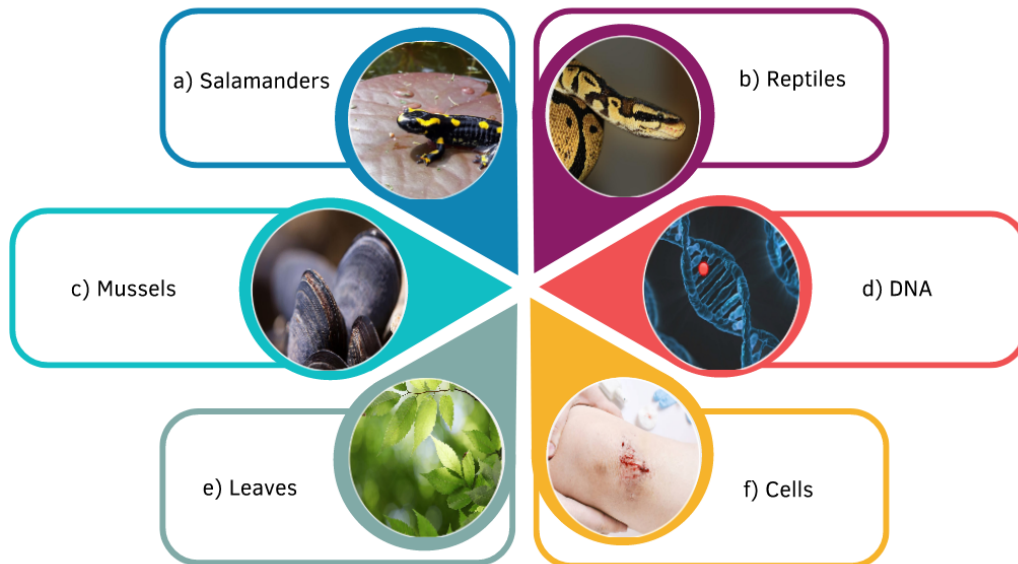
7.2. Irudia: Naturan aurkitzen diren autokonpongarritasun prozesuen adibideak: a) arrabioak, b) narrastiak, c) muskuiluak, d) DNA, e) hostoak eta f) zelulak.

Hainbat kimika mota aztertu dira autokonpongarritasun gaitasuna sartzeko material polimerikoetan, eta bi ikuspegi nagusi bereiz daitezke lotura itzulgarriaren naturaren arabera: i) lotura kobalente dinamikoetan oinarritutako materialak,[4,22–29] hala nola erabiliz retro-Diels-Alder erreakzioa,[12,30,31] lotura dikalkogenikoak,[32–36] siloxanoen kimika,[37] transesterifikazioa,[38] transkarbamilazioa,[39] transamidazioa,[40] edo alkoxiaminen kimika;[41] eta ii) interakzio ez-kobalenteetan oinarritutako materialak, esaterako, π-π pilaketak,[42–44] hidrogeno loturak,[13,45–48] metal-ioi interakzioak[49–54] edo ionomeroak.[21,55]

Polimero autokonpongarrietan interakzio ez-kobalenteak egotea (hidrogeno loturak, esaterako) garrantzitsua da, katearen dinamikak eragina baitu jariatzeko eta birmoldatzeko gaitasunean, eta horrek nabarmen baldintzatzen du materialaren konpontzeko ahalmena. Hala ere, lotura kobalente dinamikoak erabiltzeak egonkortasun mekaniko eta erresistentzia handiagoko materialak sortzen ditu. Ildo horretan, lotura kobalente ahulagoak erabiltzea onuragarria izan daiteke autonomikoki konpontzeko gaitasuna duen materiala lortzeko, lotura indarra sendo mantentzen den bitartean.[56] Dikalkogenuro aromatikoak bereziki etorkizun oparokoak dira,[33,34,57,58] eta trukatze erreakzioak giro tenperaturan ematen direla ikusi da, bai disoluzioan,[59] baita egoera solidoan ere.[60] Duela gutxi, disulfuroetan oinarritutako konposatuetan, trukatze erreakzioaren mekanismoa zein den proposatu da, teorikoki kimika teorikoa erabiliz.[35] Gainera, mekanismoa esperimentalki berretsi da katalizatzailerik gabe.[61] Bestalde, interakzio ez-kobalenteak, orokorrean, lotura kobalenteak baino joera handiagoa dute kanpo estimuluei erantzuteko, eta interakzio horietan oinarritutako materialak konpontze ezaugarri nabarmenak

dituzte.[62]

Lotura kobalente dinamikoan oinarritutako material autokonpongarrien beste adibide bat bitrimeroak dira,[63] hots, cross-linkerrak dituzten materialak lehenengoz Leiblerrek eta kolaboratzaileek proposatuak.[38] Material horiek termoplastikoen prozesagarritasunarekin termoseten sendotasuna hobetzeko diseinatu dira. Cross-linkerrek elkartrukatze dinamiko bat jasaten dute beste elkartrukatze prozesu baten bidez.[64] Prozesu horrek elkargurutzaketa dentsitate konstante bat eragiten du, denborarekin eta tenperaturarekin aldatzen ez dena. Hala, materiala ohiko beira gisa sor daiteke egoera likidoan, sarearen osotasuna galdu gabe. Hainbat material eta elkartruke erreakzio erabili dira bitrimeroak sintetizatzeko, adibidez, urea taldearen eta amina aromatiko askeen arteko trukea poli(urea-uretano) polimeroetan.[65]

Laburbilduz, autonomoa den edo estimulu ahula behar duen material autokonpongarria lortzeko, nahitaezkoa da lotura dinamikoa egoki aukeratzea. Tesi honetan Lewis bikote frustratuetan (ikusi 7.3 atala) eta metal-ligandoetan (ikusi 7.4 atala) dagoen kimika landuko dugu.

7.3 Lewis bikote frustratuetan oinarritutako lotura dinamikoak

Kimika itzulgarri asko dauden arren, oraindik zaila da lotura dinamikoetan oinarritutako material autokonpongarriak garatzea, materialaren errendimendu orokorra aldatu gabe.[66] Adibidez, zenbait lotura dinamiko polimero jakin bati soilik aplika dakizkioke, eta, beraz, komenigarria litzateke aplikazio eremua zabal dezaketen eta sistema polimeriko gehiagotan erraz integra daitezkeen lotura berriak identifikatzea. Ikuspegi horri jarraituz, Shaverrek eta kolaboratzaileek material autokonpongarri mota berri bat aztertu zuten, Lewis bikote frustratu baten (FLP) eta molekula txiki espezifiko baten (dietilo azodikarboxilatoa, DEAD) arteko interakzio itzulgarrian oinarritua.[67] Lehenengo aldiz, talde esperimental batek FLP kontzeptua eremu berri batera eraman zuen, polimero gel autokonpongarriak sortzen dituzten cross-linker sareak ekoitziz.

Stephanek eta kolaboratzaileek FLP kontzeptua sortu zuten 2006an.[68] Lewis azido baten eta Lewis base baten arteko lotura eragotzian oinarritzen den paradigma berri bat da. Azken hamarkadan, frogatu da eragozpen esterikoa edo disoziazio oreka bat sartzeak sortzen dituela elektroi emaile eta hartzaile askeak, lotura datiboak sortzeko ahalmenik ez dutenak, horrela, FLPa sortzen da[69-71] eta molekula txikien (H_2, CO_2, NO edo CO, esaterako) aktibazioa bultzatzen da. FLP kontzeptuaren deskribapena 7.3 irudian, goran, ageri da
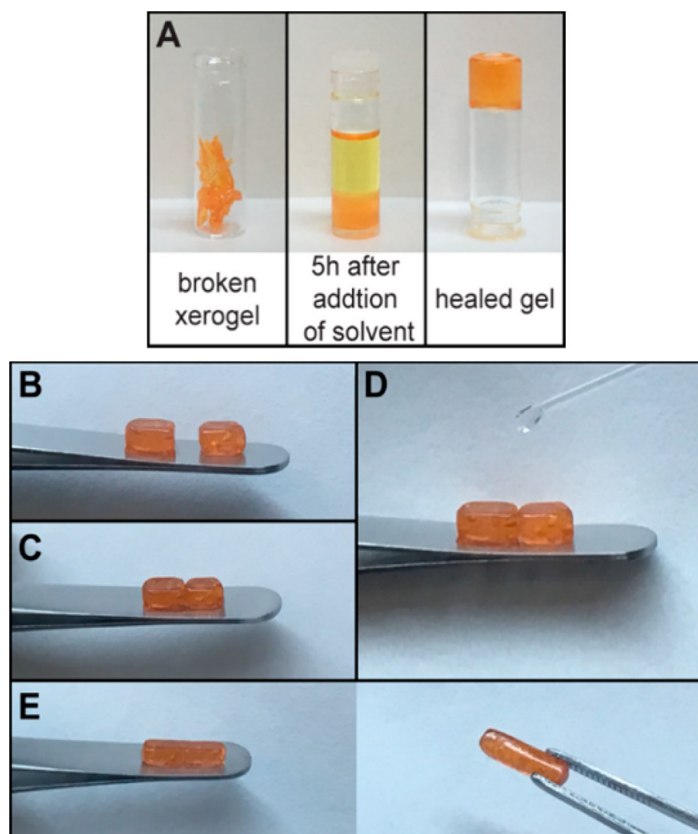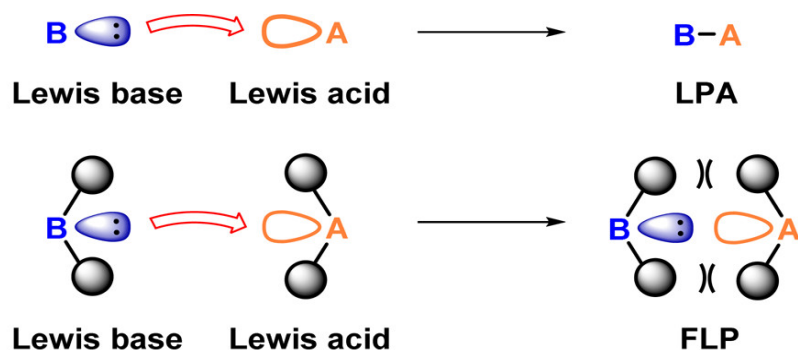
7.3. Irudia: Goran: Lewis bikote frustratuaren definizioa. Beheran: Hautsitako xerogel bat (A) eta adreilu itxurako gelaren ebakiduraren (B-E) autokonpontze prozesua. 67. erreferentziatik hartutako irudia.

Shaverrek eta kolaboratzaileek FLPn oinarritutako cross-linkerrak dituen polimero bat diseinatu zuten, hots, elektroi emaile eta hartzaile diren molekulak gehitzen, molekula txiki batekin era itzulkorrean interakzionatu dezaketenak, sare erantzule bat sortzeko. Zehazki, 4-estiril-difenilborano eta 4-estiril-dimesitilfosfina monomeroak poliestirenozko kate nagusi batean sartu ziren.

Hala, dietilo azodikarboxilato (DEAD) molekulak boro eta fosforo atomoekin erreakzionatzen du, eta gel bat sortzen du (ikusi 1.3 irudiaren behealdea). FLP-DEAD arteko elkarrekintzak dinamikoak direnez, tenperatura altuek (100°C) lotura datiboak apurtu ditzakete.[67,72] Dakigunez, lan aitzindari horretaz gain, material molekularretan FLPak sartzea ez da aintzat hartu.[73,74]

Elkarrekintza energia ahulak kalkulatu dira molekula txikien aktibazioan FLPak erabiltzean. Adibidez, CO_2ren eta fosforo-borako bikotearen arteko lotura energia 18 kcal/mol ingurukoa da,[75] hidrogeno lotura ertain-sendo baten antzekoa,[76] eta material erantzule supramolekularretan aurkitzen direnekin aldera daiteke. Hala, emaitza horietan oinarrituta, uste dugu Shaverrek proposatutako materialean dauden elkarrekintzen karakterizazio teorikoak informazio garrantzitsua emango duela, alegia, molekula txikiek aktibatutako material erantzule berriak garatzeko, FLParen loturaren izaera dinamikoa ustiatuz.

7.4 Pintza estekatzaileetan oinarritutako lotura dinamikoak

Interakzio ez-kobalenteen artean, metal-ligando elkarrekintzek moldakortasun handia erakusten dute lotura indarrari eta lotura dinamikari dagokienez, eta propietate mekaniko kontrolatuak dituzten metalopolimeroak sortzen dituzte.[77] Interakzio mota hori naturan ere badago. Adibidez, muskuiluetan, beren bizarrek substratu batean eusten dute muskuilua; han, muskuiluaren oineko proteinetan dauden Fe(III)-aminoazidoen elkarrekintza itzulgarriek zeregin garrantzitsua dute, zeren eta ur zurrunbilotsuaren estres mekanikora egokitzen dute muskuilua.[78,79] Fenomeno horretan inspiratuta, Rowanek eta Wederek lehen metalopolimero autokonpongarria deskribatu zuten.[53] Lan aitzindari horretatik abiatuta, ahalegin asko egin dira beren mekanismoa ulertzeko eta ezaugarri hobeak dituzten material berriak diseinatzeko.[80–84]

Metal-ligando lotura sorta zabal batean eralda daiteke, metala eta estekatzailea kontu handiz hautatuz,[85–87] autokonpongarritasunerako lotura indar onenak lortzeko. Gainera, egitura supramolekularretan metal-ligando loturak sartzeak funtzionalitate aurreratuak dituzten materialak garatzera darama, hala nola material termoerantzuleak[88] edo luminiszenteak.[89] Orain arte, zenbait estekatzaile erabili dira material autokonpongarriak garatzeko, adibidez, histidina,[90,91] imidazola,[92,93] karboxilatoa,[94–96] piridiloa[53,97,98] edo sulfuroa[99] duten estekatzaileak, batzuk aipatze aldera. Piridina duten ligandoak ere erabili izan dira material autokonpongarri ugari sortzeko, nitrogenoaren bikote askearen Lewis izaera basikoan oinarrituta.

Hortz anitzeko estekatzaileak erabiltzeak handitu egiten du lotura afinitatea metal sorta zabalago batera, efektu kelatzailearen[100] ondorioz, eta ligandoarekiko metalaren $d\pi$-$p\pi$ loturari esker.[101] Hala, pintza-ligando deritzenak, konfigurazio meridianoan hiru puntu planokidean elkartzen diren agente kelatzaileak dira, ikusi 7.4 irudia. Hiru hortzeko koordinazioak lotura sendoa eta egonkortasun termiko handia ematen ditu. Pintza

estekatzaileen lehen adibideak dira erdigunean karbanioia dutenak, koordinazio meridionala bultzatzen duten aldeetako lotura unitateak ere badituztenak. Lotura horiei η^3-ECE koordinazioa deritze, non E bi elektroiko emaile neutrala den, orokorrean, N eta P atomoek koordinatutakoa (NCN eta PCP motako pintza-ligandoak). Azkenaldian, *ECE* koordinazioa NNN, PNP edo SNS sistemetara zabaldu da, batzuk aipatzearren.
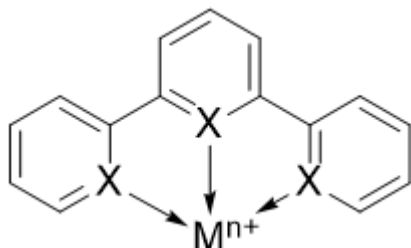
7.4. Irudia: Metal-pintza ligando konplexuaren adierazpen eskematikoa. Bertan, pintza terpiridinazko estekatzaile bat izan ohi da (X = N), eta M, berriz, dagokion oxidazio-zenbakia duen trantsizio-metala. Geziek pintzaren eta metalaren arteko elkarrekintza adierazten dute.

Hala, terpiridina (NNN koordinazioa) duten polimero mota ugari garatu dira Fe(II),[103] Cd(II),[103,104] Zn(II)[105,106] edo Co(II)[107] metalak erabiliz. Rowanek eta Wederrek garatutako metalopolimero autokonpongarria, lehen aipatu duguna, Zn(II) eta La(III) metalek duten elkarrekintzan oinarritzen da, piridiloan oinarritutako hiru hortzeko estekatzailearekin.[53] Lan horietan guztietan metalen loturaren izaerak duen garrantzia nabarmentzen da. Hala, elkarrekintza itzulgarriei dagokienez, badirudi Fe(II) dela autokonpongarritasunerako hautagairik onena; beste metal batzuek, hala nola Ru(II), elkarrekintza sendoegia eragiten dute,[101] aldiz, Cd(II) metalak, elkarrekintza ahulegia eragiten du.[105] Bistakoa da bai estekatzaileen izaerak, baita koordinatutako metalak ere, metal-ligando elkarrekintzan eragina dutela. Hori, egitura elektronikoaren adierazgarria da.

Terpiridina (TPY) ez bezala, bere analogoa den fosforoa erabiltzen duten metal-ligando konplexuei buruz ez da informaziorik eman oraindik, hain zuzen ere, terfosfinina estekatzailedunak (TPPh). Hala ere, antzeko estekatzaileak erabili dira Rh eta Ir-ren koordinaziorako, non agerikoa den fosfininen izaera π-hartzailea.[108] Zati aromatikoan fosforo atomo bat sartzeak eragina du propietate elektroniko, esteriko eta koordinazio-propietateetan. Horrela, nahiz eta fosfininak *pi* elektroi deslokalizatuak dituzten sistema aromatiko lauak izan, fosforoaren *3p* eta karbonoaren *2p* orbitalen gainazartzeagatik, fosfininen eta piridinen propietate elektronikoak oso desberdinak dira. Fosforoaren bikote askeak orbital lausoago bat betetzen du, partzialki deslokalizatua eta piridinarena baino noranzko okerragoa duena, eta maila baxuko LUMO orbital batek ahalbidetzen du fosfininak *pi*-hartzaile onak izatea.

Ikerketa gehienak metalopolimero autokonpongarri berrien sintesira eta karakterizaziora bideratu dira, ondorioz, ikerketa gutxik lotzen dituzte metal-ligando loturaren natura eta dinamika propietate autokonpongarriarekin. Azken urteotan, zenbait ikerketa bideratu dira terpiridinaren eta trantsizio-metalen arteko interakzioa aztertzera, zehazki, Fe(II), Rh(II) eta Cd(II)[101,105,109,110] metalak ikertu dira. Dakigunez, literaturan aurki

daitekeen lan konputazional bakarra, Kupfer eta kolaboratzaileek burututakoa da, [103] non Fe(II) sulfatozko eta Cd(II) bromurozko bisterpiridina konplexuetatik abiatuta metalopolimeroetan termikoki eragindako mekanismo autokonpongarriak aztertzen diren.

Beraz, argi dago metal-ligando elkarrekintzaren ikuspegi konputazionalak informazio baliotsua emango duela autokonpongarritasun gaitasuna duten material berriak garatzeko.

7.5   Argiak material autokonpongarrietan eragindako propietateak

Sarreraren hasieran emandako kimikaren definizio zabalaren arabera, materiaren eta argiaren arteko interakzioa kimikaren ikuspuntutik ere azter daiteke. Argia absorbatu edo igortzea energia xurgatzeko edo askatzeko modu bat da. UV/Vis argiaren absortzioak egoera elektronikoen arteko trantsizioak eragin ditzake, sistema egoera elektroniko natural batetik egoera kitzikatura aldatuz. Beraz, egoera kitzikatuaren joera garrantzitsua izango da sistemaren ezaugarriak ulertzeko. Material polimerikoei dagokienez, bi emaitza nabarmentzen dira. Lehenik eta behin, argia xurgatzeak autokonponketa prozesuak eragin ditzake (ikusi 7.5 irudia). Bigarrenik, autokonpongarritasun gaitasuna duten materialetan, argia xurgatzeak propietate fotoluminiszenteak eman diezazkioke sistemari, hala nola fluoreszentzia edo fosforeszentzia. Hala, argiaren eraginez, polimero fotosentikorrek beren propietateak aldatzen dituzte. Argiak eragindako aldaketa molekularra materialaren propietateen aldaketa makroskopikoan islatzen da. [111] Hori dela eta, argiaren erabilera onuragarria izan daiteke, lokalki erabil baitaiteke eta uhin-luzera kaltetutako zatian bakarrik eragiteko egokitu baitaiteke. [112]
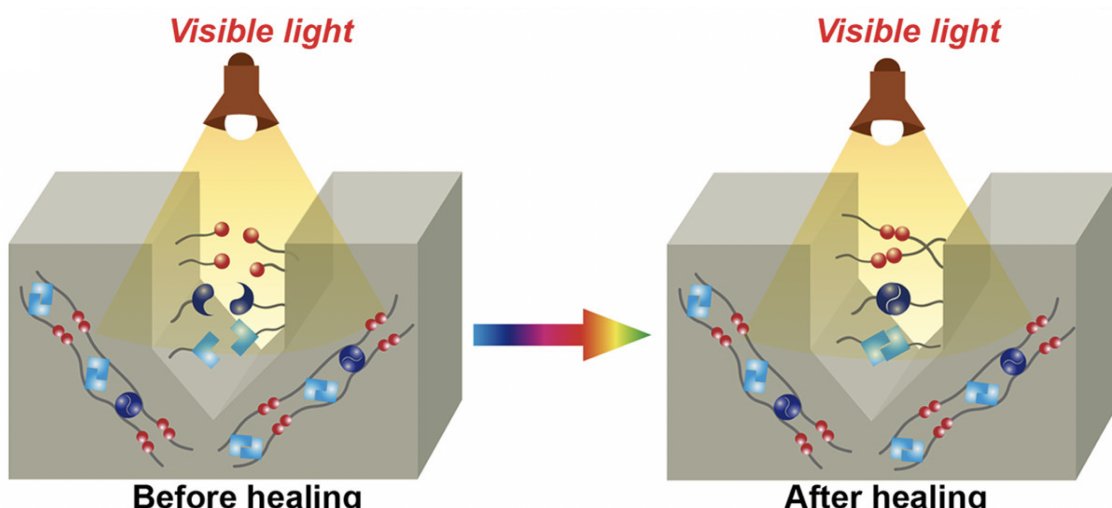
7.5. Irudia: Argiak material polimeriko batean eragindako autokonponketa prozesua. Irudia 113. erreferentziatik hartu da.

Argiak eragindako propietate autokonpongarriak dituzten material polimerikoen adibide bat, dikokalaminaz egindako materialetan aurki daiteke. Horietan, S-S edo Se-Se lotura zatitu ondoren, sufre- edo selenio-erradikalak sortzeak ematen du autokonpongarritasun gaitasuna, eta lotura UV argiaren edo argi ikuskorraren eraginpean aktiba daiteke. Ondorioz, materiala irradiatzen denean, elektroi transferentzia bat gertatzen da sigma orbital lotzailetik (σ) antilotzailera (σ^*), eta, horrek, lotura ordena murriztu eta S-S edo Se-Se lotura ahultzen du, erradikalen sorkuntza sustatuz.[36]

Argiak eragindako autokonpongarritasunaren beste adibide bat Rowanen eta Wederren lan aitzindarian aurki daiteke.[53] Bertan, konpontze prozesua UV argiarekin irradiatu ondoren gertatzen da. Egileek proposatzen dutenez, konponketa konbertsio fototermikoaren ondorioa da. Beraz, konplexuek fluoreszentzia errendimendu kuantiko txikia dute, iradokituz xurgatutako argiaren zati bat bero bihurtzen dela eta metal-ligando arteko lotura disoziatzeko erabiltzen dela. Horretaz gain, konplexua xurgatzen ez duen beste uhin-luzera batekin irradiatu ondoren, materialak ez du autokonponketarik erakusten, autokonponketa prozesua argiaren absortzioak eragiten duela berretsiz.

Metalaren izaera garrantzitsua da, bai propietate autokonpongarrian, baita metalopolimeroen propietate fotofisikoetan ere.[54,114,115] Adibidez, Ir(III) ondo ezagutzen den trantsizio-metal bat da, konposatu ziklometalikoekin konplexuak sortzen dituena.[116,117] Konplexu horien ezaugarri espektroskopiko eta elektrokimikoak hainbat aplikaziotarako erabili dira, argi igorleak diren diodo organikoetan (OLED),[118] argi igorleak diren zelula elektrokimikoetan (LEC),[119] oxigeno detekzioan,[120,121] eguzki zeluletan,[122] hidrogenoaren produkzioan[123] eta katalisi foto-erredoxean,[124] besteak beste. Adibidez, OLEDetan dopatzaile fosforeszente bezala Ir(III) konplexu ziklometalikoak erabiltzeak abantailak ditu beste konposatu batzuekin alderatuta, fosforeszentzia emisio handia baitute. Beraz, kitzikatutako egoera singleteak tripleteetan bilakatzen dira sistemarteko gurutzaketa azkar baten bidez, Ir(III) atomoak egindako espin-orbita akoplamendu handiaren ondorioz. Akoplamendu horrek ere fosforeszentziaren emisioa errazten du.[125] Gainera, gailu elektrofosforeszenteetan kolore aldaketak moldatu daitezke hainbat ligando erabiliz, hain zuzen, joera elektrokimikoa eta emisio energia alda ditzaketen estekatzaileez baliatuz. Esate baterako, [Ir(ppy)$_3$] konplexuaren igorpen berdea erraz eralda daiteke horira eta gorrira, ligando ziklometalikoak ordezkatuz eta/edo LUMO orbitala baxuagoa eginez, estekatzaile egokiak aukeratuz.[126–128]

Azken urteotan, gero eta ikerketa gehiagok jarri dute arreta argiak eragindako material autokonpongarrietan. Hori dela eta, egoera naturalaren eta egoera kitzikatuen egitura elektronikoak ikertzea, batez ere metal-ligando konplexuetan oinarritutako material autokonpongarrietan, funtsezkoa izango da ematen diren prozesuak ulertzeko eta material berriak garatzeko. Beraz, egitura elektronikoen eraldaketa konputazionalki burutzeak hainbat propietate dituzten material berriak sortzea ekar dezake.

7.6   Tesiaren motibazioa eta helburuak

Nahiz eta loturen dinamikaren eta propietate makroskopikoen arteko erlazioa zuzena ez den arren, karakterizazio zehatzak eta lotura horien diseinu zuzenak oso informazio baliotsua eman dezakete material autokonpongarri berriak sortzeko.

Argi dago interakzio edo lotura dinamiko berri baten diseinua, propietate mekaniko esanguratsuekin batera, funtsezkoa dela materialon garapenean. Horietan, kimika konputazionala tresna erabilgarria bihurtzen da, esperimentuen emaitzak ulertzen eta etorkizun oparoko hautagaiak iradokitzen lagun baitezake. Horrenbestez, tesi honetan, Lewisen bikote frustratu berrietan eta pintza ligandoetan oinarritutako lotura dinamikoen karakterizazio teorikoa egiten da. Lotura horiek erraz txerta daitezke material polimerikoetan, ezaugarri berriak hobetzeko. Egitura elektronikoaren eta elkarrekintzaren ezagutza zehatzak, lotura dinamiko berrien garapena bultzatuko du eta material autokonpongarriak hobetzen lagunduko du.

Horretarako, helburu orokor eta espezifiko hauek aurkezten dira:

1. Kate polimerikoetako cross-linkerren interakzio dinamikoen karakterizazio zehatza, 7.6 irudian azaltzen den konplexua bezala orokorki adierazi daitezkeenak, material autokonpongarri berriak garatzen lagun dezaketen joera nagusiak topatzeko. Helburu hori lortzeko, ikerketa hauek egin dira:

   (a) Lewis bikote frustratuen eta dietilo azodikarboxilato molekularen (DEAD) arteko elkarrekintzaren azterketa konputazionala. Emaitzak 8. kapituluan azaltzen dira.

   (b) Pintza estekatzaileen eta trantsizio-metalen arteko elkarrekintzaren azterketa konputazionala. Emaitzak 9. kapituluan azaltzen dira.

2. Metalopolimeroetan oinarritutako material autokonpongarriek ezaugarri fotofisikoak ikertzea, sistema horien propietate luminiszenteak eta autokonpongarritasun propietatean duten eragina ulertzeko. Helburu hori lortzeko, ikerketa hauek egin dira:

   (a) Aukeratutako metal-ligando konplexuetan argia xurgatzeko propietateen azterketa konputazionala. Emaitzak 10. kapituluan azaltzen dira.

   (b) Aukeratutako metal-ligando konplexuetan argia igortzeko propietateen azterketa konputazionala. Emaitzak 10. kapituluan azaltzen dira.
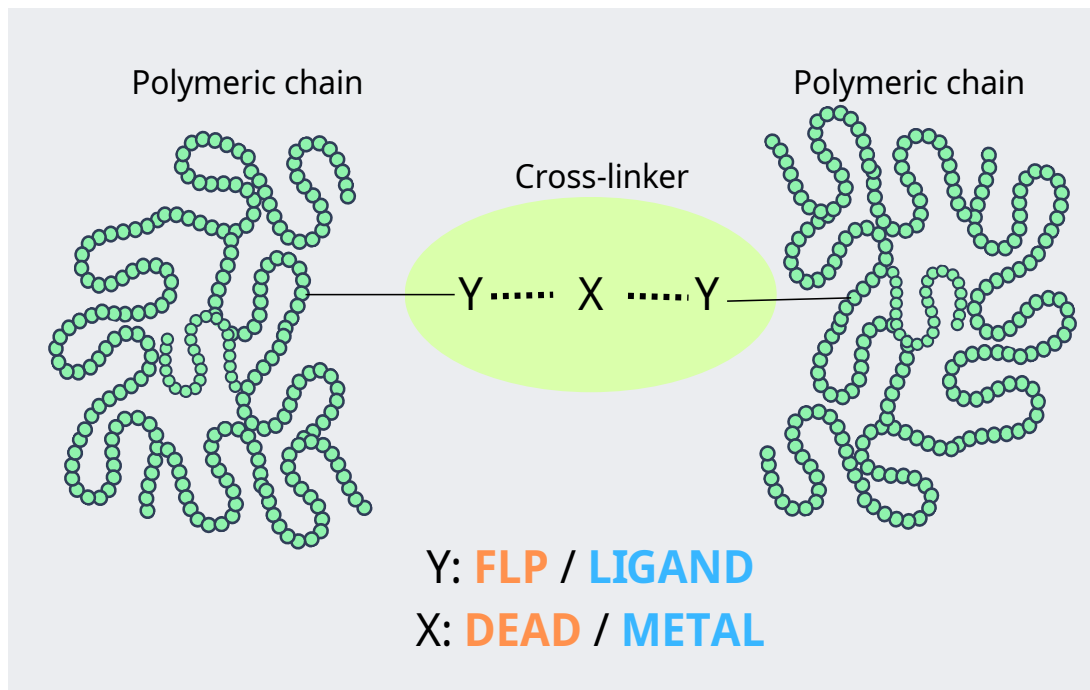
7.6. Irudia: Tesi honetan aztertutako sistemen deskribapen eskematikoa. Cross-linkerra Y-X-Y gisa irudikatzen da, non Y letra FLPri edo estekatzaileari dagokion, eta X letra, DEAD molekulari edo trantsizio-metal bati dagokion.

Lana honela antolatu da: 7. kapituluan tesiaren sarrera bat aurkezten da. Ondoren, 8., 9. eta 10. kapituluetan, tesi honen emaitzak laburbildu dira. Azkenik, ondorio nagusiak 11. kapituluan laburtzen dira.

Kapitulua 8

Material autokonpongarrietako Lewis bikote berrien karakterizazio teorikoa

Kapitulu honetan, molekula txiki baten (dietilo azodikarboxilatoa, DEAD) eta frustratutako Lewisen bikote batzuen arteko elkarrekintzaren azterketa konputazionala egiten da. Zehazki, trifenilborano (TPB) eta trifenilfosfina (TPP) deribatuetan oinarritutako Lewis azidoak eta baseak hartu dira kontuan, eta hainbat ordezkatzaile elektroi emaile (EDG) zein hartzaile (EWG) dituzte fenilo eraztunen *orto* eta *para* posizioetan. Beraz, lan honen helburu nagusia da aipatutako espezieen arteko elkarreraginak hobeto ulertzea, diseinurako garrantzitsuak diren parametroak argitzea eta material autokonpongarri berriak eta hobetuak iradokitzea.

8.1   Sarrera

Azken urteetan, lotura dinamikoak dituzten material autokonpongarriek sekulako gorazarrea izan dute material berritzaileak sortzeko. Horrez gain, material autokonpongarriak sortzeko polimero sintetikoak hautagai onak dira. Duela gutxi, Lewis bikote frustratuak (FLP) material horiek sortzeko erabili dira. Zehazki, lotura dinamikoak sortzeko, dietil azodikarboxilatoaren (DEAD, ikusi irudi hau: 8.1, goran eskuinean) aktibazioa lortu da trifenilborano (TPB) eta trifenilfosfina (TPP) konposatuetan oinarritutako FLPa erabiliz.[67,72] Atal honetan, material horietan dagoen kimika konputazionalki aztertzen dugu, FLP eta DEAD konposatuen arteko interakzio itzulkorra eta horren natura ulertzeko asmoarekin. Helburu hori ahaztu gabe, lehenik hainbat TPB eta TPP deribatuen azidotasuna eta basikotasuna karakterizatu ditugu ordezkatzaile ezberdinak erabiliz, hala nola elektroi emaileak eta elektroi hartzaileak direnak. Lortutako emaitzetan ikusten da elektroi emaile sendoek TPB konposatuaren azidotasuna handitzen eta TPP konposatuaren basikotasuna txikitzen dutela. Hala ere, FLP-DEAD interakzioa ez dute ordezkatzaile horiek mugatzen TPB edo TPP sistemetan, baizik eta ordezkatzaileen artean dauden erakarpen edo aldarapen indarrek; hidrogeno loturak edo eragozpen esterikoak, besteak

beste. Emaitza horietan oinarrituta, FLP-DEAD konplexuetan datzan material berri bat proposatu da.
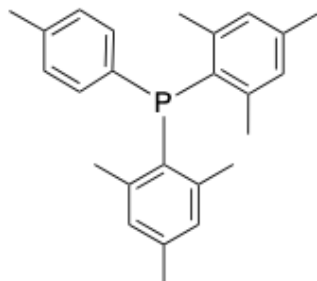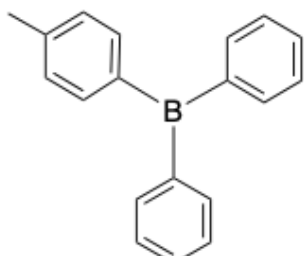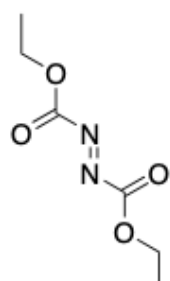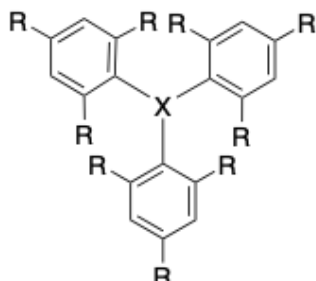
8.1. Irudia: Goran: Lewis azidoen (X = B) eta baseen (X = P) eredu molekularrak, ordezkatzaile elektroi emaile (R = CH$_3$, NH$_2$, OH, OCH$_3$ and OCOCH$_3$) eta hartzaile (R = F, CF$_3$, CN, NO$_2$ and SO$_3$H) erabilita (ezkerra), eta DEAD linker molekula (eskuina). Beheran: Lan esperimentaleko Lewis azido eta baseak.[67]

8.2   Metodologia

Geometria optimizazio eta frekuentzia bibrazionalaren kalkulu guztiak Dentsitate Funtzionalaren Teoria (DFT)[146,147] erabiliz lortu dira Gaussian 16[187] programaz baliatuz. Hain zuzen, geometriak gas fasean optimizatu dira TPSS elkartrukatze korrelazio funtzionala[188] eta def2-TZVP base sorta erabiliz.[189,190] Dispertsio interakzioak kontuan hartu dira Grimme's dispertsio bertsioaren D3 mota enpirikoa erabiliz.[191] Teoria maila hori Schrimer eta Grimme zientzialariek proposatu zuten eta egokiena da azido-base interakzio ahulak aztertzeko, esaterako, Lewis pare frustratuetan ageri diren interakzioak.[192] Geometria optimizazioak kalkulatu ondoren, frekuentzia harmoniko bibrazionalak kalkulatu dira analitikoki eta gradiente diferentziak kontuan hartu dira, teoria maila berdina erabiliz, karakterizatutako egiturak minimo errealak diren identifikatzeko. Frekuentzia horiek zero-puntuko energia bibrazionalak (ZPVE) eta entalpiaren zuzenketa bibrazional termikoak (T = 298 K) ebaluatzeko erabili dira. Interakzio energiek base sortaren superposizio errorearen (BSSE) zuzenketa barne hartzen dute. Horiek Counterpoise metodoa erabiliz kalkulatu dira.[193,194]

Azkenik, elkarrekintzaren izaera aztertzeko Orbital Natural Lotzailearen (NBO)[175,195,196] eta Energia Deskonposizio Analisia (EDA)[197,198] metodoak erabili dira. EDA kalkuluak BP86 funtzionala[199,200] erabiliz burutu dira ζ-hirukoizdun base sortarekin konbinatuz (ADF base sorta (TZP)). Horretarako, ADF2017 programa erabili da.[201]

8.3 Ondorioak

Atal honetan, konputazionalki aztertu dira Lewis pare frustratuekin sortutako hainbat konplexu eta molekula txiki bat (dietil azodikarboxilatoa, DEAD), material autokonpongarrietan lotura dinamiko berriak sortzeko asmotan. Shaver eta bere lankideek bultzatutako lanean oinarrituta,[67] FLPen sorta bat diseinatu da trifenilboranoan (TPB) eta trifenilfosfinan (TPP) datzan Lewis azidoak eta baseak erabiliz. Helburua FLPen eta DEAD molekularen arteko interakzioaren natura eta, bai azidoetan, bai baseetan, ordezkatzaileek duten eragina ulertzea izan da.

Lehenik eta behin, parametro ezberdinak erabiliz, TPB eta TPP deribatuen azidotasuna eta basikotasuna analizatu da. Lewis azidoentzat, hidruro afinitatea (HA), indar elektrohartzailea (ω^+), ^{31}P-NMR desplazamendu kimikoaren aldaera ($\Delta\delta$) eta boroaren orbital hutsaren energia (ε_B) analizatu dira; berriz; Lewis baseentzat ikertutako parametroak protoi afinitatea (PA), indar elektroemailea (ω^-), indize nukleofiloa (N) eta fosforoaren pare askearen orbital energia (ε_P) izan dira. Azidoentzat, parametro guztiek adierazten dute feniloetako ordezkatzaile elektroi hartzaileek Lewis azido sendoagoak ematen dituztela, aldiz, baseen kasuan, ordezkatzaile elektroi emaileek Lewis base sendoagoak ematen dituzte.

Aipatutako sortatik, hiru TPB eta TPP deribatu aukeratu dira, azido eta base sendo, ertain eta ahul bezala zehaztutakoak, eta 17 FLP sortzeko konbinatu dira; lan esperimentaleko erreferentzia sistema ere aztertu da. FLPa sortzeko azido-base interakzio energia (ΔH_1) eta FLPen eta DEAD molekularen arteko interakzioa (ΔH_2) kalkulatu dira. Lortutako egituratan eta interakzio energiatan oinarrituta, hidrogeno loturak edo emaile-hartzaile loturak sortzeko ahalmena duten ordezkatzaileak baztertu egin dira, FLP-DEAD interakzioa gaitzetsi baitzezakete.

Amaitzeko, NBO eta EDA analisiek FLP-DEAD interakzioaren informazio osagarria lortzeko erabili dira. NBOari dagokionez, DEAD espezieak konfigurazio elektronikoaren berrantolaketa jasaten du. Era horretan, lotura kobalente datiboak sortzen dira TPB-DEAD eta TPP-DEAD zatien artean, lotura kobalente polarrak erdietsiz. Gainera, lotura horiek polarizatuago daude B-N loturan P-N loturan baino. Erreferentzia sistemarekin alderatuz, lotura natura antzekoak kalkulatu dira gainontzeko sistementzat, NBO analisian bezala. Konplexuen artean azaltzen diren ezberdintasun txikiek ezin dituzte azaldu FLP-DEAD interakzio energian ikusten diren ezberdintasun handiak. Beraz, ezberdintasun handi horiek ordezkatzaileen arteko aldarapen esterikoarekin zerikusia dute, eta ez loturaren joeran dauden aldaketekin.

Bukatzeko, erreferentziazko materialaren ordezko errealista izateko, lan honetan FLP_4-DEAD sistema bakarrik proposatzen da. Bestela, materialean hobekuntzak egoteko, aintzat hartu behar da linkerra ordezkatzea edo beste FLP mota batzuk erabiltzea.

Amaitzeko, lanaren zati honetan FLP_4-DEAD sistema sistema proposatzen da auto-konpongarriak diren polimero berriak garatzeko. Dena den, materialotan hobekuntzak egoteko, aintzat hartu behar da linkerra ordezkatzea edo beste azido eta base zentruak (adibidez, Al, Ga edo N) dituzten FLPak erabiltzea.

Kapitulua 9

Metal-ligando elkarrekintzaren ezagutza konputazionala metalopolimero autokonpongarrietan

Kapitulu honetan, terpiridina (TPY) eta terfosfinina (TPPh) pintza estekatzaileen eta trantsizio-metalen arteko elkarrekintzaren azterketa konputazionala egin da. Helburu nagusia da elkarreragin hori hobeki ulertzea eta identifikatzea funtsezko parametroak material autokonpongarrietarako hautagai berriak diseinatzeko. Horretarako, loturaren azterketa zehatza egiten da eta ligandoaren eta metalaren eragina ikertzen da.

9.1   Sarrera

Azken urteotan, metalopolimero sintetikoak etorkizun oparoko hautagaiak izan dira material aurreratuak sortzeko. Testuinguru horretan, hainbat metal-ligando konplexu aztertu dira material autokonpongarri berriak bilatzeko asmotan. Hortz aniztun estekatzaileak erabiltzeak (terpiridina, esaterako) handitu egiten du metalekin lotzeko ahalmena, efektu kelatzaileari esker,[100] eta metal-ligando $d\pi$-$p\pi$ lotura.[101] Ondorioz, TPY duten polimeroak garatu dira trantsizio metalak erabiliz, adibidez, Fe(II),[103] Cd(II),[103,104] Zn(II),[105,106] eta Co(II).[107] Baita Rowan eta Wederren metalopolimeroa, autokonpongarritasun gaitasuna duena. Azken hori, Zn(II) eta La(III) trantsizio metalek hiru horzdun piridina estekatzailearekin duten interakzioan oinarritzen da.[53]

Metal-ligando interakzio hori alda daiteke, bai estekatzailea, baita trantsizio-metala ere aldatuz. Dena den, gure ezagutzaren arabera, terpiridinaren analogoa den terfosfinina (TPPh) oraindik ez da erabili metalopolimeroen pintza estekatzaile gisa. Gainera, fosfininen ezaugarri elektronikoak eta piridinenak oso desberdinak dira, hala nola pi-hartzaile izaera handia dute.

Kapitulu honetan, metodo konputazionalak erabili ditugu metalopolimero horien ki-mika dinamikoa aztertzeko. Hain zuzen ere, cross-linker itxurako ligandoak erabili di-tugu, 9.1 irudian definitu direnak. Bertan ageri dira ligando batekin (ezkerrean) eta bi ligandorekin (eskuinean) erabilitako konplexuak, non X = N TPYri eta X = P TPPhri dagokion. Bestalde, elektroi hartzaile (EWG) eta emaile (EDG) taldeekin (R) ordezkatu ditugu ligandoak, eta hainbat trantsizio metal katioi erabili ditugu (M).
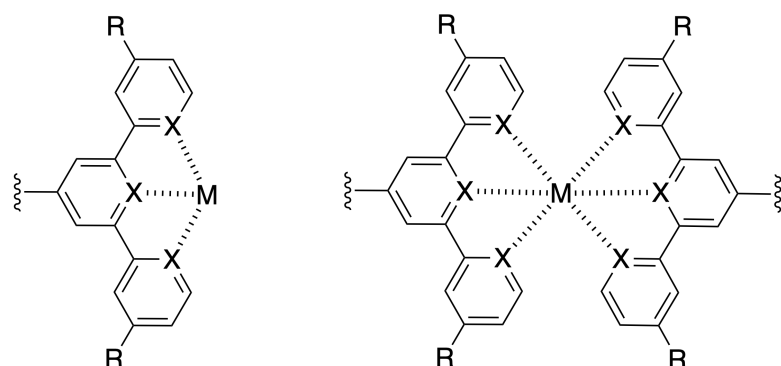
9.1. Irudia: Aztertutako sistemen eredu molekularra. Ezkerrean, pintza estekatzaile batekin, eskuinean, birekin. X = N kasurako, ligandoa terpiridina da eta, X = P kasurako, terfosfinina. Estekatzaileak elektroi emaile (EDG, R = NH$_2$) eta hartzaile (EWG, R = CN) taldeekin ordezkatu dira. Konplexatutako metal ioiak M = Fe(II), Cu(I), Zn(II), Ru(II), Cd(II), Sc(I), Sc(II) eta Sc(III) dira.

Eredu horietan oinarrituta, identifika ditzakegu metal-ligando elkarrekintzen funtsez-ko ezaugarri elektronikoak, horrela, material autokonpongarri eraginkorragoak diseina-tzeko. Zehazki, trantsizio-metalek duten eragina aztertuko dugu TPY ligandoa duten metalopolimeroetan. Ondoren, TPY estekatzaileen fenilo eraztunetan elektroiak har-tzaile eta emaile taldea ipiniko da, nitrogenoaren $sigma$-emaile izaera aldatzeko, eta, azkenik, nitrogenoa fosforoz aldatzearen eragina aztertuko dugu, TPPh estekatzailea erabiliz. Gure aurkikuntzek adierazten dute periodo batean ezkerraldean kokatutako trantsizio-metalek elkarrekintza indartsuagoak sortzen dituztela eskuineko aldean daude-nekin alderatuta. Gainera, estekatzailean ordezkoak sartzeak eragin txiki bat izan dezake interakzioan, hala ere, ordezko horiek egoteak ez du metal-ligando elkarrekintza mota zehazten. Bestalde, TPY TPPh estekatzailearekin ordezkatuz gero, elkarrekintza ener-giak txikitu egiten dira. Emaitza horietan oinarrituta, zenbait konplexu proposatzen dira polimero autokonpongarri hobeak sortzeko.

9.2   Metodologia

Geometria optimizazio kalkulu guztiak Dentsitate Funtzionalaren Teoria (DFT)[146,147] erabiliz lortu dira, ωB97XD funtzionalaz[203] eta 6-31+G(d,p)[204] base-sortaz baliatuz. Lortutako egiturak optimoak direla baieztatzeko, frekuentzia kalkuluak egin dira teoria

maila berdina erabiliz. Gero, frekuentzia horiek zero-puntuko energia bibrazionalak (ZP-VE) eta entalpiaren zuzenketa bibrazional termikoak (T = 298 K) ebaluatzeko erabili dira. Azkenik, egitura optimoetan, single-point kalkuluak burutu dira energia balioak hobetzeko 6-311++G(2df,2p) base sorta[205] erabiliz.

Azkenik, elkarrekintzaren izaera aztertzeko Orbital Natural Lotzailearen (NBO)[175,195,196] eta Energia Deskonposizio Analisia (EDA)[197,198] metodoak erabili dira. EDA kalkuluak BP86 funtzionala[199,200] erabiliz burutu dira ζ-hirukoizdun base sortarekin konbinatuz (ADF base sorta (TZP)). Horretarako, ADF2017 programa erabili da.[201]

Elkarrekintzaren izaera aztertzeko, bi metodologia erabili dira: batetik, Orbital Natural Lotzailearen (NBO)[175,195,196] eta, bestetik, atomoak molekuletan teoria kuantikoa (QTAIM)[206,207]. Azken horrek puntu kritikoak identifikatzen ditu, adibidez, elektroi dentsitatearen gradientea desagertzen den espazioko puntuak ($\nabla\rho$). Puntu kritikoak elektroi dentsitatearen Laplaziarraren zeinuaren arabera identifikatzen ditu ($\nabla^2\rho$). Bi atomoren arteko lotura puntu kritikoa (BCP), bi atomoak lotzen diren bidean aurkitzen da, zehazki, elektroi dentsitateak balio minimoa duen puntuan.Elektroi dentsitatea eta BCP puntuko Laplaziarra (ρ_{BCP} eta $\nabla^2\rho_{BCP}$), dagokion loturaren izaera identifikatzeko erabil daitezke, hurrengo erlazioetan oinarrituz:

$$\frac{1}{4}\nabla^2\rho = 2G + V \tag{9.1}$$

$$H = G + V \tag{9.2}$$

non G, V eta H BCP puntuko energia dentsitate zinetikoa, potentziala eta totala diren. Beraz, G positiboa denez eta V negatiboa, orduan, baldin eta $|V| > 2G$ bada, Laplaziarra negatiboa izango da ($\nabla^2\rho < 0$) eta elkarrekintza kobalentea izango da. Aldiz, $|V| > G$ bada, Laplaziarra positiboa izango da ($\nabla^2\rho > 0$), baina dentsitate energia totala negatiboa (H < 0). Kasu horretan, interakzioa partzialki kobalentea izango da. Azkenik, $|V| < G$ bada, Laplaziarra eta dentsitate energia totala positiboak izango dira ($\nabla^2\rho$, H > 0), interakzio ez kobalentea adieraziz.[183–186] Gainera, ρ balioa nahiko handia ($\rho > 0.03$) eta H < 0 badira, interakzioa partzialki kobalentea dela esaten da.

Kalkulu guztiak egiteko, Gaussian 16[187] eta AIMAII[208] programak erabili dira.

9.3   Ondorioak

Kapitulu honetan, konputazionalki aztertu dira terpiridina (TPY) eta terfosfinina (TPPh) pintza estekatzaileak zenbait trantsizio-metalekin batera, hala nola Cd(II), Zn(II), Cu(I), Fe(II), Ru(II) eta Sc(III). Era horretan, interakzioaren natura ulertzea izan da helburua,

material autokonpongarrietan erabilgarriak izan daitezken lotura dinamikoak sor baiti-
tzakete.

Lehenik, trantsizio-metalaren efektua aztertu da. Horretarako, disoziazio energiak
aztertu dira. Ikusi denez, disoziazio energiak txikitzeko joera du periodoan zehar ezke-
rretik eskuinera. Joera hori ligandotik metalera dagoen karga transferentziagatik izan
daiteke, d orbital hutsak daudelako, eta, ondorioz, lotura sendoagoak sortzen dira. Joera
hori bat dator N-M lotura distantziaren aldaketarekin, zeina handiagoa den Cu(I), Cd(II)
eta Zn(II) metalentzat, eta txikiagoa Fe(II) eta Ru(II) metalentzat. Sc(III) kasu berezia
da, izan ere, karga transferentzia orbital birtual energetiko altuagoetan gertatzen da, eta
elkarrekintza energia handia bere karga ioniko handiak sortzen du. Horrek, ioi-dipolo
elkarrekintza sendoak eragiten baititu. Gainera, eragozpen esterikoak M-N loturaren lu-
zera ere handitu dezake. Bestalde, loturaren analisiak adierazten du interakzioa partzialki
kobalentea dela.

Bigarrenik, estekatzailearen fenilo eraztunetan talde elektroi emaileak eta hartzaileak
duten eragina aztertu da. Horretarako, TPY eta TPPh ligandoak EDG (NH_2) eta EWG
(CN) taldeekin ordezkatu dira. Oro har, ikusi da talde elektroi emaileak interakzio energia
handiagotzen duela, aldiz, talde elektroi hartzaileak txikitu egiten du. Hala ere, ordez-
katzaileek interakzio energian duten eragina oso urria da eta parametro geometrikoetan
ez da aldaketarik antzematen. Horiek horrela, esan daiteke lotura indarra ez dutela talde
funtzional horiek zehazten, baizik eta metalaren eta estekatzailearen naturak.

Azkenik, koordinazio atomoak (X) estekatzailean duen eragina aztertu da, Fe(II)-
TPY eta Fe(II)-TPPh konplexuak alderatuz. Gainera, TPPh ligandoan NH_2 eta CN tal-
deak txertatu dira. Ikusi denez, TPPh estekatzailea duten konplexuek disoziazio energia
baxuagoak dituzte TPY konplexuenak baino. Izan ere, ligandoaren egitura elektronikoak
zerikusia du metalaren d orbitalen eta estekatzailearen interakzioan. Hori dela eta, fosfo-
roaren bikote askea ez da HOMO orbitala eta nitrogenoen bikote askeak baino $3s$ izaera
sendoagoa erakusten du (sp^2 izaera ahulagoa). Hala, σ-emaile ahalmena txikitzen da
eta interakzio ahulagoak sortzen dira. Gainera, $d\pi$-$p\pi$ donazioa antzematen bada ere,
TPPh-ren pi-hartzaile gaitasuna agerian utziz, ez dirudi nahikoa denik σ-emaile gaita-
sun ahula orekatzeko. Bestalde, NH_2 duten TPPh ligandoen kasuan, disoziazio energia
handiagoak bildu dira, eta, CN duten TPPh ligandoentzat baxuagoak. Emaitza horiek
TPY estekatzailearen emaitzekin bat datoz.

Laburbilduz, karga handiek interakzio energia handiak direla eta, erronka handia
da autokonpongarritasun propietatea lortzeko konplexu bat proposatzea. Giro tenpe-
raturatik hurbil dauden tenperaturetan, materialok 40-60 kcal/mol-eko interakzio ener-
giak dituzte. Horrek, aztertutako kasuetan kontraioien garrantzia erakusten du. Beraz,
kontraioien eragina kontuan hartu behar da materialon interakzio energia kuantitatibo
egokiak erreproduzitzeko. Hala ere, oso zaila da metalopolimero horietako ioi-metal -
kontraioi egitura erreala zein den esatea, izan ere, esperimentuak handizka egiten dira,
eta, ziur aski, metala eta kontraioiaren klusterrak sortuko dira (ikusi etorkizuneko lana
xehetasun gehiagorako). Dena den, espero dugu katioi metalikoen ereduetan oinarritu-
tako joerak eta kontraioiak gehitzean egongo direnak antzekoak izatea. Gure emaitzetan

oinarrituta, uste dugu interesgarria litzatekeela zenbait alderdiren konbinazioa aztertzea, nahi den elkarreragina lortzeko. Adibidez, estekatzailea periodo baten eskuinean dagoen trantsizio-metal batekin konbinatuz gero, interakzio ahulagoa lortuko litzateke, ezkerrean dagoen trantsizio-metal batekin alderatuta. Horretaz gain, pintza estekatzailean ordezkatzaileak gehitzeak oso gutxi eragiten du elkarrekintzan. Gainera, TPPh estekatzailea erabiltzea beste aukera bat izan daiteke interakzio energia handiak txikitzeko. Bada, espekula daiteke [TPY-Fe-TPY]$^{+2}$, [TPPh-Fe-TPPh]$^{+2}$ eta [TPY-Zn-TPY]$^{+2}$ konplexuek autokonpongarritasun propietatea erakutsi dezaketela. Alabaina, TPPh estekatzailea gehiago ikertzea beharrezkoa da etorkizunerako.

Kapitulua 10

Metal-ligandoz osatutako metalopolimeroen propietate fotofisikoak

Kapitulu honetan, aztertzen da hainbat metal-ligando konplexuk (9 atalean aztertu dituzunen antzekoak) argiarekin nola jarduten duten, zehazki, metalopolimeroetan cross-linker gisa erabiltzen direnak. Hala, kapitulu honen helburu nagusia propietate fotofisikoak ulertzea da, hain zuzen, konplexu horietan gerta daitezkeen absortzio eta emisio prozesuak ulertzea. Horiek horrela, polimero berritzaileak sortzeko aukera egongo litzateke, autokonpongarritasun propietateaz gain propietate fluoreszente edo fosforeszente interesgarriak dituztenak, alegia.

10.1   Sarrera

Argiaren eta materiaren arteko elkarreraginak prozesu fotokimikoak (argiak eragindako erreakzio kimikoak) nahiz fotofisikoak (argiarekin edo gabe kitzikatzeko eta desaktibatzeko prozesuak) barne hartzen ditu. Azken horretan, hasiera batean, ez dago erreakzio kimikorik, eta gure materialotan aztertu nahi ditugun prozesuak biltzen dituzte. Zehazki, fotoeszitazioan, molekulak eraginda daude egoera elektroniko naturaletik egoera elektroniko kitzikatura, fotoiaren absortzioa dela eta. Prozesu horrek molekulen absortzio espektroak eragiten ditu, alegia, UV/Vis espektroak. Absortzio prozesuan, egoera kitzikatua eta egoera naturala spin berekoak dira, hautatze arauen ondorioz. Absortzioa gertatzen denean, kitzikatutako egoera elektroniko horien bilakaera ezberdina izan daiteke. Prozesu nagusiak lau kategoriatan bana daitezke, **??** irudian ikusten den bezala Jablonskiren diagraman. Egoera eszitatu elektronikoa spin egoera berean gera daiteke, eta egoera eszitatu baxuenetik irradiatu dezake fluoreszentzia emanez, edo egoerara naturalera itzul daiteke barne-konbertsioaren bidez (IC). Horrez gain, egoera kitzikatua beste spin egoe-

ra batera eralda daiteke sistemarteko gurutzaketa bidez (ISC). Bertan, fosforeszentzia eman dezake argia igorriz edo egoera naturalera igaro daiteke argirik igorri gabe bigarren ISC baten bidez. Laburbilduz,badira prozesu ez-erradiatiboak eta erradiatiboak (fluoreszentzia eta fosforeszentzia). Gure helburua hautatutako sistemetan erradiatzen duten prozesuak aztertzean datza.
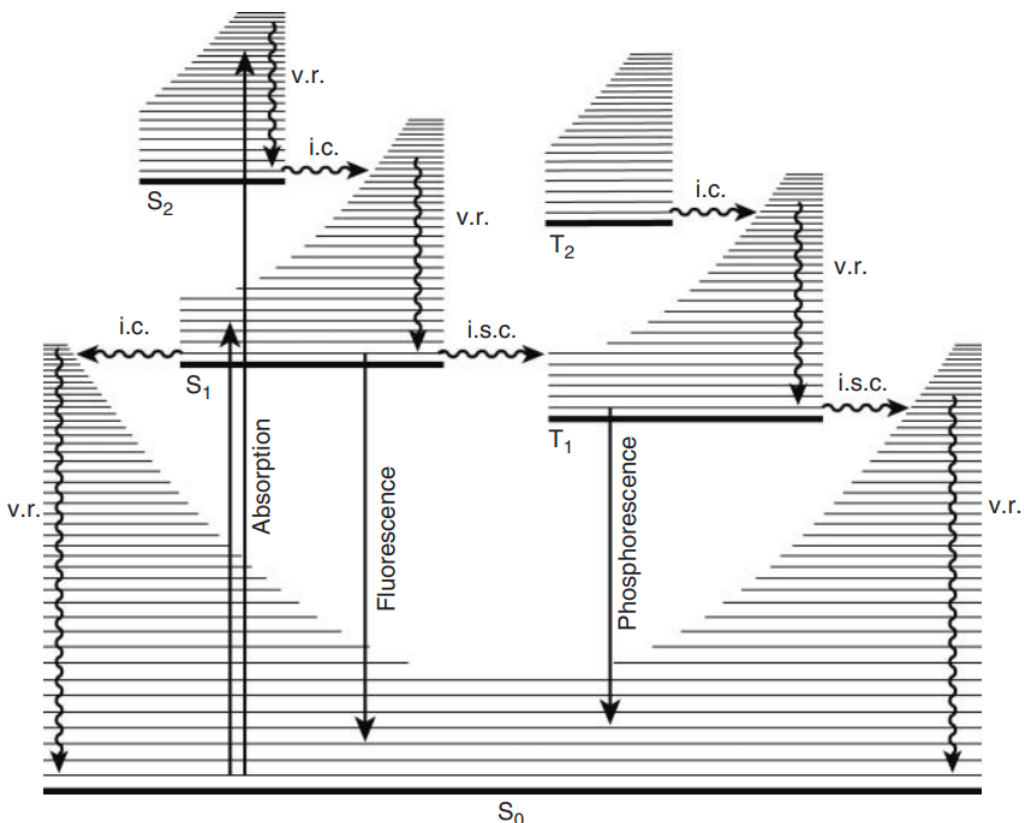
10.1. Irudia: Jablonskiren diagrama. Molekula baten egoera naturala (S_0) eta egoera kitzikatuak (S_1, S_2 eta T_1) adierazten ditu, bai eta honako prozesu fotofisiko hauek ere: absortzioa, fluoreszentzia, fosforeszentzia, erlaxazio-bibrazionala (v.r.), barne-konbertsioa (i.c) eta sistemarteko gurutzaketa (i.s.c). 218 erreferentziatik hartutako irudia da.

Jakina da trantsizio-metalek uhin-luzera desberdineko fotoiak absorbatu eta igor ditzaketela, egitura elektronikoa dela eta. Molekula ez-organikoen artean, trantsizio-metalak dituzten konplexuak dira fotokimika eta fotofisikari dagokionez garrantzitsuenak. Oro har, konplexu horiek oso simetrikoak dira, eta trantsizio-metalek bete gabeko d-orbital konfigurazioa erakusten dute, egoera naturalaren hainbat multiplizitaterekin. Gainera, atomo astunak egoteak orbita-akoplamendu handia eragin dezake, batez ere bigarren eta hirugarren periodoetako trantsizio-metaletan, eta horrek ISC prozesuak errazten ditu. Adibidez, platinozko konplexuek debekatutako spinen absortzio banda dute. Absortzio banda hori baimendutako spinen antzekoa da intentsitatean. Kasu horietan, egoera naturala singletea duten konplexuentzat (S_0), $S_1 \rightarrow T_1$ sistemarteko gurutzaketaren eraginkortasuna unitatetik hurbil egon ohi da, eta fluoreszentziaren errendimendu kuantikoa zerotik hurbil egon ohi da.[219,220] Rutenioaren kasuan, esaterako, Ru(II)-polipiridinak eta Ru(II)-2,2'-bipiridina konplexuek luminiszentzia erakusten dute, zehazki,

fosforeszentzia. Konplexu horietan, egoera kitzikatu baxuenaren natura alda daiteke metal eta/edo estekatzaile egokiak erabiliz. Beraz, egoera kitzikatuaren energia asko alda daiteke, metal-ligando karga transferentzian (MLCT) parte hartzen duten estekatzaileak aldatuz, energia zorrotz egokitu baitaiteke bere egitura aldatuz. Egoera kitzikatuaren energia moldatzeko beste aukera bat da MLCT trantsizioetan parte hartzen ez duten estekatzaileak ordezkatzea.[221,222]

Material autokonpongarriei dagokienez, argi dago prozesu fotofisikoak funtsezkoak direla material berritzaileen garapenean.

Bi alderdi horiek lotuta egon daitezke, Sarreran ikusi den bezala. Rowan eta Wederrek frogatu zuten metalopolimeroen autokonponketa prozesuan beroa askatzen dela barne-konbertsioaren eraginez, argi ultramorearen eraginpean egon ondoren, eta errendimendu txikiko fluoreszentzia ematen dela.[53] Hala ere, dakigunez, ez da informazio gehiago eman konplexuaren egitura elektronikoari eta behatutako fluoreszentziaren jatorriari buruz. Beraz, konplexu horietan gertatzen diren egoera elektronikoak eta prozesu fotofisikoak zehatz-mehatz ezagutzea funtsezkoa da materialon prozesu autokonpongarriak ulertzeko. Horiek horrela, kapitulu honen helburua da aurreko kapituluan aztertutako zenbait konplexuren propietate fotofisikoak aztertzea, alegia, [TPY-M-TPY]$^{n+}$ konplexuak Fe(II), Ru(II), Cd(II), Zn(II) eta Ir(III) metalekin. Azken metal hori ere ikertzea erabaki da beren konplexuek erakusten dituzten propietate luminiszente interesgarriak direla eta.[223] Gainera, [TPPh-Fe-TPPh]$^{2+}$ konplexua ere ikertu da estekatzaileak eragiten duen efektua ulertzeko.

10.2   Metodologia

Geometria optimizazio kalkulu guztiak Dentsitate Funtzionalaren Teoria (DFT)[144,145] erabiliz lortu dira, ωB97XD funtzionalaz[203] eta 6-31+G(d,p)[204] base-sortaz baliatuz. Lortutako egiturak optimoak direla baieztatzeko, frekuentzia kalkuluak egin dira teoria maila berdina erabiliz. Gero, frekuentzia horiek zero-puntuko energia bibrazionalak (ZPVE) eta entalpiaren zuzenketa bibrazional termikoak (T = 298 K) ebaluatzeko erabili dira. Behin egoera naturaleko geometriak optimizatuta eta egitura elektronikoak karakterizatuta, propietate fotofisikoak kalkulatu dira TDDFT[156] erabiliz, teoria maila berean. Absortzio propietateak aztertzeko, trantsizio gertagarrienak identifikatzeko, trantsizio bertikaleko 20 energia baxuenak eta haien indar oszilatzaileak kalkulatu dira. Gero, singlete eta triplete egoera kitzikatu baxuenen bilakaera aztertu da haien geometriak optimizatzen, eta egoeren gurutzaketa eta oszilatzaileak aztertu dira emisio propietateak aurresateko, hala nola fluoreszentzia eta fosforeszentzia ematen diren aurresateko. Kalkulu guztiak Gaussian 16[187] programa erabiliz burutu dira.

10.3 Ondorioak

Kapitulu honetan, materialak sintetizatzeko hainbat metal-ligando konplexuen propietate optikoak aztertu ditugu. Hain zuzen ere, $[M\text{-}XXX]^{n+}$ eta $[XXX\text{-}M\text{-}XXX]^{n+}$ konplexuen absortzio eta emisio propietateak ikertu dira, M trantsizio-metala izanik, esaterako, Zn(II), Cd (II), Fe(II), Ru (II) eta Ir(III), eta XXX pintza estekatzailea izanik, hala nola terpiridina (TPY) eta terfosfinina (TPPh).

Konposatu horien absortzio propietateek erakusten dute absortzioa UV eremuan gertatzen dela bai ligando baten kasuan, baita bi ligandoren kasuan ere. Eskuinaldean kokatutako transtsizio-metalak, Cd(II) eta Zn(II), absortzio pikoak energia altuagoetan erakusten dituzte. Bi kasuotarako, bat edo bi estekatzaile izanik ere, absortzio energiak 4.0 eV-tik gorakoak dira, eta txikiagoak dira ligando bakarreko konplexuentzat bi ligando dituztenentzat baino. Erdialdean kokatzen diren trantsizio metalak malguagoak dira, eta eskuinaldeko trantsizio-metalen intentsitate antzeko pikoak erakusten dituzte, baina badituzte beste piko ez hain intentsu batzuk energia baxuagoko (uhin-luzera handiagoak) trantsizioei dagozkienak. Oro har, piko horiek UV eremuan daude, baina, Fe(II) eta Ru(II) konplexuetan eremu ikuskorretik gertu azaltzen dira. Azkenik, TPY ligandoa TPPh ligandoarekin ordezkatzeak espektroa gorriruntz mugitzen du.

Fluoreszentzia propietateak aztertzeko, sistema guztietarako energia baxueneko singlete egoera elektroniko kitzikatua optimizatu da. Absortzio propietateei dagokienez, eskuinaldeko eta erdialdeko trantsizio-metalen konplexuek joera ezberdina dute. Erdialdeko trantsizio-metalen kasuan, joera posibleena barne-konbertsio ez erradiatiboa izango litzateke, berriz, eskuinaldeko trantsizio-metalen kasuan, hasiera batean ez litzateke prozesu hori emango egoera singlete baxuena energia altuagoetan baitute. Bi ligando dituzten konplexuei dagokienez, konplexu guztietan ez litzateke inolako barne-konbertsiorik gertatuko, baizik eta konplexu guztiek UV eremuan igorriko lukete. Dena den, $[TPY\text{-}Ru\text{-}TPY]^{2+}$ konplexua salbuespena da, gure datuen arabera fluoreszentzia emango lukeelako.

Dena den, singlete egoeren bilakaerak triplete egoeran amai dezake sistemarteko gurutzaketa ematen bada. Gure aurretiazko kalkuluen arabera, $[TPY\text{-}Zn\text{-}TPY]^{2+}$ eta $[TPY\text{-}Ru\text{-}TPY]^{2+}$ konplexuentzat, S_1 egoeraren lasaikuntzan ikusi da triplete egoera gurutzatu dezakeela, eta, noiz edo noiz, energia baxuagoko T_1 egoerara igaro.

Bi kasuetan, egoera horretarako geometria optimizatuan, egoera naturalarekiko energia desberdintasuna eremu ikuskorrean aurkitzen da. Hori dela eta, material horiek fosforeszenteak direnik ondorioztatzerik ez dugun arren, ikus daiteke fosforeszentzia egoera kitzikatuaren bilakaera posibleetako bat dela. Horregatik, sistema horien egoera kitzikatuen bilakaera nahiko korapilatsua izan daiteke, erorketa ez erradiatibotik, barne-konbertsioa dela eta, erorketa erradiatibora igaroz, eta fluoreszentzia edo fosforeszentzia lortuz.

Kapitulua 11

Laburpena, ondorio orokorrak eta etorkizuneko lana

Tesi honetan, zenbait lotura dinamiko mota ikertu ditugu, hala nola FLP-linker eta metal-ligando elkarrekintzak, propietate mekaniko egokiekin, material polimerikoetan txertatzeko. Horretaz gain, metal-ligando konplexuen propietate fotofisikoak aztertu dira, autokonpongarritasun propietateaz gain beste propietate osagarri batzuk dituzten materialak lortzeko. Era horretan, material autokonpongarri eraginkorragoak diseinatzeko, propietate optiko interesgarriak izan ditzaketenak, funtsezko faktore batzuk ulertu ahal izan ditugu. Elkarrekintza horien egitura elektronikoa eta elkarrekintzak ulertzea funtsezkoa da lotura dinamiko berriak garatzeko. Hain zuzen, 11.1 irudian definitutako egitura orokorrean cross-linkerrak ageri dira, eta ikerketak cross-linker horien interakzio dinamikoak aztertzen ditu, zehatz-mehatz karakterizatuz. Sistema horiek eta beren elkarrekintza mekanismoak ezagutarazteko, metodo konputazionalak erabili dira, alegia, Dentsitate Funtzionalaren Teoria (DFT). Gainera, metal-ligando batzuen propietate fotofisikoak aztertu ditugu, material autokonpongarrietan oinarritutakoak, Denboraren Mendeko Dentsitate Funtzionalaren Teoria (TDDFT) erabiliz, absortzio eta emisio propietatean karakterizatuz.

11.1   FLP-DEAD materialak

Tesi honen lehen zatian (8 kapituluan), Frustrated Lewis Pair (FLP) oinarri duten lotura dinamikoen karakterizazio teorikoa aztertu da. Shaver-en eta kolaboratzaileen lan esperimentalean oinarrituta, FLPen multzo bat diseinatu da trifenilboranoan (TPB) eta trifenilfosfinan (TPP) oinarritutako Lewis azidoak eta baseak eta horien deribatuak erabiliz, DEAD molekularekin duten elkarreragina ulertzeko (ikusi 11.2 bola-marratxo errepresentaziorako). Hasteko, ordezkatutako TPB eta TPPen azidotasuna eta basikotasuna karakterizatu dira. Gero, azido zatien eta base zatien arteko elkarrekintza energiak aztertu dira, Lewis bikote isolatuan eta Lewis bikote frustratuan linker molekularekin batera.

Zehazki, aztertzen ari diren TPB eta TPP sistemetan hainbat ordezkatzaile jarri dira *ortho* eta *para* posizioetan, hala nola EDG taldeak (R = CH_3, NH_2, OH, OCH_3, $OCOCH_3$) edo EWG taldeak (R = F, CF_3, CN, NO_2, SO_3H). Konposatu horien azidotasuna eta basikotasuna aztertzeko zenbait parametro erabili dira. Azidoen kasuan, erabilitako parametroak hidruroaren afinitatea (HA), indar elektrohartzailea (ω^+), ^{31}P-NMR desplazamendu kimikoaren aldaera ($\Delta\delta$) eta boroaren orbital hutsaren energia (ε_B) izan dira. Protoi afinitatea (PA), indar elektroemailea (ω^-), indize nukleofiloa (N) eta fosforoaren pare askearen orbital energia (ε_P) eta okupazio zenbakiak ($\eta(\sigma_P)$) erabili dira. Emaitza horiek aztertuta, ondorio batzuk atera dira. Azidoei dagokienez, HA, ω^+, $\Delta\delta$, eta LP parametroek emaitza bera eman dute, hots, EWG ordezkatzaileek EDG ordezkatzaileek baino Lewis azido sendoagoak lortzen dituztela. Aldiz, $\eta(\sigma_B)$ parametroak ez du balio azidotasuna neurtzeko. Baseei dagokienez, PA, ω^-, N, eta LP parametroek joera sendoa adierazi dute, alegia, EDG konposatuek EWG konposatuek baino Lewis base sendoagoak ematen dituztela. Hala eta guztiz ere, Lewisen basikotasuna neurtzeko $\eta(\sigma_P)$ ez da eraginkorra.
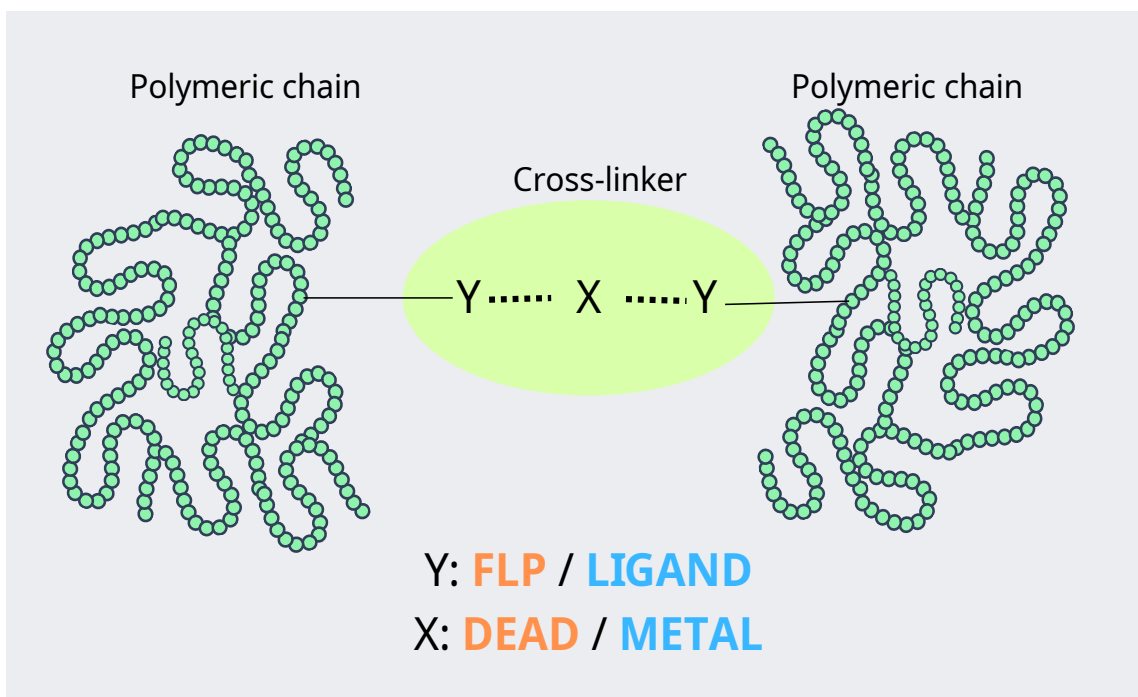
11.1. Irudia: Tesi honetan aztertutako sistemen deskribapen eskematikoa. Cross-linkerra Y-X-Y gisa irudikatzen da, non Y letra FLPri edo estekatzaileari dagokion, eta X letra, DEAD molekulari edo trantsizio-metal bati dagokion.

Emaitza horietan oinarrituta, zenbait TPB eta TPP deribatu aukeratu dira FLP eratzeko elkarrekintza eta horiek DEAD molekularekin duten elkarrekintza aztertzeko. Zehazki, azido eta base indar desberdinak dituzten bost TPB eta TPP deribatu aukeratu eta konbinatu dira 17 FLPs sortzeko, sistema esperimentala erreferentzia gisa hartuta. Emaitza horiek ikusirik, ondorioztatu da hidrogeno-loturak edo emaile-hartzaile loturak sortzeko gai diren ordezkoak saihestu behar direla, FLP eta DEADen arteko interakzio egokia eragotz dezaketelako. Horretaz gain, azido eta base ertainak diren TPB eta TPP

konposatuak dira egokienak DEAD molekularekiko elkarrekintza orekatzeko eta, beraz, materialei autokonpongarriak sortzeko.
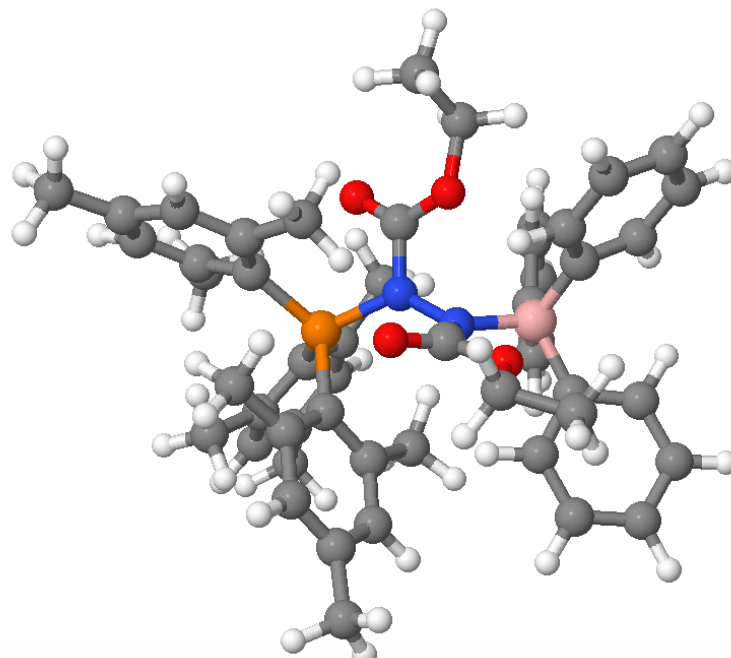
11.2. Irudia: Shaverrek eta kolaboratzaileek garatutako sistema esperimentalerako FLP-DEAD eredua.

NBO eta EDA analisiek ideia osagarriak eman dituzte FLP-DEAD sistemen barneko elkarrekintzen izaerari buruz. NBO analisiak erakutsi duenez, TPB-DEAD eta TPP-DEAD zatiek lotura datibo kobalenteak eratu dituzte, eta horrek lotura polar kobalenteak sortu ditu. Lotura horien polaritatea handiagoa izan da B-N loturarentzat P-N loturarentzat baino. Emaitza horiek EDA analisiak berretsi ditu. Konplexuen interakzio energien arteko desberdintasunak ordezkatzaileen arteko aldarapen esterikoaren ondorio izan daitezke, eta ez loturen aldaketen ondorio. Gainera, NBOren laguntzarekin, ulertu ahal izan da linkerrean gertatzen den egitura elektronikoaren aldaketa; izan ere, B-N eta N-P lotura berriak sortu dira, eta nitrogeno atomoen arteko lotura bikoitza bi bikote askeko orbitaletan banatu da.

Laburbilduz, FLP$_4$-DEAD sistema proposatzen dugu polimero autokonpongarri berriak garatzeko etorkizun oparoko hautagaitzat. Hala ere, beste aukera batzuk kontuan hartzea azpimarratzen dugu, hala nola beste linker molekula edo FLP bikote batzuk, azkenok zentro azido eta basiko desberdinekin (Al, Ga, N) osatuak, etorkizunean hobekuntzak egiteko.

11.2   Metal-ligando materialak

Lan honen bigarren zatian, trantsizio-metalen eta pintza estekatzaileetan oinarrituta-ko materialen interakzioak eta propietatea optikoak aztertu dira. Trantsizio-metalen eta pintzen arteko elkarrekintzaren izaerari dagokionez, kontuan hartu dira terpiridina (TPY) eta terfosfinina (TPPh) estekatzaileak eta beren deribatuak. Pintza estekatzai-leok trantsizio-metalekin (Cd(II), Zn(II), Cu(I), Fe(II), Ru(II) eta Sc(III), zehazki) duten elkarrekintza eztabaidatu da 4 kapituluan. Elkarrekintza-energiak kalkulatu ziren eta elkarrekintzaren izaerari buruzko azterketa sistematikoa egin zen, NBO eta QTAIM ana-lisien bidez, elkarrekintzaren alderdi fisikoak ulertzeko eta interakzioari eragiten dioten funtsezko parametroak identifikatzeko asmotan. Horrela, linker horiek dituzten material polimerikoen autokonpongarritasun gaitasuna hobetzeko xedearekin. Rowan eta Wede-rrek egindako ikerketa esperimentalean oinarritu zen ikerketaren zati hori.[53]
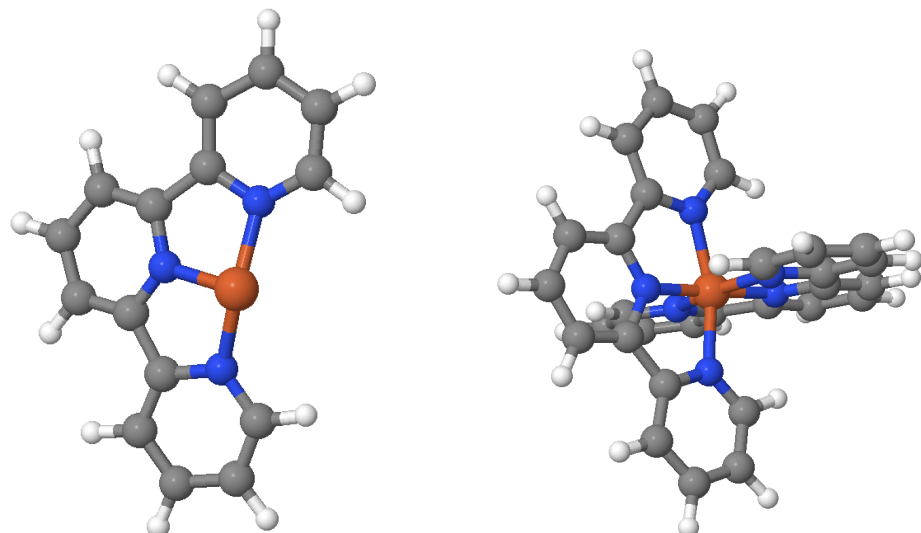
11.3. Irudia: P ptimizatutako $[Fe\text{-}TPY]^{2+}$, ezkerraldean, eta $[TPY\text{-}Fe\text{-}TPY]^{2+}$, eskui-naldean, konplexu egiturak.

   Lehenik eta behin, trantsizio-metalek elkarrekintza energian duten eragina aztertu zen lehen aipatutako metal-ligando konplexuen sortze energiak kalkulatuz eta aztertuz. Ikusi zen, interakzio energian eragina dutela bai metalaren kargak, baita d orbital me-talikoaren okupazioak ere; izan ere, d orbital hutsak dituzten metalek N bikoteen karga elektronikoa onar dezakete, eta, hala, elkarrekintza handitu. M-N lotura distantziei dago-kienez, elkarrekintza energiarekin bat datorren joera ikusten da, eta, 1 eta 2 estekatzaile dituzten konplexuak alderatuz, distantzia luzeagoak ikusten dira $[TPY\text{-}M\text{-}TPY]^{[n+]}$ kon-plexuetan, seguruenik eragozpen esterikoak eraginda. Testuinguru horretan, Sc(III) kasu berezia da, haren karga transferentzia orbital birtual eta energetiko altuagoetan gerta-tzen baita. Erakusten duen elkarrekintza energia handia ioi karga handiaren ondorioa da, ioi-dipolo elkarrekintza handiak eragiten baititu.

Metalen eraginaz gain, EDG eta EWG talde funtzionalek (R = H, NH$_2$ eta CN) estekatzailearen eraztun fenilikoetan duten eragina ere aztertu da. Lortutako emaitzetan oinarrituta, ondoriozta dezakegu EDG baten presentziak interakzio energia handitzen duela, eta EWG baten presentziak, berriz, kontrako eragina duela. Hala ere, talde horien eragina metalarena baino askoz txikiagoa da, eta interakzioa doitzeko erabil daiteke metal egokia aukeratu ondoren. Beraz, lotura indarra nagusiki metalaren eta ligandoaren izaerak zehazten du, EDG eta EWG taldeen presentziak baino.

Azkenik, TPY estekatzailearen ordez bere fosforo analogoa (TPPh) erabiltzearen efektua ikertu dugu. Ikusi denez, TPPh estekatzaileekin sortutako Fe(II) konplexuen disoziazio energiak TPY estekatzaileenak baino txikiagoak izan dira, fosforo/metal interakzio ahulagoa izan dutelako, egitura elektroniko desberdinaren ondorioz. Halaber, EDGek eta EWGek (R = H, NH$_2$ eta CN) TPPh ligandoetan duten eragina kalkulatu da, eta EDG taldeentzat disoziazio energia handiagoak aurkitu dira. NBO analisiaren arabera, lotura bat sortu da [Fe-TPPh-NH$_2$]$^{2+}$ konplexuan, aldiz, beste kasuetan elkarrekintza nagusiki elektrostatikoa da. Horretaz gain, hainbat lotura sortu dira [TPPh-Fe-TPPh]$^{2+}$ (R = H, NH$_2$ and CN) sistemetan. Dena den, QTAIM analisiaren arabera, konplexu horietako M-P elkarrekintzak partzialki kobalenteak dira.

Emaitza horietan oinarrituta, ikusi dugu faktore garrantzitsuenak estekatzaileak (TPY vs TPPh) eta ioi metalikoa direla. Hala ere, kalkulatutako elkarrekintza energiak altuegiak dira lotura dinamikotzat hartzeko. Kontuan izan behar da ohiko lotura dinamikoak, hala nola disulfuro edo FLP-DEAD sisteman aurkitzen direnak, 40 eta 50 kcal/mol bitartekoak direla, eta metal-ligando konplexu horietan topatzen direnak magnitude orden bat handiagokoak dira. Desadostasun hori egoera esperimentalean gatz metalikoak guztiz disoziatzen ez direlako izan daiteke, beraz, gatz klusterren eragina garrantzitsua izan daiteke, kontraioi efektua barne. Ildo horretan, aurretiazko kalkuluak egin dira FeCl$_2$ gatzarekin. Zehazki, TPY estekatzaile batek eta bik Fe$_6$Cl$_{12}$ kluster txiki batekin duten elkarreragina kalkulatu da. 11.4 irudian, kluster isolatuaren eta bi TPY estekatzailerekin osatutako konplexuaren optimizatutako egiturak irudikatzen dira. Kalkulatutako elkarrekintza energiak hauek dira, gutxi gorabehera: 50 kcal/mol pintza estekatzaile batentzat eta 150 kcal/mol birentzat.

Balio baxuago horiek adierazten dute garrantzitsua dela esperimentu baldintzen modelizazio egokia. Etorkizunean, kontuan hartu behar da ioi metalikoak segur aski ez direla espezie libreak izango material horiek sintetizatzen diren baldintza esperimentaletan. Beraz, funtsezkoa da gatz klusterren eta kontraioien efektua kontuan hartzea. Nolanahi ere, uste dugu tesi honetan aztertutako faktoreen eragina antzekoa izango litzatekeela kasu horietan.
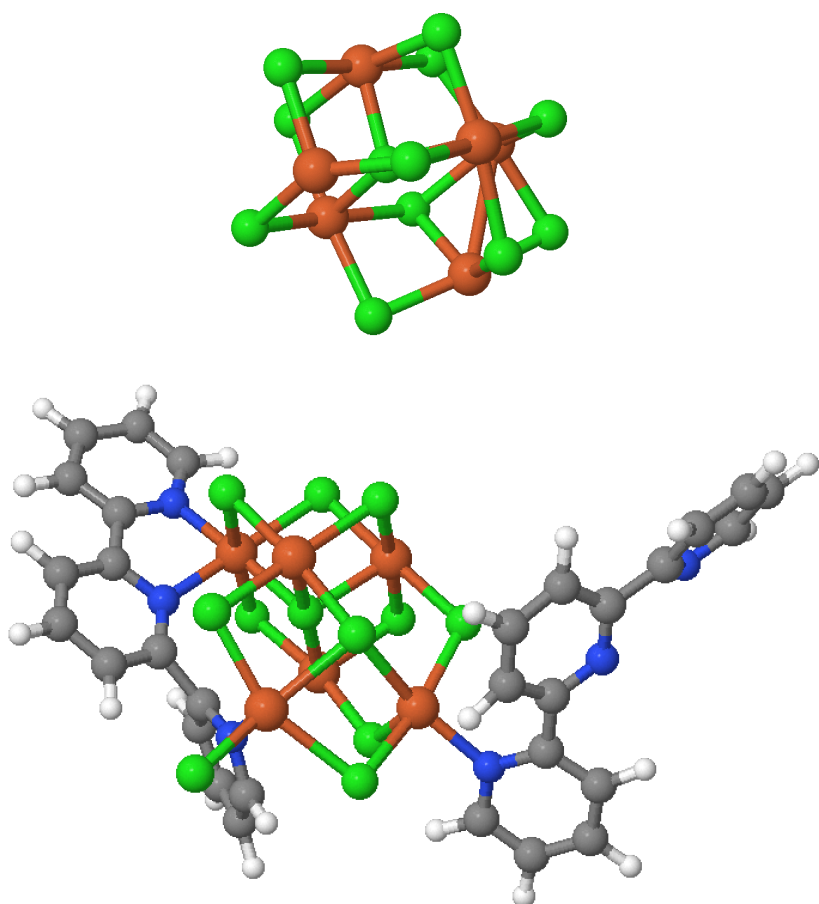
11.4. Irudia: Goran, isolatutako Fe_6Cl_{12} klusterra. Beheran, kluster horrek bi TPY estekatzailerekin duen interakzioa.

Behin interakzioaren natura ulertuta, $[M\text{-}XXX]^{n+}$ eta $[XXX\text{-}M\text{-}XXX]^{n+}$ konplexuen propietate optikoak ikertu ditugu. Zehazki, propietate optikoak Zn(II), Cd (II), Fe(II), Ru (II) eta Ir(III) metalentzat, eta terpiridina (TPY) eta terfosfinina (TPPh) pintza estekatzaileentzat aztertu dira. Konposatu horiek material mota hauetan duten erabilera esperimentalaren ondorioz aukeratu dira. Aztertutako propietate optikoak UV/Vis absortzioa eta emisioa (fluoreszentzia eta fosforeszentzia) izan dira.

Gure emaitzen arabera, oro har, eskuinaldean dauden trantsizio-metalek absortzioa eta emisio fluoreszentea erakusten dute UV eremuan, berriz, fosforeszentziaren emisioari buruzko aurretiazko kalkuluek agerian uzten dute $[TPY\text{-}Zn\text{-}TPY]^{2+}$ konplexuak eremu ikuskorrean igortzeko ahalmena izan dezakeela. Erdialdean kokatuta dauden trantsizio-metalak malguagoak dira. Ligando bakarreko konplexuek barne-konbertsio ez erradiatiboak jasan ditzakete, aldiz, bi ligando dituzten konplexuek ez dute prozesu hori jasango, egoera kitzikatuko singleteak energia altuagokoak direlako. Printzipioz, UV eremu hurbilean igorriko lukete, $[TPY\text{-}Ru\text{-}TPY]^{2+}$ konplexua salbuespena izanik, zeinak eremu ikuskorrean igorri dezakeen. Horretan gain, $[TPY\text{-}Zn\text{-}TPY]^{2+}$ eta $[TPY\text{-}Ru\text{-}TPY]^{2+}$ konplexuen triplete egoerari buruzko lehen emaitzek erakusten dute egoera horretatik igorri

dezaketela eremu ikuskorrean, fosforeszentzia propietatea eskuratuz. Bestalde, TPY eta TPPh estekatzaileak alderatuz, ikusi da TPPh ligandoak espektroaren aldaketa eragiten duela eremu gorrira.

Fluoreszentzia propietateak aztertzeko, sistema guztietarako energia baxueneko singlete egoera elektroniko kitzikatua optimizatu da. Absortzio propietateei dagokienez, eskuinaldeko eta erdialdeko trantsizio-metalen konplexuek joera ezberdina dute. Erdialdeko trantsizio-metalen kasuan, joera posibleena barne-konbertsio ez erradiatiboa izango litzateke, berriz, eskuinaldeko trantsizio-metalen kasuan, hasiera batean ez litzateke prozesu hori emango egoera singlete baxuena energia altuagoetan baitute. Bi estekatzaile dituzten konplexuei dagokienez, konplexu guztietan ez litzateke inolako barne-konbertsiorik gertatuko, baizik eta konplexu guztiek UV eremuan igorriko lukete. Dena den, [TPY-Ru-TPY]$^{2+}$ konplexua salbuespena da, gure datuen arabera fluoreszentzia emango lukeelako.

Konplexu horien propietate optikoei buruzko azterketa hau propietate horiek aztertzeko lehen hurbilketatzat har daiteke. Izan ere, lan asko egiteko dago material metalopolimerikoen propietate optikoak behar bezala ulertzeko. Adibidez, kontuan hartu behar da, lehen aipatu dugun bezala, kontraioien eragina eta ioi metaliko isolatuak ez aurkitzea sistema horietan. Gainera, sistema horietan egoera kitzikatuaren bilakaera oso korapilatsua denez, barne-konbertsioaren eta barne sistemarteko gurutzaketen azterketa zehatza egitea aintzat hartu behar da, aurreikuspen kualitatiboa ez ezik, kuantitatiboa ere emateko. Gainera, behin prozesu horiek hobeto ulertuz gero, lantano (III), kobalto (II) edo platino (II) bezalako trantsizio-metalen eraginak ere lagunduko luke beren aplikazio ugariren berri ematen.

Appendix A

Photophysical properties of metal-ligand based metallopolymers

A.1 Absorption spectra

Calculated TDDFT most significant vertical transitions to S_0 at the optimized geometry of S_1 electronic state for $[M\text{-}XXX]^{n+}$ and $[XXX\text{-}M\text{-}XXX]^{n+}$ complexes. For each system, the starting singlet states (State, S_i), transition energies (ΔE) in eV and corresponding photon wavelengths (λ values in parenthesis) in nm, and oscillator strengths (f) are given. Orbitals involved in the transition are denoted as H for HOMO, L for LUMO. Besides, its contribution (Contribution) is also given. Finally, the metal contribution (Metal %) of each orbital is provided.

Table A.1: Results for $[Cd\text{-}TPY]^{2+}$ complex.

$[Cd\text{-}TPY]^{2+}$						
State	ΔE (λ)	f	Transition		Orbital	
			Transition	Contribution	Orbital	Metal %
S_1	4.08 (304)	0.000	H → L	0.702	H-7	0.08
S_2	4.12 (301)	0.305	H-1 → L+2	-0.111	H-6	0.00
			H → L+1	0.669	H-5	0.01
S_3	4.73 (262)	0.202	H-2 → L	0.390	H-4	0.01
			H-1 → L+1	-0.332	H-3	0.00
			H → L+2	0.445	H-2	0.13
S_5	4.98 (249)	0.055	H-2 → L	0.558	H-1	0.00
			H-1 → L+1	0.203	H	0.00
			H → L+2	-0.314	L	1.18
S_{14}	6.13 (202)	0.112	H-6 → L+2	0.136	L+2	0.00
Continued on next page						

[Cd-TPY]$^{2+}$						
State	$\Delta E\ (\lambda)$	f	Transition		Orbital	
			Transition	Contribution	Orbital	Metal $\%$
			H-5 $\rightarrow$ L+1	0.477	L+3	0.00
			H-3 $\rightarrow$ L+1	0.376	L+4	0.03
			H-3 $\rightarrow$ L+4	0.124	L+6	0.04
			H-1 $\rightarrow$ L+4	-0.131	L+7	0.02
			H $\rightarrow$ L+3	-0.193		
S$_{15}$	6.19 (200)	0.739	H-7 $\rightarrow$ L	0.483		
			H-6 $\rightarrow$ L+1	-0.112		
			H-3 $\rightarrow$ L+2	-0.178		
			H-1 $\rightarrow$ L+2	0.244		
			H-1 $\rightarrow$ L+3	-0.131		
			H $\rightarrow$ L+4	-0.328		
S$_{20}$	6.39 (194)	0.052	H-5 $\rightarrow$ L+1	0.350		
			H-4 $\rightarrow$ L+2	-0.196		
			H-4 $\rightarrow$ L+3	-0.120		
			H-3 $\rightarrow$ L+1	-0.323		
			H-1 $\rightarrow$ L+1	0.130		
			H-1 $\rightarrow$ L+6	0.101		
			H $\rightarrow$ L+3	0.389		
			H $\rightarrow$ L+7	-0.113		

Table A.2: Results for [Zn-TPY]$^{2+}$ complex.

[Zn-TPY]$^{2+}$						
State	$\Delta E\ (\lambda)$	f	Transition		Orbital	
			Transition	Contribution	Orbital	Metal $\%$
S$_1$	4.06 (305)	0.288	H-1 $\rightarrow$ L+1	-0.110	H-6	0.00
			H $\rightarrow$ L	0.673	H-5	0.02
S$_2$	4.77 (260)	0.279	H-1 $\rightarrow$ L	-0.431	H-4	0.16
			H $\rightarrow$ L+1	0.513	H-3	0.01
S$_7$	5.64 (220)	0.037	H-4 $\rightarrow$ L+2	-0.192	H-2	0.00
			H-3 $\rightarrow$ L+1	0.202	H-1	0.00
			H-2 $\rightarrow$ L	0.354	H	0.00
			H-1 $\rightarrow$ L	0.375	L	0.10
			H-1 $\rightarrow$ L+4	-0.143	L+1	0.00
			H $\rightarrow$ L+1	0.282	L+2	0.84
			H $\rightarrow$ L+3	0.185	L+3	0.01
S$_{12}$	6.08 (204)	0.145	H-6 $\rightarrow$ L+1	-0.122	L+4	0.02
			H-5 $\rightarrow$ L	0.480	L+5	0.01
			H-2 $\rightarrow$ L	0.366		
			H-2 $\rightarrow$ L+4	-0.125		
Continued on next page						

			[Zn-TPY]$^{2+}$			
State	ΔE (λ)	f	Transition		Orbital	
			Transition	Contribution	Orbital	Metal %
S$_{13}$	6.29 (197)	0.442	H-1 → L+4	0.132		
			H → L+3	-0.190		
			H-6 → L	0.108		
			H-3 → L	-0.294		
			H-2 → L+1	-0.298		
			H-1 → L+1	0.272		
			H-1 → L+3	-0.115		
			H → L+4	0.422		
S$_{17}$	6.51 (190)	0.692	H-5 → L+1	0.257		
			H-3 → L	-0.314		
			H-3 → L+4	-0.151		
			H-2 → L+1	0.346		
			H-2 → L+3	-0.166		
			H-1 → L+3	-0.213		
			H → L	-0.145		
			H → L+4	0.159		
S$_{20}$	6.70 (185)	0.147	H-6 → L	0.590		
			H-1 → L+1	-0.226		
			H → L+5	-0.172		

Table A.3: Results for [Fe-TPY]$^{2+}$ complex.

			[Fe-TPY]$^{2+}$			
State	ΔE (λ)	f	Transition		Orbital	
			Transition	Contribution	Orbital	Metal %
S$_1$	0.08 (16235)	0.000	H-11 → L	0.108	H-16	0.04
			H-8 → L	0.314	H-15	0.03
			H-6 → L	0.140	H-11	0.11
			H-3 → L	0.309	H-10	0.10
			H-2 → L	0.699	H-9	0.11
			H-2 → L+3	-0.158	H-8	0.26
			H-2 → L+5	0.146	H-7	0.03
			H-1 → L	0.350	H-6	0.16
			H-8 ← L	-0.243	H-4	0.73
			H-3 ← L	-0.265	H-3	0.24
			H-2 ← L	-0.376	H-2	0.56
			H-1 ← L	-0.342	H-1	0.45
S$_8$	3.93 (315)	0.133	H-3 → L	-0.275	H	0.00
			H-1 → L	0.206	L	0.78
			H → L+1	0.588	L+1	0.09
			Continued on next page			

State	$\Delta E\ (\lambda)$	f	Transition		Orbital	
			Transition	Contribution	Orbital	Metal %
S_{10}	4.31 (288)	0.083	H-8 $\rightarrow$ L	0.152	L+2	0.74
			H-3 $\rightarrow$ L	0.420	L+3	0.06
			H-3 $\rightarrow$ L+3	-0.126	L+4	0.14
			H-1 $\rightarrow$ L	-0.378	L+5	0.05
			H $\rightarrow$ L+1	0.321	L+6	0.79
S_{13}	4.93 (251)	0.279	H-8 $\rightarrow$ L+1	-0.123	L+7	0.16
			H-3 $\rightarrow$ L+1	-0.385		
			H-1 $\rightarrow$ L+2	0.102		
			H-1 $\rightarrow$ L+6	0.117		
			H $\rightarrow$ L+3	0.477		
S_{14}	4.95 (250)	0.068	H-15 $\rightarrow$ L	-0.137		
			H-10 $\rightarrow$ L	0.123		
			H-6 $\rightarrow$ L	0.527		
			H-3 $\rightarrow$ L	0.187		
			H-2 $\rightarrow$ L	-0.189		
			H-1 $\rightarrow$ L+3	0.271		
S_{17}	5.17 (239)	0.223	H-7 $\rightarrow$ L+1	-0.128		
			H-6 $\rightarrow$ L	-0.246		
			H-1 $\rightarrow$ L+3	0.549		
			H-1 $\rightarrow$ L+5	-0.111		
			H $\rightarrow$ L+4	0.146		
			H $\rightarrow$ L+7	-0.100		
S_{19}	5.42 (230)	0.058	H-16 $\rightarrow$ L	0.113		
			H-9 $\rightarrow$ L	0.392		
			H-4 $\rightarrow$ L	-0.113		
			H-3 $\rightarrow$ L+1	0.138		
			H-3 $\rightarrow$ L+2	0.132		
			H-2 $\rightarrow$ L+6	-0.134		
			H-1 $\rightarrow$ L+1	-0.133		
			H-1 $\rightarrow$ L+2	-0.150		
			H-1 $\rightarrow$ L+6	-0.101		
			H $\rightarrow$ L+3	0.352		

Table A.4: Results for [Ru-TPY]$^{2+}$ complex.

State	$\Delta E\ (\lambda)$	f	Transition		Orbital	
			Transition	Contribution	Orbital	Metal %
S_1	0.77 (1600)	0.000	H-6 $\rightarrow$ L	0.114	H-6	0.09
			H-1 $\rightarrow$ L	0.203	H-4	0.04
			Continued on next page			

			[Ru-TPY]$^{2+}$			
State	ΔE (λ)	f	Transition		Orbital	
			Transition	Contribution	Orbital	Metal $\%$
			H $\rightarrow$ L	0.649	H-3	0.86
			H $\rightarrow$ L+2	0.125	H-2	0.01
			H $\rightarrow$ L	-0.107	H-1	0.69
S$_{10}$	3.99 (310)	0.117	H-4 $\rightarrow$ L	-0.153	H	0.73
			H-3 $\rightarrow$ L+1	-0.159	L	0.73
			H-3 $\rightarrow$ L+3	-0.139	L+1	0.09
			H-2 $\rightarrow$ L+1	0.610	L+2	0.06
S$_{15}$	4.61 (269)	0.110	H-4 $\rightarrow$ L	0.515	L+3	0.68
			H-2 $\rightarrow$ L+1	0.157	L+4	0.03
			H-2 $\rightarrow$ L+3	-0.224	L+5	0.41
			H-1 $\rightarrow$ L+2	-0.342	L+6	0.62
S$_{16}$	4.75 (261)	0.175	H-4 $\rightarrow$ L+1	0.253	L+7	0.36
			H-2 $\rightarrow$ L+2	0.463		
			H-1 $\rightarrow$ L+5	0.300		
			H-1 $\rightarrow$ L+6	-0.150		
			H-1 $\rightarrow$ L+7	0.113		
			H $\rightarrow$ L+5	0.188		
S$_{17}$	4.96 (250)	0.106	H-4 $\rightarrow$ L	0.143		
			H-3 $\rightarrow$ L+3	0.114		
			H-2 $\rightarrow$ L+3	0.636		
			H-1 $\rightarrow$ L+2	-0.185		
S$_{18}$	5.07 (245)	0.125	H-4 $\rightarrow$ L+1	-0.156		
			H-3 $\rightarrow$ L+2	0.260		
			H-2 $\rightarrow$ L+2	-0.289		
			H-1 $\rightarrow$ L+1	-0.148		
			H-1 $\rightarrow$ L+5	0.359		
			H-1 $\rightarrow$ L+6	-0.299		
			H-1 $\rightarrow$ L+7	0.148		
S$_{19}$	5.27 (235)	0.069	H-4 $\rightarrow$ L+1	0.150		
			H-3 $\rightarrow$ L	-0.121		
			H-3 $\rightarrow$ L+2	0.605		
			H-3 $\rightarrow$ L+4	0.125		
			H-2 $\rightarrow$ L+2	0.129		
			H-1 $\rightarrow$ L+5	-0.113		
			H-1 $\rightarrow$ L+6	0.122		

Table A.5: Results for [Ir-TPY]$^{2+}$ complex.

State	ΔE (λ)	f	Transition		Orbital	
			Transition	Contribution	Orbital	Metal %
S$_1$	1.03 (1205)	0.002	H-5 → L	0.375	H-12	0.16
			H-3 → L	-0.294	H-9	0.10
			H-2 → L	0.405	H-8	0.48
			H-1 → L	-0.316	H-7	0.56
S$_{11}$	3.86 (321)	0.086	H-12 → L+1	0.151	H-6	0.14
			H-7 → L+1	0.422	H-5	0.44
			H-7 → L+2	-0.106	H-4	0.07
			H-6 → L+1	0.237	H-3	0.19
			H-5 → L	-0.228	H-2	0.40
			H-4 → L+1	-0.134	H-1	0.19
			H-2 → L	0.113	H	0.01
			H → L+2	0.318	L	0.61
S$_{12}$	3.90 (318)	0.187	H-12 → L+1	-0.106	L+1	0.69
			H-8 → L	0.192	L+2	0.17
			H-7 → L+1	-0.286	L+3	0.04
			H-7 → L+2	0.102		
			H-6 → L+1	-0.184		
			H-5 → L	-0.283		
			H-3 → L	-0.195		
			H-1 → L	-0.155		
			H → L+2	0.365		
S$_{14}$	4.28 (289)	0.018	H-5 → L+2	-0.169		
			H-3 → L+2	0.256		
			H-1 → L+1	0.305		
			H-1 → L+2	0.455		
			H → L+3	0.227		
S$_{15}$	4.31 (287)	0.230	H-8 → L	0.533		
			H-7 → L+1	0.105		
			H-3 → L	-0.216		
			H-2 → L	-0.264		
			H → L+2	-0.213		
S$_{17}$	4.64 (267)	0.030	H-9 → L	-0.207		
			H-5 → L+2	0.156		
			H-3 → L+2	-0.128		
			H-2 → L+1	0.192		
			H-2 → L+2	0.495		
			H-1 → L+1	-0.137		
			H-1 → L+2	0.114		
			H → L+3	0.230		

[Ir-TPY]$^{2+}$						
State	ΔE (λ)	f	Transition		Orbital	
			Transition	Contribution	Orbital	Metal %
S$_{18}$	4.98 (249)	0.366	H-8 → L+2	-0.148		
			H-3 → L+2	-0.393		
			H-2 → L+2	-0.25		
			H → L+3	0.434		

Table A.6: Results for [Fe-TPPh]$^{2+}$ complex.

[Fe-TPPh]$^{2+}$						
State	ΔE (λ)	f	Transition		Orbital	
			Transition	Contribution	Orbital	Metal %
S$_1$	0.01 (105745)	0.000	H-15 → L+1	0.195	H-15	0.18
			H-11 → L	-0.435	H-12	0.21
			H-11 → L+1	-0.782	H-11	0.43
			H-11 → 90	0.107	H-10	0.80
			H-9 → L	0.383	H-9	0.31
			H-9 → L+1	0.683	H-8	0.36
			H-7 → L	-0.339	H-7	0.44
			H-7 → L+1	-0.585	H-6	0.17
			H-4 → L	0.232	H-5	0.30
			H-3 → L	0.202	H-4	0.05
			H-3 → L+1	0.359	H-3	0.06
			H-1 → L	-0.231	H-2	0.04
			H-1 → L+1	-0.408	H-1	0.03
			L+1 → H-15	-0.178	H	0.04
			L → H-11	0.383	L	0.39
			L+1 → H-11	0.712	L+1	0.68
			L → H-9	-0.337	L+2	0.45
			L+1 → H-9	-0.622		
			L → H-7	0.298		
			L+1 → H-7	0.532		
			L → H-4	-0.204		
			L+1 → H-4	-0.367		
			L → H-3	-0.177		
			L+1 → H-3	-0.325		
			L → H-1	0.201		
			L+1 → H-1	0.371		
S$_5$	2.03 (611)	0.009	H-12 → L	-0.121		
			H-10 → L	-0.279		
			H-10 → L+2	0.188		
			H-6 → L	-0.167		
Continued on next page						

			[Fe-TPPh]$^{2+}$			
State	ΔE (λ)	f	Transition		Orbital	
			Transition	Contribution	Orbital	Metal %
			H-6 $\rightarrow$ L+2	0.116		
			H-5 $\rightarrow$ L	-0.187		
			H-5 $\rightarrow$ L+2	0.142		
			H-2 $\rightarrow$ L	-0.184		
			H $\rightarrow$ L	0.407		
S$_8$	2.74 (452)	0.082	H-10 $\rightarrow$ L	0.260		
			H-10 $\rightarrow$ L+2	-0.189		
			H-8 $\rightarrow$ L	-0.101		
			H-2 $\rightarrow$ L	0.284		
			H $\rightarrow$ L	0.483		
			H $\rightarrow$ L+2	0.161		
S$_{10}$	2.95 (421)	0.008	H-11 $\rightarrow$ L	-0.157		
			H-11 $\rightarrow$ L+2	0.121		
			H-9 $\rightarrow$ L	0.137		
			H-9 $\rightarrow$ L+2	-0.109		
			H-7 $\rightarrow$ L+1	0.234		
			H-7 $\rightarrow$ L+2	0.105		
			H-3 $\rightarrow$ L	0.125		
			H-1 $\rightarrow$ L	0.457		
			H-1 $\rightarrow$ L+1	-0.249		
S$_{11}$	3.07 (403)	0.003	H-11 $\rightarrow$ L+1	-0.120		
			H-7 $\rightarrow$ L	0.205		
			H-7 $\rightarrow$ L+1	0.309		
			H-3 $\rightarrow$ L	0.225		
			H-3 $\rightarrow$ L+1	0.414		
			H-1 $\rightarrow$ L+1	0.288		
S$_{12}$	3.56 (348)	0.014	H-10 $\rightarrow$ L	-0.188		
			H-10 $\rightarrow$ L+1	-0.126		
			H-10 $\rightarrow$ L+2	0.110		
			H-2 $\rightarrow$ L	0.479		
			H-2 $\rightarrow$ L+1	0.391		
			H $\rightarrow$ L+2	-0.115		
S$_{13}$	3.66 (338)	0.004	H-7 $\rightarrow$ L+1	-0.125		
			H-3 $\rightarrow$ L	0.563		
			H-3 $\rightarrow$ L+1	-0.187		
			H-2 $\rightarrow$ 89	0.101		
			H-1 $\rightarrow$ L+2	-0.248		
S$_{14}$	3.64 (337)	0.084	H-10 $\rightarrow$ L+1	-0.166		
			H-10 $\rightarrow$ L+2	-0.132		
			H-2 $\rightarrow$ L	-0.315		
			H-2 $\rightarrow$ L+1	0.515		
			H $\rightarrow$ L+2	0.155		
Continued on next page						

State	ΔE (λ)	f	Transition		Orbital	
			[Fe-TPPh]$^{2+}$			
			Transition	Contribution	Orbital	Metal %
S_{15}	3.86 (321)	0.003	H-11 → L	0.108		
			H-11 → L+1	0.244		
			H-9 → L+1	-0.211		
			H-7 → L	-0.181		
			H-7 → L+1	-0.291		
			H-3 → L+1	0.454		
S_{17}	3.94 (317)	0.008	H-10 → L	-0.252		
			H-8 → L+1	-0.238		
			H → L+2	0.546		
S_{18}	4.05 (306)	0.003	H-7 → L	0.132		
			H-4 → L	-0.263		
			H-4 → L+1	0.103		
			H-3 → L	0.158		
			H-3 → L+1	-0.111		
			H-1 → L+2	0.548		
S_{19}	4.28 (290)	0.082	H-11 → L	0.134		
			H-9 → L	-0.173		
			H-4 → L	0.574		
			H-4 → L+1	0.199		
			H-1 → L+2	0.185		

Table A.7: Results for [TPY-Cd-TPY]$^{2+}$ complex.

State	ΔE (λ)	f	Transition		Orbital	
			[TPY-Cd-TPY]$^{2+}$			
			Transition	Contribution	Orbital	Metal %
S_1	4.41 (281)	0.362	H-1 → L	-0.298	H-16	0.00
			H-1 → L+1	0.332	H-13	0.13
			H → L	0.402	H-12	0.14
			H → L+1	-0.276	H-11	0.03
S_2	4.41 (281)	0.363	H-1 → L	0.356	H-10	0.02
			H-1 → L+1	0.330	H-9	0.01
			H → L	0.249	H-8	0.01
			H → L+1	0.374	H-7	0.01
S_6	4.95 (250)	0.384	H-3 → L+1	-0.206	H-6	0.00
			H-2 → L	-0.196	H-5	0.06
			H-1 → L+2	0.428	H-4	0.00
			H → L+3	-0.404	H-3	0.00
S_{15}	5.75 (216)	0.248	H-16 → L	0.109	H-2	0.00
			H-11 → L+2	-0.112	H-1	0.00
			Continued on next page			

			[TPY-Cd-TPY]$^{2+}$			
State	ΔE (λ)	f	Transition		Orbital	
			Transition	Contribution	Orbital	Metal %
			H-9 → L+1	-0.128	H	0.00
			H-8 → L+3	0.107	L	0.00
			H-7 → L+2	-0.106	L+1	0.00
			H-7 → L+3	-0.119	L+2	0.00
			H-6 → L	-0.149	L+3	0.00
			H-5 → L+2	0.133	L+4	0.01
			H-4 → L	0.122	L+5	0.00
			H-3 → L+3	0.263	L+6	0.03
			H-3 → L+4	-0.119	L+7	0.03
			H-2 → L+2	-0.244		
			H-2 → L+5	-0.121		
			H-1 → L+7	-0.179		
			H → L+6	0.172		
S$_{16}$	5.75 (216)	0.241	H-16 → L+1	0.117		
			H-10 → L+2	-0.123		
			H-9 → L	0.122		
			H-8 → L+3	-0.120		
			H-7 → L+3	-0.110		
			H-6 → L+1	0.141		
			H-5 → L	0.102		
			H-5 → L+3	0.149		
			H-4 → L+1	0.127		
			H-3 → L+2	0.252		
			H-3 → L+5	0.118		
			H-2 → L+3	-0.230		
			H-2 → L+4	0.112		
			H-1 → L+6	-0.180		
			H → L+7	0.163		
S$_{17}$	5.80 (214)	0.033	114 → L+3	0.119		
			H-16 → L+2	-0.241		
			H-13 → L	0.136		
			H-12 → L+1	-0.134		
			H-11 → L	0.146		
			H-10 → L+1	0.148		
			H-5 → L+3	0.318		
			H-5 → L+4	-0.151		
			H-4 → L+5	0.249		
			H-2 → L+3	0.161		
S$_{20}$	5.84 (212)	0.026	114 → L+2	0.125		
			H-16 → L+3	-0.212		
			H-13 → L+1	-0.146		
			H-12 → L	0.143		

[TPY-Cd-TPY]$^{2+}$						
State	ΔE (λ)	f	Transition		Orbital	
			Transition	Contribution	Orbital	Metal %
			H-11 → L+1	-0.151		
			H-10 → L	-0.156		
			H-5 → L+2	0.249		
			H-5 → L+5	0.163		
			H-4 → L+4	-0.247		
			H-2 → L+2	0.117		
			H-1 → L	-0.196		
			H → L+1	0.188		

Table A.8: Results for [TPY-Zn-TPY]$^{2+}$ complex.

[TPY-Zn-TPY]$^{2+}$						
State	ΔE (λ)	f	Transition		Orbital	
			Transition	Contribution	Orbital	Metal %
S$_1$	4.38 (283)	0.348	H-1 → L	0.401	H-12	0.00
			H-1 → L+1	0.229	H-11	0.00
			H → L	-0.330	H-10	0.00
			H → L+1	-0.333	H-9	0.01
S$_2$	4.38 (282)	0.348	H-1 → L	-0.229	H-8	0.01
			H-1 → L+1	0.410	H-7	0.01
			H → L	-0.333	H-6	0.00
			H → L+1	0.329	H-3	0.00
S$_6$	4.95 (251)	0.405	H-3 → L	-0.165	H-2	0.00
			H-3 → L+1	0.131	H-1	0.00
			H-2 → L	0.131	H	0.00
			H-2 → L+1	0.165	L	0.00
			H-1 → L+2	0.443	L+1	0.00
			H → L+3	0.402	L+2	0.00
S$_{11}$	5.43 (228)	0.025	H-12 → L	0.117	L+3	0.00
			H-10 → L+2	0.106	L+4	0.01
			H-10 → L+3	-0.113	L+5	0.00
			H-9 → L	0.126	L+6	0.00
			H-6 → L	-0.136	L+7	0.00
			H-6 → L+1	-0.125	L+8	0.00
			H-2 → L+2	0.285	L+9	0.00
			H-2 → L+3	-0.201		
			H-2 → L+4	0.148		
			H-2 → L+5	0.166		
			H-1 → L+6	-0.105		
			H-1 → L+7	0.172		
	Continued on next page					

State	ΔE (λ)	f	Transition		Orbital	
			Transition	Contribution	Orbital	Metal %
			H → L+6	0.138		
			H → L+7	-0.153		
			H → L+9	-0.107		
S_{12}	5.43 (228)	0.025	H-12 → L+1	-0.117		
			H-11 → L+2	-0.106		
			H-11 → L+3	-0.113		
			H-9 → L+1	-0.126		
			H-6 → L	0.125		
			H-6 → L+1	-0.136		
			H-3 → L+2	0.285		
			H-3 → L+3	0.201		
			H-3 → L+4	0.148		
			H-3 → L+5	-0.166		
			H-1 → L+6	0.172		
			H-1 → L+7	0.105		
			H → L+6	0.153		
			H → L+7	0.138		
			H → L+8	-0.107		
S_{17}	5.73 (216)	0.277	H-9 → L+1	0.108		
			H-8 → L+2	0.123		
			H-7 → L+3	0.135		
			H-6 → L	-0.161		
			H-3 → L+2	0.133		
			H-2 → L+2	-0.256		
			H-2 → L+3	0.324		
			H-2 → L+4	0.136		
			H-2 → L+5	0.124		
			H-1 → L+6	-0.149		
			H-1 → L+7	0.126		
			H → L+7	-0.183		
S_{18}	5.73 (216)	0.277	H-9 → L	-0.109		
			H-8 → L+3	0.135		
			H-7 → L+2	0.123		
			H-6 → L+1	0.161		
			H-3 → L+2	0.256		
			H-3 → L+3	0.324		
			H-3 → L+4	-0.136		
			H-3 → L+5	0.124		
			H-2 → L+2	0.133		
			H-1 → L+6	-0.126		
			H-1 → L+7	-0.149		
			H → L+6	-0.182		

<div align="center">Continued on next page</div>

[TPY-Zn-TPY]$^{2+}$						
State	ΔE (λ)	f	Transition		Orbital	
			Transition	Contribution	Orbital	Metal %
S$_{19}$	5.95 (208)	0.014	H-8 → L	0.156		
			H-7 → L+1	-0.155		
			H-6 → L+2	-0.108		
			H-3 → L	0.283		
			H-3 → L+1	-0.224		
			H-2 → L	-0.226		
			H-2 → L+1	-0.284		
			H-1 → L+2	0.314		
			H-1 → L+4	0.118		

Table A.9: Results for [TPY-Fe-TPY]$^{2+}$ complex.

[TPY-Fe-TPY]$^{2+}$						
State	ΔE (λ)	f	Transition		Orbital	
			Transition	Contribution	Orbital	Metal %
S$_1$	2.09 (594)	0.000	H-13 → L+11	0.140	H-13	0.13
			H-4 → L+11	0.141	H-4	0.06
			H → L+11	0.602	H-3	0.00
			H → L+14	-0.220	H-2	0.80
			H → L+21	0.170	H-1	0.80
S$_4$	3.13 (396)	0.005	H-1 → L+11	-0.338	H	0.73
			H-1 → L+12	0.348	L	0.01
			H-1 → L+14	0.120	L+1	0.01
			H → L	0.107	L+2	0.00
			H → L+1	0.417	L+3	0.01
S$_5$	3.13 (396)	0.005	H-2 → L+11	-0.338	L+6	0.09
			H-2 → L+12	-0.348	L+7	0.09
			H-2 → L+14	0.121	L+11	0.50
			H → L	0.417	L+12	0.66
			H → L+1	-0.107	L+14	2.11
S$_{10}$	3.48 (356)	0.064	H-2 → L+1	0.484	L+21	1.57
			H-1 → L	0.484		
S$_{13}$	3.94 (314)	0.020	H-2 → L+2	0.177		
			H-2 → L+3	0.349		
			H-1 → L+2	-0.200		
			H-1 → L+3	0.506		
S$_{14}$	3.94 (314)	0.020	H-2 → L+2	0.201		
			H-2 → L+3	0.505		
			H-1 → L+2	0.177		
			H-1 → L+3	-0.350		
Continued on next page						

[TPY-Fe-TPY]$^{2+}$						
State	ΔE (λ)	f	Transition		Orbital	
			Transition	Contribution	Orbital	Metal %
S$_{15}$	4.03 (308)	0.056	H → L+2	0.686		
S$_{19}$	4.47 (277)	0.319	H-4 → L+1	0.447		
			H-3 → L	-0.147		
			H-3 → L+1	-0.438		
			H → L+7	-0.104		
S$_{20}$	4.47 (277)	0.319	H-4 → L	0.448		
			H-3 → L	0.437		
			H-3 → L+1	-0.147		
			H → L+6	-0.104		

Table A.10: Results for [TPY-Ru-TPY]$^{2+}$ complex.

[TPY-Ru-TPY]$^{2+}$						
State	ΔE (λ)	f	Transition		Orbital	
			Transition	Contribution	Orbital	Metal %
S$_1$	2.94 (421)	0.013	H → L+1	0.687	H-4	0.02
S$_5$	3.18 (421)	0.110	H-2 → L	0.139	H-3	0.00
			H-2 → L+1	0.469	H-2	0.73
			H-1 → L	0.469	H-1	0.73
			H-1 → L+1	-0.139	H	0.70
S$_{10}$	3.62 (343)	0.084	H → L+2	0.690	L	0.05
S$_{16}$	4.42 (280)	0.054	H-4 → L	0.121	L+1	0.05
			H-4 → L+1	-0.212	L+2	0.00
			H-3 → L	-0.157	L+3	0.02
			H-3 → L+1	0.184	L+4	0.00
			H-2 → L+11	-0.168	L+5	0.08
			H-2 → L+12	0.134	L+6	0.08
			H-2 → L+17	0.294	L+11	0.41
			H-2 → L+20	-0.132	L+12	0.63
			H-1 → L+11	-0.109	L+17	0.47
			H-1 → L+17	0.282	L+20	4.64
			H-1 → L+20	-0.126		
			H → L+5	0.122		
S$_{17}$	4.42 (280)	0.054	H-4 → L	0.212		
			H-4 → L+1	0.121		
			H-3 → L	0.184		
			H-3 → L+1	0.157		
			H-2 → L+11	0.109		
			H-2 → L+17	0.282		
			H-2 → L+20	-0.126		
Continued on next page						

[TPY-Ru-TPY]$^{2+}$						
State	ΔE (λ)	f	Transition		Orbital	
			Transition	Contribution	Orbital	Metal %
			H-1 → L+11	-0.168		
			H-1 → L+12	0.134		
			H-1 → L+17	-0.294		
			H-1 → L+20	0.132		
			H → L+6	-0.122		
S$_{18}$	4.46 (278)	0.100	H-4 → L	0.272		
			H-4 → L+1	-0.197		
			H-3 → L+1	0.326		
			H-2 → L+17	-0.259		
			H-2 → L+20	0.118		
			H-1 → L+11	0.100		
			H → L+5	0.194		
			H → L+6	-0.197		
S$_{19}$	4.46 (278)	0.100	H-4 → L	0.196		
			H-4 → L+1	0.272		
			H-3 → L	0.325		
			H-2 → L+11	-0.100		
			H-1 → L+17	0.259		
			H-1 → L+20	-0.118		
			H → L+5	-0.198		
			H → L+6	-0.194		
S$_{20}$	4.55 (272)	0.044	H-4 → L+2	-0.119		
			H-3 → L+3	-0.102		
			H-2 → L+5	0.116		
			H-1 → L+6	0.116		
			H → L+4	0.635		

Table A.11: Results for [TPY-Ir-TPY]$^{3+}$ complex.

[TPY-Ir-TPY]$^{3+}$						
State	ΔE (λ)	f	Transition		Orbital	
			Transition	Contribution	Orbital	Metal %
S$_1$	4.00 (309)	0.055	H-2 → L	0.135	H-6	0.03
			H-1 → L	-0.285	H-5	0.03
			H-1 → L+1	0.152	H-4	0.47
			H → L	0.568	H-3	0.47
			H → L+1	-0.112	H-2	0.35
S$_2$	4.00 (309)	0.055	H-2 → L+1	0.135	H-1	0.00
			H-1 → L	0.152	H	0.18
			H-1 → L+1	0.285	L	0.02
Continued on next page						

State	ΔE (λ)	f	Transition		Orbital	
			Transition	Contribution	Orbital	Metal %
			H → L	0.112	L+1	0.02
			H → L+1	0.568	L+2	0.00
S_6	4.54 (273)	0.265	H-2 → L	0.510	L+3	0.01
			H-2 → L+1	-0.191	L+4	0.00
			H-1 → L	0.348	L+6	0.07
			H-1 → L+1	-0.118	L+8	0.76
S_7	4.54 (273)	0.265	H-2 → L	0.191		
			H-2 → L+1	0.510		
			H-1 → L	-0.118		
			H-1 → L+1	-0.348		
S_{12}	4.90 (253)	0.302	H-2 → L+2	0.277		
			H-1 → L+3	-0.163		
			H → L+2	0.564		
S_{13}	4.93 (251)	0.082	H-4 → L+2	-0.298		
			H-4 → L+3	-0.100		
			H-4 → L+8	-0.161		
			H-3 → L+2	0.269		
			H-3 → L+3	0.460		
			H → H-1	0.136		
S_{14}	4.03 (251)	0.082	H-4 → L+2	-0.269		
			H-4 → L+3	0.460		
			H-3 → L+2	-0.298		
			H-3 → L+3	0.100		
			H-3 → L+8	0.161		
			H → L+6	0.136		
S_{17}	5.11 (242)	0.462	H-6 → L+1	0.214		
			H-5 → L	0.214		
			H-4 → L	-0.112		
			H-3 → L+1	-0.112		
			H-2 → L+2	0.389		
			H-1 → L+3	0.339		
			H → L+4	0.153		

Table A.12: Results for [TPPh-Fe-TPPh]$^{2+}$ complex.

State	ΔE (λ)	f	Transition		Orbital	
			Transition	Contribution	Orbital	Metal %
S_1	2.27 (547)	0.000	H-14 → L+4	0.356	H-14	0.55
			H-6 → L+4	0.366	H-12	0.47

			[TPPh-Fe-TPPh]$^{2+}$			
State	ΔE (λ)	f	Transition		Orbital	
			Transition	Contribution	Orbital	Metal %
			H-3 → L+4	0.475	H-11	0.47
S$_5$	3.36 (369)	0.001	H-12 → L+6	-0.266	H-9	0.08
			H-11 → L+4	0.144	H-8	0.08
			H-9 → L+6	0.178	H-7	0.00
			H-5 → L+6	-0.269	H-6	0.18
			H-4 → L+4	0.169	H-5	0.14
			H-3 → L+1	0.197	H-4	0.14
			H-2 → L+4	0.205	H-3	0.18
			H-1 → L+6	0.336	H-2	0.08
S$_6$	3.36 (369)	0.001	H-12 → L+4	-0.144	H-1	0.08
			H-11 → L+6	0.266	H	0.00
			H-8 → L+6	-0.178	L	0.05
			H-5 → L+4	-0.169	L+1	0.13
			H-4 → L+6	0.269	L+2	0.13
			H-3 → L+2	-0.197	L+3	0.00
			H-2 → L+6	0.336	L+4	0.49
			H-1 → L+4	0.205	L+5	0.06
S$_9$	3.60 (345)	0.015	H-11 → L+4	-0.100	L+6	0.37
			H-3 → L+1	0.481	L+7	0.04
			H-2 → L+4	-0.157	L+8	0.04
			H-1 → L	-0.228		
			H → L+2	-0.324		
S$_{10}$	3.60 (345)	0.015	H-12 → L+4	-0.100		
			H-3 → L+2	0.481		
			H-2 → L	-0.228		
			H-1 → L+4	0.157		
			H → L+1	-0.324		
S$_{11}$	3.86 (321)	0.059	H-3 → L+2	0.139		
			H-2 → L	0.541		
			H-1 → L+3	0.284		
			H → L+1	-0.145		
S$_{12}$	3.86 (321)	0.059	H-3 → L+1	0.139		
			H-2 → L+3	0.284		
			H-1 → L	0.541		
			H → L+2	-0.145		
S$_{14}$	4.19 (295)	0.023	H-14 → L+2	0.139		
			H-6 → L+2	0.360		
			H-3 → L+2	0.242		
			H-1 → L+4	0.139		
			H → L+1	0.454		
S$_{15}$	4.19 (295)	0.023	H-14 → L+1	0.139		
			H-6 → L+1	0.360		

[TPPh-Fe-TPPh]$^{2+}$						
State	ΔE (λ)	f	Transition		Orbital	
			Transition	Contribution	Orbital	Metal %
			H-3 → L+1	0.242		
			H-2 → L+4	-0.139		
			H → L+2	0.454		
S_{17}	4.26 (291)	0.496	H-7 → L	-0.191		
			H-5 → L+2	-0.344		
			H-4 → L+1	0.344		
			H-3 → L+3	0.217		
			H → L	-0.320		
S_{19}	4.31 (287)	0.003	H-7 → L+1	-0.231		
			H-6 → L+2	0.129		
			H-5 → L+3	-0.150		
			H-4 → L	0.362		
			H-3 → L+2	-0.127		
			H-3 → L+7	0.111		
			H-2 → L+5	-0.267		
			H-1 → L+3	-0.242		
			H → L+1	-0.139		
S_{20}	4.31 (287)	0.003	H-7 → L+2	0.231		
			H-6 → L+1	-0.129		
			H-5 → L	0.362		
			H-4 → L+3	-0.150		
			H-3 → L+1	0.127		
			H-3 → L+8	0.111		
			H-2 → L+3	0.242		
			H-1 → L+5	0.267		
			H → L+2	0.139		

Bibliography

[1] C. H. Heathcock, *Angew. Chem.* **1992**, *104*, 675–691.

[2] K. C. Nicolaou, D. Vourloumis, N. Wissinger, P. S. Baran, *Angew. Chem.* **2000**, *112*, 46–126.

[3] J.-M. Lehn, *Chem. Eur. J.* **1999**, *5*, 2455–2463.

[4] Z. P. Zhang, M. Z. Rong, M. Q. Zhang, *Prog. Polym. Sci.* **2018**, *80*, 39.

[5] M. Frenette, C. Aliaga, E. Font-Sanchís, J. C. Scaiano, *Org. Lett.* **2004**, *6*, 2579.

[6] K. Imato, M. Nishihara, T. Kanehara, Y. Amamoto, A. Takahara, H. Otsuka, *Angew. Chem. Int. Ed.* **2012**, *51*, 1138.

[7] H. Ying, Y. Zhang, J. Cheng, *Nat. Commun.* **2014**, *5*, 3218.

[8] Z. P. Zhang, M. Z. Rong, M. Q. Zhang, C. Yuan, *Polym. Chem.* **2013**, *4*, 4648.

[9] Z. P. Zhang, M. Z. Rong, M. Q. Zhang, *Polymer* **2014**, *55*, 3936.

[10] T. Manouras, M. Vamvakaki, *Polym. Chem.* **2017**, *8*, 74.

[11] S. R. White, N. R. Sottos, P. H. Geubelle, J. S. Moore, M. R. Kessler, S. R. Sriram, E. N. Brown, S. Viswanathan, *Nature* **2001**, *409*, 794.

[12] X. Chen, M. A. Dam, K. Ono, A. K. Mal, H. Shen, S. R. Nutt, K. Sheran, F. Wudl, *Science* **2002**, *295*, 1698.

[13] P. Cordier, F. Tournilhac, C. Soulié-Ziakovic, L. Leibler, *Nature* **2008**, *451*, 977.

[14] S. J. Rowan, S. J. Cantrill, G. R. L. Cousins, J. K. M. Sanders, J. F. Stoddart, *Angew. Chem. Int. Ed.* **2002**, *41*, 898.

[15] S. J. Rowan, J. P. Capadona, K. Shanmuganathan, D. J. Tyler, C. Weder, *Science* **2008**, *319*, 1370.

[16] R. Abbel, C. Grenier, M. J. Pouderoijen, J. W. Stouwdam, P. E. L. G. Leclère, R. P. Sijbesma, E. W. Meijer, A. P. H. J. Schenning, *J. Am. Chem. Soc.* **2009**, *131*, 833.

[17] N. Roy, B. Bruchmann, J.-M. Lehn, *Chem. Soc. Rev.* **2015**, *44*, 3786.

[18] M. D. Hager, P. Greil, C. Leyens, S. van der Zwaag, U. S. Schubert, *Adv. Mater.* **2010**, *22*, 5424.

[19] M. Q. Zhang, M. Z. Rong, *Polym. Chem.* **2013**, *4*, 4878.

[20] S. Billiet, X. K. D. Hillewaere, R. F. A. Teixiera, F. E. Du Prez, *Macromol. Rapid. Commun.* **2013**, *34*, 290.

[21] D. Y. Wu, S. Meure, D. Solomon, *Prog. Polym. Sci.* **2008**, *33*, 479.

[22] J. W. Kamplain, C. W. Bielawski, *Chem. Commun.* **2006**, 1727.

[23] Y. Ruff, J.-M. Lehn, *Biopolymers* **2008**, *89*, 486.

[24] H. Otsuka, T. Muta, M. Sakada, T. Maeda, A. Takahara, *Chem. Commun.* **2009**, 1073.

[25] Y. Amamoto, T. Maeda, M. Kikuchi, H. Otsuka, A. Takahara, *Chem. Commun.* **2009**, 689.

[26] T. Maeda, H. Otsuka, A. Takahara, *Prog. Polym. Sci.* **2009**, *34*, 581.

[27] X. K. D. Hillewaere, F. E. Du Prez, *Prog. Polym. Sci.* **2015**, *49-50*, 121.

[28] W. Zou, J. Dong, Y. Luo, Q. Zhao, T. Xie, *Adv. Mater.* **2017**, *29*, 1606100.

[29] J. Dahlke, S. Zechel, M. D. Hager, U. S. Schubert, *Adv. Mater. Interfaces* **2018**, *5*, 1800051.

[30] X. Chen, F. Wudl, A. K. Mal, H. Shen, S. R. Nutt, *Macromolecules* **2003**, *36*, 1802.

[31] Y.-L. Liu, Y.-W. Chen, *Macromol. Chem. Phys.* **2007**, *208*, 224.

[32] A. Rekondo, R. Martin, A. Ruiz de Luzuriaga, G. Cabañero, H. J. Grande, I. Odriozola, *Mater. Horiz.* **2014**, *1*, 237.

[33] I. Azcune, I. Odriozola, *Eur. Polym. J.* **2016**, *84*, 147.

[34] R. Martin, A. Rekondo, A. Ruiz de Luzuriaga, P. Casuso, D. Dupin, G. Cabañero, H.-J. Grande, I. Odriozola, *Smart Mater. Struct.* **2016**, *25*, 084017.

[35] J. M. Matxain, J. M. Asua, F. Ruipérez, *Phys. Chem. Chem. Phys.* **2016**, *18*, 1758.

[36] F. Ruipérez, M. Galdeano, E. Gimenez, J. M. Matxain, *ChemistryOpen* **2018**, *7*, 248.

[37] P. Zheng, T. J. McCarthy, *J. Am. Chem. Soc.* **2012**, *134*, 2024.

[38] D. Montarnal, M. Capelot, F. Tournilhac, L. Leibler, *Science* **2011**, *134*, 965.

[39] D. J. Fortman, J. P. Brutman, C. J. Cramer, M. A. Hillmyer, W. R. Dichtel, *J. Am. Chem. Soc.* **2015**, *137*, 14019.

[40] W. Denissen, G. Rivero, R. Nicolaÿ, L. Leibler, J. M. Winne, F. E. Du Prez, *Adv. Funct. Mater.* **2015**, *25*, 2451.

[41] C. Yuan, M. Rong, M. Zhang, Z. Zhang, Y. Yuan, *Chem. Mater.* **2011**, *23*, 5076.

[42] S. Burattini, H. M. Colquhoun, J. D. Fox, D. Friedmann, B. W. Greenland, P. J. F. Harris, W. Hayes, M. E. Mackay, S. J. Rowan, *Chem. Commun.* **2009**, 6717.

[43] S. Burattini, B. W. Greenland, D. Hermida-Merino, W. Weng, J. Seppala, H. M. Colquhoun, W. Hayes, M. E. Mackay, I. W. Hamley, S. J. Rowan, *J. Am. Chem. Soc.* **2010**, *132*, 12051.

[44] S. Burattini, B. W. Greenland, W. Hayes, M. E. Mackay, S. J. Rowan, H. M. Colquhoun, *Chem. Mater.* **2011**, *23*, 6.

[45] B. A. Blight, C. A. Hunter, D. A. Leigh, H. McNab, P. I. T. Thomson, *Nat. Chem.* **2011**, *3*, 246.

[46] Y. Chen, A. M. Kushner, G. A. Williams, Z. Guan, *Nat. Chem.* **2012**, *4*, 467.

[47] J. Cortese, C. Soulié-Ziakovic, S. Tencé-Girault, L. Leibler, *J. Am. Chem. Soc.* **2012**, *134*, 3671.

[48] F. Herbst, S. Seiffert, W. H. Binder, *Polym. Chem.* **2012**, *3*, 3084.

[49] N. Giuseppone, J.-M. Lehn, *J. Am. Chem. Soc.* **2004**, *126*, 11448.

[50] H. Hofmeier, U. S. Schubert, *Chem. Soc. Rev.* **2004**, *33*, 373.

[51] C.-F. Chow, S. Fujii, J.-M. Lehn, *Angew. Chem. Int. Ed.* **2007**, *46*, 5007.

[52] S. D. Bergman, F. Wudl, *J. Mater. Chem.* **2008**, *18*, 41.

[53] M. Burnworth, L. M. Tang, J. R. Kumpfer, A. J. Duncan, F. L. Beyer, G. L. Fiore, S. J. Rowan, C. Weder, *Nature* **2011**, *472*, 334.

[54] J. R. Kumpfer, S. J. Rowan, *J. Am. Chem. Soc.* **2011**, *133*, 12866.

[55] M. Q. Zhang, M. Z. Rong, *J. Polym. Sci., Part B: Polym. Phys.* **2012**, *50*, 229.

[56] J. Canadell, H. Goossens, B. Klumperman, *Macromolecules* **2011**, *44*, 2536.

[57] X. An, R. H. Aguirresarobe, L. Irusta, F. Ruipérez, J. M. Matxain, X. Pan, N. Aramburu, D. Mecerreyes, H. Sardon, *Polym. Chem.* **2017**, *8*, 3641.

[58] M. Irigoyen, A. Fernández, A. Ruiz, F. Ruipérez, J. M. Matxain, *J. Org. Chem.* **2019**, *84*, 4200.

[59] R. J. Sarma, S. Otto, J. R. Nitschke, *Chem. Eur. J.* **2007**, *13*, 9542.

[60] A. M. Belenguer, T. Friščić, G. M. Day, J. K. M. Sanders, *Chem. Sci.* **2011**, *2*, 696.

[61] S. Nevejans, N. Ballard, J. I. Miranda, B. Reck, J. M. Asua, *Phys. Chem. Chem. Phys.* **2016**, *18*, 27577.

[62] C.-H. Li, J.-L. Zuo, *Adv. Mater.* **2020**, *32*, 1903762.

[63] W. Denissen, J. M. Winne, F. E. Du Prez, *Chem. Sci.* **2016**, *7*, 30.

[64] C. N. Bowman, C. J. Kloxin, *Angew. Chem. Int. Ed.* **2012**, *51*, 4272.

[65] E. Erice, A. R. de Luzuriaga, J. M. Matxain, F. Ruipérez, J. M. Asua, H.-J. Grande, A. Rekondo, *Polymer* **2018**, *145*, 127–136.

[66] N. K. Guimard, K. K. Oehlenschlaeger, J. Zhou, S. Hilf, F. G. Schmidt, C. Barner-Kowollik, *Macromol. Chem. Phys.* **2012**, *213*, 131.

[67] M. Wang, F. Nudelman, R. R. Matthes, M. P. Shaver, *J. Am. Chem. Soc.* **2017**, *139*, 14232.

[68] G. C. Welch, R. R. San Juan, J. D. Masuda, D. W. Stephan, *Science* **2006**, *314*, 1124.

[69] D. W. Stephan, *Org. Biomol. Chem.* **2008**, *6*, 1535.

[70] D. W. Stephan, G. Erker, *Angew. Chem. Int. Ed.* **2015**, *54*, 6400.

[71] D. W. Stephan, *Science* **2016**, *354*, aaf7229.

[72] U. Yolsal, M. Wang, J. R. Royer, M. P. Shaver, *Macromolecules* **2019**, *52*, 3417–3425.

[73] L. Chen, R. Liu, Q. Yan, *Angew. Chem. Int. Ed.* **2018**, *57*, 9336.

[74] L. Chen, R. Liu, X. Hao, Q. Yan, *Angew. Chem. Int. Ed.* **2018**, *58*, 264.

[75] C. Mömming, E. Otten, G. Kehr, R. Frölich, S. Grimme, D. W. Stephan, G. Erker, *Angew. Chem. Int. Ed.* **2009**, *48*, 6643.

[76] T. Steiner, *Angew. Chem. Int. Ed.* **2002**, *41*, 48.

[77] K. C. Bentz, S. M. Cohen, *Angew. Chem. Int. Ed.* **2018**, *57*, 14992–15001.

[78] C. Sun, J. H. Waite, *J. Biol. Chem.* **2005**, *280*, 39332–39336.

[79] M. J. Harrington, A. Masicniels, N. Holten-Andersen, H. Waite, P. Fratzl, *Science* **2010**, *328*, 216–220.

[80] N. Holten-Andersen, M. J. Harrington, H. Birkedal, B. P. Lee, P. B. Messersmith, K. Y. C. Lee, J. H. Waite, *Proc. Natl. Acad. Sci. USA* **2010**, *108*, 2651–2655.

[81] N. Holten-Andersen, A. Jaishankar, M. J. Harrington, D. E. Fullenkamp, G. Di-Marco, L. He, G. H. McKinley, P. B. Messersmith, K. Y. C. Lee, *J. Mater. Chem. B* **2014**, *2*, 2467–2472.

[82] M. Krogsgaard, V. Nue, H. Birkedal, *Chem. Eur. J.* **2016**, *22*, 844–857.

[83] S. Zechel, M. D. Hager, T. Priemel, M. J. Harrington, *Biomimetics* **2019**, *4*, 20.

[84] A. Andersen, Y. Chen, H. Birkedal, *Biomimetics* **2019**, *4*, 30.

[85] G. I. Dzhardimalieva, B. C. Yadav, S. Singh, I. E. Uflyand, *Dalton Trans.* **2020**, *49*, 3042–3087.

[86] J.-F. Gohy, *Coord. Chem. Rev.* **2009**, *253*, 2214–2225.

[87] G. A. Lawrence in *Introduction to Coordination Chemistry*, John Wiley & Sons, Ltd, London, UK, **2010**.

[88] J. Lee, E. J. Choi, I. Varga, P. M. Claesson, S.-H. Yun, C. Song, *Polym. Chem.* **2018**, *9*, 1032–1039.

[89] M. Mauro, S. Bellemin-Laponnaz, C. Cebrián, *Chem. Eur. J.* **2017**, *23*, 17626–17636.

[90] M. Enke, L. Köps, S. Zechel, J. C. Brendel, J. Vitz, M. D. Hager, U. S. Schubert, *Macromol. Rapid Commun.* **2018**, *39*, 1700742.

[91] M. Enke, R. K. Bose, S. Zechel, J. Vitz, R. Deubler, S. J. García, S. van der Zwaag, F. H. Schacher, M. D. Hager, U. S. Schubert, *Polym. Chem.* **2018**, *9*, 3543–3551.

[92] D. Mozhdehi, S. Ayala, O. R. Cromwell, Z. Guan, *J. Am. Chem. Soc.* **2014**, *136*, 16128–16131.

[93] D. Mozhdehi, J. A. Neal, S. C. Grindy, S. Ayala, N. Holten-Andersen, Z. Guan, *Macromolecules* **2016**, *49*, 6310–6321.

[94] J.-C. Lai, L. Li, D.-P. Wang, M.-H. Zhang, S.-R. Mo, X. Wang, K.-Y. Zeng, C.-H. Li, Q. Jiang, X.-Z. You, J.-L. Zuo, *Nat. Commun.* **2018**, *9*, 2725.

[95] J.-C. Lai, X.-Y. Jia, D.-P. Wang, Y.-B. Deng, P. Zheng, C.-H. Li, J.-L. Zuo, Z. Bao, *Nat. Commun.* **2019**, *10*, 1164.

[96] Y. Lei, W. Huang, Q. Huang, A. Zhang, *New J. Chem.* **2019**, *43*, 261–268.

[97] B. Yang, H. Zhang, H. Peng, Y. Xu, B. Wu, W. Weng, L. Li, *Polym. Chem.* **2014**, *5*, 1945–1953.

[98] B. Sandmann, B. Happ, S. Kupfer, F. H. Schacher, M. D. Hager, U. S. Schubert, *Macromol. Rapid Commun.* **2014**, *36*, 604–609.

[99] S. Götz, R. Geitner, M. Abend, M. Siegmann, S. Zechel, J. Vitz, S. Gräfe, M. Schmitt, J. Popp, M. D. Hager, U. S. Schubert, *Macromol. Rapid Commun.* **2018**, *39*, 1800495.

[100] A. Wild, A. Winter, F. Schlütter, U. S. Schubert, *Chem. Soc. Rev.* **2011**, *40*, 1459–1511.

[101] P. R. Andres, U. S. Schubert, *Advanced Materials* **2004**, *16*, 1043–1068.

[102] M. A. W. Lawrence, K.-A. Green, P. N. Nelson, S. C. Lorraine, *Polyhedron* **2018**, *143*, 11–27.

[103] S. Kupfer, L. Zedler, J. Guthmuller, S. Bode, M. D. Hager, U. S. Schubert, J. Popp, S. Gräfe, B. Dietzek, *Phys. Chem. Chem. Phys.* **2014**, *16*, 12422–12432.

[104] S. Bode, R. K. Bose, S. Matthes, M. Ehrhardt, A. Seifert, F. H. Schacher, R. M. Paulus, S. Stumpf, B. Sandmann, J. Vitz, A. Winter, S. Hoeppener, S. J. García, S. Spange, S. van der Zwaag, M. D. Hager, U. S. Schubert, *Polym. Chem.* **2013**, *4*, 4966–4973.

[105] S. Bode, R. K. Bose, S. Matthes, M. Ehrhardt, A. Seifter, F. H. Schacher, R. M. Paulus, S. Stumpf, B. Sandmann, J. Vitz, A. Winter, S. Hoeppener, S. J. Garcia, S. Spange, S. can der Zwaag, M. D. Hager, U. S. Schubert, *Polymer Chemistry* **2013**, *4*, 4966–4973.

[106] E. Borré, J.-F. Stumbé, S. Bellemin-Laponnaz, M. Mauro, *Angew. Chem. Int. Ed.* **2016**, *55*, 1313–1317.

[107] E. Borré, J.-F. Stumbé, S. Bellemin-Laponnaz, M. Mauro, *Chem. Commun.* **2017**, *53*, 8344–8347.

[108] N. Mézailles, N. Avarvari, L. Ricard, F. Mathey, P. Le Floch, *Inorg. Chem.* **1998**, *37*, 5313–5316.

[109] M. Burnworth, L. Tang, J. R. Kumpfer, A. J. Duncan, F. L. Beyer, G. L. Fiore, S. J. Rowan, C. Weder, *Nature* **2011**, *472*, 334–338.

[110] C. Müller, L. E. E. Broeckx, I. de Krom, J. J. M. Weemers, *ejic* **2013**, 187–202.

[111] X. Xion, A. del Campo, J. Cui, *Photoresponsive polymers*, chapter 4, Smart polymers and their applications, Elsevier, second edition edition, **2019**, 1–18.

[112] G. L. Fiore, S. J. Rowan, C. Weder, *Chem. Soc. Rev.* **2013**, *42*, 7278–7288.

[113] W. Fan, Y. Jin, L. Shi, W. Du, R. Zhou, S. Lai, Y. Shen, Y. Li, *ACS Appl. Mater. Interfaces* **2020**, *12*, 6383–6395.

[114] D. Knapton, M. Burnworth, S. J. Rowan, C. Weder, *Angew. Chem. Int. Ed.* **2006**, *45*, 5825–5829.

[115] J. R. Kumpfer, J. Jin, S. J. Rowan, *J. Mater. Chem.* **2010**, *20*, 145–151.

[116] L. Flamigni, A. Barbieri, C. Sabatini, B. Ventura, F. Barigelletti in *Photochemistry and photophysics of coordination compounds: iridium*, Springer, Berlin, Heidelberg, **2007**.

[117] Y. You, W. Nam, *csr* **2012**, *41*, 7061–7084.

[118] M. A. Baldo, M. E. Thompson, S. R. Forrest, *nature* **2000**, *403*, 750–753.

[119] R. D. Costa, E. Ortí, H. J. Bolink, F. Monti, G. Accorsi, N. Armaroli, *Angewandte Reviews* **2012**, *51*, 8178–8211.

[120] Z. Xie, L. Ma, K. E. deKrafft, A. Jin, W. Lin, *jacs* **2009**, *132*, 922–923.

[121] A. Ruggia, F. W. Leeuwenb, A. H.Veldersac, *Elsevier* **2011**, *225*, 2542–2554.

[122] G. L. Schulz, S. Holdcroft, *Chem. Mater.* **2008**, *20*, 5351–5355.

[123] J. I. Goldsmith, W. R. Hudson, M. S. Lowry, T. H. Anderson, S. Bernhard, *jacs* **2005**, *127*, 7502–7510.

[124] J. D. Nguyen, J. W. Tucker, M. D. Konieczynska, C. R. J. Stephenson, *jacs* **2011**, *133*, 4160–4163.

[125] B. H. Jhun, D. Song, S. Y. Park, Y. You, *Top Curr. Chem. (Z)* **2022**, *380*, 35.

[126] T. Sajoto, P. Djurovich, A. Tamayo, M. Yousufuddin, R. Bau, M. Thompson, R. Holmes, S. Forrest, *Inorg. Chem.* **2005**, *44*, 7992–8003.

[127] C. Adachi, M. Baldo, S. Forrest, S. Lamansky, M. Thompson, R. Kwong, *Appl. Phys. Lett.* **2001**, *78*, 1622–1624.

[128] A. Tsuboyama, H. Iwawaki, M. Furugori, T. Mukaide, J. Kamatani, S. Igawa, T. Moriyama, S. Miura, T. Takiguchi, S. Okada, M. Hoshino, K. Ueno, *J. Am. Chem. Soc.* **2003**, *125*, 12971–12979.

[129] E. Schrödinger, *Ann. Physik.* **1926**, *79*, 361.

[130] E. Schrödinger, *Ann. Physik.* **1926**, *79*, 734.

[131] P. A. M. Dirac, *Proc. R. Soc. London, Ser. A* **1926**, *113*, 621.

[132] M. Born, J. Oppenheimer, *Ann. Phys.* **1927**, *44*, 455.

[133] P. A. M. Dirac, *Proc. R. Soc. London, Ser. A* **1930**, *126*, 360.

[134] E. Schrödinger, *Phys. Rev.* **1926**, *28*, 1049.

[135] W. Heisenberg, *Z. Physik* **1925**, *33*, 879.

[136] W. Heisenberg, *Z. Physik* **1927**, *43*, 172.

[137] W. Pauli, *Z. Physik* **1925**, *31*, 765.

[138] M. Born, R. Oppenheimer, *Ann. Phys.* **1927**, *84*, 457.

[139] D. R. Hartree, *Proc. Cambridge Phil. Soc.* **1928**, *24*, 89.

[140] V. Fock, *Z. Phys.* **1930**, *61*, 126.

[141] W. Kutzelnigg, *J. Mol. Struct. (THEOCHEM)* **1988**, *181*, 33.

[142] C. Møller, M. S. Plesset, *Phys. Rev.* **1934**, *46*, 618.

[143] R. J. Bartlett in *Recent Advances in Coupled-Cluster Methods*, World Scientific, Singapur, **1997**.

[144] R. G. Parr, W. Yang in *Density Functional Theory of Atoms and Molecules*, Oxford Science Publications, New York, **1989**.

[145] E. Kryachko, ed. in *Energy Density Functional Theory of Many-Electron Systems*, Kluwer Academic Publishers, London, **1990**.

[146] P. Hohenberg, W. Kohn, *Phys. Rev. B* **1964**, *136*, B864.

[147] W. Kohn, L. J. Sham, *Phys. Rev.* **1965**, *140*, A1133.

[148] R. Stowaser, R. Hoffmann, *J. Am. Chem. Soc.* **1999**, *121*, 3414.

[149] O. Gunnarsson, B. I. Lundqvist, *Phys. Rev. B* **1976**, *13*, 4274.

[150] T. Kar, J. Angyan, A. Shannigrahi, *J. Phys. Chem. A* **2000**, *104*, 9953.

[151] S. Vosko, L. Wilk, M. Nusair, *Can. J. Phys.* **1980**, *58*, 1299.

[152] J. Labanowski, J. Andelzelm, eds. in *Density Functional Methods in Chemistry*, Spring-Verlag, New York, **1991**.

[153] V. Tschinke, T. Ziegler, *Theor. Chim. Acta* **1991**, *81*, 651.

[154] B. Johnson, P. Gill, J. Pople, *J. Chem. Phys.* **1993**, *98*, 5612.

[155] T. Ziegler, *Chem. Rev.* **1991**, *91*, 651.

[156] E. Runge, E. K. U. Gross, *Phys. Rev. Lett.* **1984**, *52*, 997.

[157] M. E. Casida **1995**, 155–192.

[158] C. Jamorski, M. E. Casida, D. R. Salahub, *J. Chem. Phys.* **1998**, *104(13)*, 5134.

[159] M. Petersilka, U. J. Gossman, E. K. U. Gross, *Phys. Rev. Lett.* **1996**, *76(8)*, 1212–1215.

[160] M. Petersilka, E. K. U. Gross, *Int. J. Quantum Chem. 7*, 1393–1401.

[161] R. Bauernschmitt, R. Ahlrichs, *Chem. Phys. Lett.* **1996**, *256(4-5)*, 454–464.

[162] S. Hirata, M. Head-Gordon, *Chem. Phys. Lett.* **1999**, *302(5-6)*, 375–382.

[163] S. Hirata, M. Head-Gordon **nov 1999**, *111(19)*, 8904.

[164] N. N. Matsuzawa, A. Ishitani, D. A. Dixon, T. Uda, *J. Phys. Chem. A* **2001**, *105*, 4953–4962.

[165] Z.-L. Cai, J. R. Reimers, *J. Chem. Phys.* **1999**, *112(2)*, 527.

[166] R. Bauernschmitt, R. Ahlrichs, H. H. Frank, M. M. Kappes **1998**.

[167] E. K. U. Gross, W. Kohn, *Adv. Quantum. Chem.* **1990**, *21*, 255.

[168] R. E. Stratmann, G. E. Scuseria, M. J. Frisch, *J. Chem. Phys.* **1998**, *109(19)*, 8218.

[169] M. E. Casida, C. Jamorski, K. C. Casida, D. R. Salahub, *J. Chem. Phys.* **1998**, *108(11)*, 4439.

[170] R. G. Parr, L. Von Szentpaly, S. B. Liu, *J. Am. Chem. Soc.* **1999**, *121*, 1922.

[171] J. L. Gázquez, A. Cedillo, A. Vela, *J. Phys. Chem. A* **2007**, *111*, 1966.

[172] S. Partihar, S. Roy, *J. Org. Chem.* **2010**, *75*, 4957.

[173] S. Partihar, S. Roy, *J. Org. Chem.* **2011**, *76*, 4219.

[174] V. Gutmann, *Coord. Chem. Rev.* **1976**, *18*, 225.

[175] A. E. Reed, L. A. Curtiss, F. Weinhold, *Chem. Rev.* **1988**, *88*, 899.

[176] J. P. Foster, F. Weinhold, *J. Am. Chem. Soc.* **1980**, *102*, 7211.

[177] F. Weinhold, C. R. Landis, E. D. Glendening, *Int. Rev. Phys. Chem.* **2016**, *35*, 399.

[178] M. von Hopffgarten, G. Frenking, *WIREs Comput. Mol. Sci.* **2012**, *2*, 43–62.

[179] K. J. Morokuma, *J. Chem. Phys.* **1971**, *55*, 1236–1244.

[180] F. M. Bickelhaupt, E. J. Baerends, *Reviews in Computational Chemistry* **2000**, 1–86.

[181] S. Grimme, *J. Comput. Chem.* **2004**, *25*, 1463.

[182] S. Grimme, *J. Comput. Chem.* **2006**, *27*, 1787.

[183] D. Cremer, E. Kraka, *Croat. Chem. Acta* **1984**, *57*, 1259–1281.

[184] S. Jenkins, I. Morrison, *Chem. Phys. Lett.* **2000**, *317*, 97–102.

[185] S. J. Grabowski, *Relationships between QTAIM and the decomposition of the interaction energy - Comparison of different kinds of hydrogen bond*, The quantum theory of atoms in molecules. From solid state to DNA and drug design, Wiley-VCH, Weinheim, **2007**, 453–469.

[186] S. J. Grabowski, *Chem. Rev.* **2011**, *111*, 2597–2625.

[187] M. J. Frisch, G. W. Trucks, H. B. Schlegel, G. E. Scuseria, M. A. Robb, J. R. Cheeseman, G. Scalmani, V. Barone, G. A. Petersson, H. Nakatsuji, X. Li, M. Caricato, A. V. Marenich, J. Bloino, B. G. Janesko, R. Gomperts, B. Mennucci, H. P. Hratchian, J. V. Ortiz, A. F. Izmaylov, J. L. Sonnenberg, D. Williams-Young, F. Ding, F. Lipparini, F. Egidi, J. Goings, B. Peng, A. Petrone, T. Henderson, D. Ranasinghe, V. G. Zakrzewski, J. Gao, N. Rega, G. Zheng, W. Liang, M. Hada, M. Ehara, K. Toyota, R. Fukuda, J. Hasegawa, M. Ishida, T. Nakajima, Y. Honda, O. Kitao, H. Nakai, T. Vreven, K. Throssell, J. A. Montgomery, Jr., J. E. Peralta, F. Ogliaro, M. J. Bearpark, J. J. Heyd, E. N. Brothers, K. N. Kudin, V. N. Staroverov, T. A. Keith, R. Kobayashi, J. Normand, K. Raghavachari, A. P. Rendell, J. C. Burant, S. S. Iyengar, J. Tomasi, M. Cossi, J. M. Millam, M. Klene, C. Adamo, R. Cammi, J. W. Ochterski, R. L. Martin, K. Morokuma, O. Farkas, J. B. Foresman, D. J. Fox, *Gaussian 16 Revision A.03*, **2016**, gaussian Inc. Wallingford CT.

[188] J. Tao, J. P. Perdew, V. N. Staroverov, G. E. Scuseria, *Phys. Rev. Lett.* **2003**, *91*, 146401.

[189] F. Weigend, R. Ahlrichs, *Phys. Chem. Chem. Phys.* **2005**, *7*, 3297–3305.

[190] F. Weigend, *Phys. Chem. Chem. Phys.* **2006**, *8*, 1057–1065.

[191] S. Grimme, S. Ehrlich, L. Goerigk, *J. Comput. Chem.* **2011**, *32*, 1456–1465.

[192] B. Schirmer, S. Grimme, in G. Erker, D. Stephan, eds., *Frustrated Lewis Pairs I. Topics in Current Chemistry*, Springer, Berlin, Heidelberg, **2013**, 213–230.

[193] S. Simon, M. Duran, J. J. Dannenberg, *J. Chem. Phys.* **1996**, *105*, 11024–11031.

[194] S. F. Boys, F. Bernardi, *Mol. Phys.* **1970**, *19*, 553–566.

[195] A. E. Reed, R. B. Weinstock, F. Weinhold, *J. Chem. Phys.* **1985**, *83*, 735.

[196] A. E. Reed, F. Weinhold, *J. Chem. Phys.* **1985**, *83*, 1736.

[197] T. Ziegler, A. Rauk, *Inorg. Chem.* **1979**, *18*, 1755–1759.

[198] M. Van Hopffgarten, G. Frenking, *WIREs Comput. Mol. Sci.* **2012**, *2*, 43–62.

[199] A. D. Becke, *Phys. Rev. A* **1988**, *38*, 3098.

[200] J. P. Perdew, *Phys. Rev. B* **1986**, *33*, 8822.

[201] G. te Velde, F. M. Bickelhaupt, E. J. Baerends, C. Fonseca Guerra, S. J. A. van Gisbergen, J. G. Snijders, T. Ziegler, *J. Comput. Chem.* **2001**, *22*, 931–967, ISSN 1096-987X.

[202] S. J. Grabowski, W. A. Sokalski, E. Dyguda, J. Leszczyński, *J. Phys. Chem. B* **2006**, *110*, 6444–6446.

[203] J.-D. Chai, M. Head-Gordon, *Phys. Chem. Chem. Phys.* **2008**, *10*, 6615.

[204] W. J. Hehre, R. Ditchfield, J. A. Pople, *J. Chem. Phys.* **1972**, *56*, 2257.

[205] R. Krishnan, J. S. Binkley, R. Seeger, J. A. Pople, *J. Chem. Phys.* **1980**, *72*, 650.

[206] R. F. W. Bader in *Atoms in molecules: a quantum theory*, Clarendon Press, Oxford, UK, **1990**.

[207] R. F. W. Bader, *Chem. Rev.* **1991**, *91*, 893–928.

[208] A. Todd, T. A. Keith, **2011**, aIMAll (Version 11.08.23), TK Gristmill Software, Overland Park KS, USA (http://aim.tkgristmill.com).

[209] R. G. Pearson, *J. Am. Chem. Soc.* **1963**, *85*, 3533–3539.

[210] A. Loibl, I. de Krom, E. A. Pidko, M. Weber, J. Wiecko, C. Müller, *Chem. Commun.* **2014**, *50*, 8842–8844.

[211] B. Breit, R. Winde, T. Mackewitz, R. Paciello, K. Harms, *Chem. Eur. J.* **2001**, *7*, 3106–3121.

[212] N. Mézailles, L. Ricard, F. Mathey, P. Le Floch, *Organometallics* **2001**, *20*, 3304–3307.

[213] C. Elschenbroich, J. Six, K. Harms, G. Frenking, G. Heydenrych, *Eur. J. Inorg. Chem.* **2008**, *2008*, 3303–3309.

[214] D. Carmichael, P. Le Floch, L. Ricard, F. Mathey, *Inorg. Chim. Acta* **1992**, 437–441.

[215] P. Le Floch, S. Mansuy, L. Ricard, F. Mathey, A. Jutand, C. Amatore, *Organometallics* **1996**, *15*, 3267–3274.

[216] M. Doux, N. Mézailles, L. Ricard, P. Le Floch, *Eur. Jour. Inorg. Chem.* **2003**, *2003*, 3878–3894.

[217] T. Müller, E. A. Pidko, M. Lutz, A. L. Spek, D. Vogt, *Chem. Eur. J.* **2008**, *14*, 8803–8807.

[218] V. Balzani, P. Ceroni, A. Juris in *Photochemistry and photophysics: concepts, research, applications*, Wiley-VCH Verlag GmbH, Boschstr. 12, 69469 Weinheim, Germany, **2014**.

[219] R. F. Borkman, D. R. Kearns, *Chemical Comunications (London)* **1966**, 446–447.

[220] L. S. Foster, *Coordination Chemistry Reviews* **2002**, *227*, 59–92.

[221] A. Juris, F. Barigelletti, V. Balzani, P. Belser, A. von Zelewsky, *Journal of the Chemical Society, Faraday Transactions 2: Molecular and Chemical Physics* **1987**, *83*, 2295–2306.

[222] A. Juris, V. Balzani, F. Barigelletti, S. Campagna, P. Belser, A. von Zelewsky, *Coordination Chemistry Review* **1988**, *84*, 85–277.

[223] S. Shaikh, Y. Wang, F. Rehman, H. Jiang, X. Wang, *Coord. Chem. Rev.* **2020**, *416*, 213344.